Check for updates

NIST Technical Note
NIST TN 2254

Sensitivity Analysis of Reinforced Concrete Structures

A Review

Mohammad Amin Hariri-Ardebili
Siamak Sattar

This publication is available free of charge from:
https://doi.org/10.6028/NIST.TN.2254

NATIONAL INSTITUTE OF STANDARDS AND TECHNOLOGY
U.S. DEPARTMENT OF COMMERCE

NIST Technical Note
NIST TN 2254

Sensitivity Analysis of Reinforced Concrete Structures

A Review

Mohammad Amin Hariri-Ardebili
Siamak Sattar
Materials and Structural Systems Division
Engineering Laboratory

This publication is available free of charge from:
https://doi.org/10.6028/NIST.TN.2254

July 2023

U.S. Department of Commerce
Gina M. Raimondo, Secretary

National Institute of Standards and Technology
Laurie E. Locascio, NIST Director and Under Secretary of Commerce for Standards and Technology

NIST TN 2254
July 2023

NIST Technical Series Policies

Publication History
Approved by the NIST Editorial Review Board on 2023-04-13

How to cite this NIST Technical Series Publication:
Mohammad Amin Hariri-Ardebili, Siamak Sattar (2023) Sensitivity Analysis of Reinforced Concrete Structures: A Review. (National Institute of Standards and Technology, Gaithersburg, MD), NIST TN 2254. https://doi.org/10.6028/NIST.TN.2254

NIST Author ORCID iDs
Mohammad Amin Hariri-Ardebili: 0000-0001-6772-1468
Siamak Sattar: 0000-0003-1096-7015

Abstract

Sensitivity analysis is a crucial step in computational mechanics and earthquake engineering. Sensitivity analysis of a model (either numerical or physical) aims at quantifying the relative importance of each input parameter, their potential interaction, and their effects on the model response. Sensitivity analysis has a long-term application in structural engineering more specifically on reinforced concrete RC structures. Many researchers benefited from the results of sensitivity analysis to reduce the uncertainty domain to those variables which are very important. This further helps in uncertainty quantification by accelerating the entire process. This state-of-the-art technical report provides a comprehensive review of classical sensitivity analysis techniques, followed by an in-depth review of all the related documents that implemented a full sensitivity analysis or partially adopted it for uncertainty quantification-related discussions. This review report on sensitivity analysis of reinforced concrete structures is a valuable contribution to the field of computational mechanics and earthquake engineering. This review highlights the importance of selecting an appropriate sensitivity analysis technique to achieve reliable results in structural analysis and design. By providing insights into the advantages and limitations of various sensitivity analysis techniques, this report can guide researchers, practitioners, and decision-makers in selecting the most appropriate technique for their specific applications. It is observed that the outcome of a sensitivity analysis depends heavily on the applied technique to perform the sensitivity assessment which eventually may cause a significant bias during the decision-making. This report paves the road for better selection of a sensitivity analysis technique in problems related to structural and earthquake engineering. The findings of this review have significant implications for improving the accuracy and reliability of structural analysis, ultimately leading to safer and more resilient structures.

Keywords

Local and global sensitivity; Modeling parameters; Material randomness; Reinforced concrete; Sensitivity; Seismic response; Tornado diagram; Uncertainty quantification.

Table of Contents

List of Tables

List of Figures

Acknowledgments

The authors would like to thank Dr. Katherine Johnson and Dr. Christine Z. Beyzaei at NIST and Professor Victor Saouma and Dr. Golsa Mahdavi at the University of Colorado Boulder for their reviews and constructive comments. Dr. Christopher Segura from NIST provided constructive comments and discussions about the sensitivity analysis methods, as well as a major contribution to the "Uncertainty Quantification" project.

Author Contributions

Mohammad Amin Hariri-Ardebili: Conceptualization, Methodology, Software, Data curation, Writing- Original draft preparation, Visualization, Investigation, Supervision, Writing- Reviewing and Editing; **Siamak Sattar**: Conceptualization, Writing- Reviewing and Editing, Investigation.

1. Introduction

Sensitivity analysis is an essential part of every risk assessment, either quantitative or qualitative. The gaps in our knowledge are bridged by assumptions, probability distributions, expert opinions, approximations, and a variety of other techniques. Sensitivity analysis is a systematic investigation of the means by which assessors bridge these uncertainty gaps. Sensitivity analysis seeks to learn such things as how sensitive model outputs are to changes in inputs and how that sensitivity might affect decisions. A good sensitivity analysis increases overall confidence in a risk assessment [27]. At present, the codified approaches for seismic performance evaluation of structural systems do not explicitly account for the application of sensitivity analysis, which is indeed a required tool to quantify the epistemic and aleatory uncertainty sources.

In engineering applications, sensitivity analysis is used both in the framework of design and analysis. In structural engineering and mechanics, sensitivity analysis has been widely used to evaluate the important/sensitive parameters in existing structural systems. The robustness and adequacy of the models can be best understood by means of sensitivity analysis [28–30].

Applications of sensitivity analysis of structural systems can be found in [31] for steel jacket-type offshore platforms with soil-pile-structure interaction, [32] for cohesive crack models with different fracture mechanism modes, [33] for structural and material level assessment of alkali aggregate reaction induced models, [34] for sensitivity analysis of creep models, [35] for global sensitivity analysis of gravity dams with structural health monitoring applications, [36] for arch dam-foundation-reservoir coupled system, [37] for steel frames with bolted-angle connections, [38] for steel moment-resisting frames, [39] for highway bridges, [40] for port structures, [41] for tunnel face stability, [42] for reinforced masonry buildings, [43] for unreinforced masonry structures, [44] for gravity quay walls, [45] for base-isolation structures, [46] for double-circuit steel tubular transmission towers, [47] for design of ship-to-shore container crane, [48] for pile-supported wharves and so on. Since the focus of this report will be on reinforced concrete components, these examples are studied in detail in Section 3.

Sensitivity analysis methods can be classified in a variety of ways. Although the review of all these methods is not the objective of this report, a brief review is provided in Section 2, including the main classifications by different researchers. Next, we move to reinforced concrete (RC) components (since they are used as a case study in this report) and we will provide a detailed review of the papers that provided a sensitivity analysis, including the Tornado diagram, see Section 3. The state-of-the-review in this section will help in the verification of the results and justification of (sometimes diverse) results. Section 4 discusses the topics in the sensitivity analysis that are beyond the typical material and modeling variability. For example, this section covers the sensitivity in software used, types of sensitivity analysis techniques, indirect sensitivity analysis methods, etc. Section 5.2 provides a theoretical classification of different sensitivity analysis methods and Tornado diagrams in the context of earthquake engineering.

This report does compare different sensitivity analysis methods (such as those briefly reviewed in Section 2). The objective of this report is to expand the Tornado diagram sensitivity analysis method (also known as the one-at-a-time (OAT) method, nominal range sensitivity method, local sensitivity method, or Threshold method) using assumptions that are beyond the initial epistemic random variables (RVs) by incorporating the particular features of earthquake engineering. It has been shown that the outcome of sensitivity analyses depends on the objective of sensitivity assessment, the subsequent uncertainty quantification (UQ), the choice of the structural analysis technique, the choice of stressor, as well as demand parameters.

2. Classification of Sensitivity Analysis Techniques

This section provides a general overview of different sensitivity analysis techniques classification. Depending on the application, capability, and applied methodology, a variety of (sometimes diverse) classifications have been proposed over the past three decades. Christopher Frey and Patil (2002) [1] classified the sensitivity analysis methods into three groups: mathematical, statistical, and graphical approaches. A summary is also provided in Table 1.

2.1. Mathematical Methods

Mathematical methods refer to those that evaluate the sensitivity of a quantity of interest (QoI) to the variation of an input parameter. In these methods, the QoIs are typically computed for those values that represent the entire range of the input [49]. These methods are not capable of outputting the variance in QoIs due to the variance in the input parameters, and they only can provide the impact of the range of variation in the input parameters on the QoIs [50]. They are indeed a great tool to screen the most sensitive input parameters [51]. Examples of mathematical methods are break-even analysis, nominal range sensitivity analysis, automatic differentiation, and difference in the log-odds ratio [1].

2.1.1. Nominal Range Sensitivity

Nominal Range Sensitivity (NRS) evaluates the effect on model QoI by individually varying only one input parameter across its entire range of plausible values while holding all others at their nominal/base-case values [52, 53]. The difference in the model output, Δy, due to the change in the input parameter, Δx, is known as swing weight:

$$\Delta_i^{\pm} y = g\left(x_i + \Delta^{\pm} x_i, \mathbf{x^0}_{\sim i}\right) - g\left(\mathbf{x^0}\right) \tag{1}$$

where g defines an explicit or implicit function, the subscript i refers to an individual input parameter, and superscript $\mathbf{0}$ refers to the base case with all input parameters in their

Table 1. Summary of some of sensitivity analysis techniques; adapted from [1].

Technique	Applicability	Computational Issues	Representation of Sensitivity
NRS	Deterministic model	Need nominal range for each input; potentially time consuming.	Ratios, percentages. Does not include effect of interactions or correlated inputs. Easy to understand.
DLOR	Deterministic model with output as a probability	Need nominal range for each input; potentially time-consuming.	Ratios, percentages. Does not include effect of interactions or correlated inputs. Easy to understand.
BEA	Models used to choose among alternatives	Complex for model with many decision options and/or more than two inputs, potentially time consuming.	Graphical representation.
ADT	Locally differentiable models	Requires specific software	Local sensitivity measures, such as sensitivity coefficients.
Regression	Results from probabilistic simulation	Must specify functional form, computation time and value of solution depends on specific techniques used.	R2, t-ratios for regression coefficients, standard regression coefficients, and others.
ANOVA	Probabilistic models	Time consuming for a large number of inputs with interactions.	F-value, Tukey test coefficients, and others that are calculated at different stages of ANOVA.
RSM	Deterministic model	Developed using a variety of techniques; some require functional forms, others do not; may require extensive runs to generate a calibration data set.	Graphical, evaluation of functional form, method-dependent measures.
FAST	Probabilistic models	Better with no interactions/higher-order input. Caution against discrete inputs.	Portion of output variance attributable to each input.
MII	Probabilistic model	Complex, no computer code available, time-consuming.	Amount of mutual information about the output provided by each input, also graphs of intermediate stages.
Scatter Plots	Probabilistic model	Easy; time requirement depends on the number of input/outputs.	Graphical, no quantitative sensitivity.

mean/median values. Plus and minus signs indicate an increase or decrease in the parameter, respectively.

The outcome of this technique is most valid for linear systems. For nonlinear systems, this method neglects the interactions among input parameters and can be misleading. There are some recommended options on how to vary the parameters:

- OAT with $\pm$ 1 STD (standard deviation): change one parameter at-a-time by its standard deviation

- OAT with $\pm$ 20%: change one parameter at-a-time by 20% of its mean/base value
- Factorial design [54]: is another OAT method that requires a lot of simulations when dealing with large models. A two-level factorial design (with lower and upper bounds) requires 2^N model runs.
- Sentime-consuming (SC): This method determines the output percentage difference when varying one input parameter from its minimum value to its maximum value [55]:

$$\mathrm{SC} = \frac{y_{max} - y_{min}}{y_{max}} \tag{2}$$

  where y_{min} and y_{max} represent the minimum and maximum output values, respectively, resulting from varying the input over its entire range.
- Importance Factors: This method has been introduced by [56] in three levels. These measures are calculated from data collected after a five-point OAT analysis (model at mean value, ± 2 STD, and ± 4 STD).
  - First importance factor: is determined as parameter uncertainty (defined as two standard deviations of the input) multiplied by parameter sensitivity (defined as the change in output divided by change in input).
  - Second importance factor: It is the positive difference in the maximum output value and the minimum output value.
  - Third importance factor: is estimated utilizing the output sample variance.

2.1.2. Difference in Log-Odds Ratio

The difference in Log-Odds Ratio (DLOR) is a specific application of nominal range sensitivity. The odds ratio of an event is a ratio of the probability of occurrence, $\mathbb{P}(.)$, to the probability of not occurrence, $1-\mathbb{P}(.)$, and can be presented as $\frac{\mathbb{P}(.)}{1-\mathbb{P}(.)}$. Taking the log of this ratio scales the probabilities [57]. Next, the change in QoI is computed as:

$$\mathrm{DLOR} = \log\left[\frac{\mathbb{P}\left(E|\Delta^{\pm}\mathbf{x}\right)}{\mathbb{P}\left(\bar{E}|\Delta^{\pm}\mathbf{x}\right)}\right] - \log\left[\frac{\mathbb{P}\left(E|\mathbf{x}\right)}{\mathbb{P}\left(\bar{E}|\mathbf{x}\right)}\right] \tag{3}$$

where E refers to an event and $\bar{E}$ means not the event; $\mathbf{x}$ are input parameters. Positive DLOR shows that changes in input parameters enhance the probability of the specified event. It is a useful method when the QoI has a probabilistic nature.

2.1.3. Break-Even Analysis

Break-Even Analysis (BEA) is a more conceptual method that tries to evaluate the robustness of a decision to variations in input parameters [58]. The objective is to find values of input parameters that provide the outcome for which a decision-maker would be indifferent among multiple risk management options.

2.1.4. Automatic Differentiation Technique

Automatic Differentiation Technique (ADT) is used to calculate the local sensitivities for large models (i.e., resource-demanding). This technique is based on first-order partial derivatives of QoI with respect to small changes in the input parameters. The normalized local sensitivity coefficients for ith QoI and jth input parameter are:

$$\alpha_{i,j} = \frac{\left(\frac{\Delta y_i}{\Delta x_j}\right)}{\left(\frac{y_i}{x_j}\right)} \tag{4}$$

2.2. Statistical Methods

Statistical methods refer to those simulation-based methods in which the input parameters follow a pre-defined distributional model, and the impact of input parameters' variance is evaluated on the QoI distribution [59]. The interaction among the input parameters can be identified if more than one parameter is varied at a time (i.e., the correlation concept). Uncertainty in inputs can be propagated using one of the Monte Carlo simulation family methods. Examples of statistical methods are regression analysis, analysis of variance, response surface meta-models, mutual information index, and Fourier amplitude sensitivity test.

2.2.1. Relative Deviation

The relative deviation method (RDM) measures the amount of variability in the QoI while varying each input parameter OAT according to its probability density function (PDF). This method simply covers the entire input parameter domain. Next, for each QoIs, the ratio of the PDF's standard deviation to its mean (i.e., coefficient of variation - COV) is calculated and compared to each other.

Relative Deviation Ratio (RDR) is presented based on the ratio of the QoI's COV to the input distribution's COV.

$$\mathrm{RDR} = \frac{\mathrm{COV}_{QoI}}{\mathrm{COV}_{input}} \tag{5}$$

It is similar to the importance index method. The larger the RDR value, the more sensitive the model is to the input parameter.

2.2.2. Analysis of Variance

Analysis of Variance (ANOVA) is a model-independent probabilistic sensitivity analysis technique and is used to determine if there is a statistical association between the QoI and one or more input parameters [60]. As opposed to regression analysis, there is no assumption in ANOVA regarding the functional form of relationships. This is a non-parametric method and the QoI is assumed to be normally distributed.

2.2.3. Importance Index

Importance Index (II) is based on the ratio of the variance of the parameter value, s_X^2, to the variance of the dependent values, s_Y^2:

$$\mathrm{II} = \frac{s_X^2}{s_Y^2} \tag{6}$$

For additive models, the variance of the raw data is used, while for simple multiplicative models, the variance is based on the log-transformed data [55, 61].

2.2.4. First order-second-moment

First-order-second-moment (FOSM) is a general technique that is used in structural reliability analysis [62, 63], uncertainty quantification [64, 65] and sensitivity analysis [66]. Due to its simplicity and efficiency, the FOSM method is a useful tool for sensitivity studies where Monte Carlo Simulation (MCS) is not affordable [67]. FOSM procedure provides a linear approximation of the structural response concerning fluctuations in RVs [68]. Therefore, the applicability of a general form of FOSM is limited, and might not be exact for nonlinear cases.

Therefore, another version of the FOSM method is provided which is formulated in the logarithmic domain of data. This is especially useful for the seismic response of structures because the probabilistic seismic demand models typically take exponential form in the Cartesian coordinate system (and thus, linear form in a logarithmic coordinate system) [69, 70].

The first-order approximations for mean QoI and the associated variance in the logarithmic domain are:

$$\mu_{\ln Y} \approx g\left(\mu_{\ln X_1}, \mu_{\ln X_2}, \ldots, \mu_{\ln X_n}\right) \tag{7}$$

$$\sigma_{\ln Y}^2 \approx \sum_{i=1}^{n}\sum_{j=1}^{n} \left.\frac{\partial g}{\partial \ln x_i}\right|_{\mu_{\ln X}} \left.\frac{\partial g}{\partial \ln x_j}\right|_{\mu_{\ln X}} \rho_{\ln X_i \ln X_j}\sigma_{\ln X_i}\sigma_{\ln X_j} \tag{8}$$

where the function g is the relationship between the logarithm QoI and the logarithms of input RVs, X_i. $\mu_{\ln X}$ is the vector of RV $\ln X_i$ taken at their median values, ρ presents the correlation coefficient, and $\sigma_{\ln X_i}$ is the standard deviations of the RV $\ln X_i$.

The partial derivatives $\frac{\partial g}{\partial \ln x_j}$ can be calculated approximately using a finite difference approach. By selecting one increment of the standard deviation $\sigma_{\ln X_i}$ above and below the mean values $\mu_{\ln X_i}$ of the RVs:

$$\left.\frac{\partial g}{\partial \ln x_i}\right|_{\mu_{\ln X}} \approx \frac{\ln Y^+ - lnY^-}{2\sigma_{\ln X_i}} \tag{9}$$

where $\ln Y^+$ and $\ln Y^-$ are the logarithms of QoIs calculated for the two perturbed values of the RV X_i.

2.2.5. Response Surface Method

Response Surface Method (RSM) is used to build a meta-model in linear and nonlinear form and is capable to identify the curvatures in the QoIs. MCS is typically used to generate multiple realizations for the input parameters to calculate the corresponding QoIs. Usually, a least squares regression method is used to fit the response surface. Having a response surface, the sensitivity of the input parameters can be obtained by statistical analysis.

2.2.6. Fourier Amplitude Sensitivity Test

Fourier Amplitude Sensitivity Test (FAST) is a technique that is used to estimate the expected value and variance of the QoI and the contribution of input parameters to the variance of QoI [71]. The main advantage of the FAST relies on a specific search pattern to select the initial points from the input parameters which is faster than MCS. In a sense, it is similar to Sobol's sensitivity method [72]. In this method, first, a frequency is specified for each input parameter. Then, the values of inputs are converted along the search curve using a transformation function. Finally, the variance of QoI is evaluated using Fourier coefficients which show the contribution of each input parameter. The ratio of the contribution of each input parameter to QoI's variance is called the first-order sensitivity index (which does not account for the interaction terms).

2.2.7. Mutual Information Index

Mutual Information Index (MII) is a technique in which the sensitivity index is calculated based on conditional probabilistic analysis. Comparing the magnitude of this index provides information about the importance of each input parameter on QoI [52]. MII involves calculation of overall, $\mathbb{P}_y$, and conditional, $\mathbb{P}_{y|x}$, confidence measures. The overall confidence is measured from the CDF of QoI. The conditional confidence is measured by keeping an input parameter constant and varying all others and then using its CDF. The natural sensitivity index is computed as:

$$\alpha_{xy} = \frac{I_{xy}}{I_{yy}} \tag{10}$$

$$I_{xy} = \sum_x \sum_y \mathbb{P}_x \mathbb{P}_{y|x} \log_n \left(\frac{\mathbb{P}_{y|x}}{\mathbb{P}_y} \right) \tag{11}$$

$$I_{yy} = \sum_y \mathbb{P}_y \log_n \left(\frac{1}{\mathbb{P}_y} \right) \tag{12}$$

where $n = 2$ indicates (for example) binary QoI. If I_{xy} is large, then x provides a great deal of information about y. On the other hand, if x and y are statistically independent, then I_{xy} is zero.

2.2.8. Pearson's r Method

Pearson's product moment correlation coefficient provides a quantitative estimate of the linear correlation between the input parameters and QoIs. This method is applied to the data obtained from Monte Carlo simulation and shows the contribution of each input parameter to prediction uncertainty [73].

$$r_{x_i,y} = \frac{\sum_{j=1}^{n}\left(x_{i,j} - \bar{x}_i\right)\left(y_j - \bar{y}\right)}{\left[\sum_{j=1}^{n}\left(x_{i,j} - \bar{x}_i{}^2 \sum_{j=1}^{n}\left(y_j - \bar{y}^2\right)\right)\right]^{1/2}} \tag{13}$$

where x_i and y are one of the input parameters and the QoI.

A higher value for absolute r presents a stronger degree of linear relationship. The major drawback lies in the assumption of a linear relationship between input/output data, and any potential strong correlation between any pairs of two input parameters.

2.2.9. Spearman's ρ Method

For the monotonic input/output pairs, the rank transformations (i.e. replacing the values with their ranks) of the input and output values will have a linear relationship. In this method, the rank correlation coefficient is indicative of the degree of monotonicity between the input/output pair. Spearman's rank correlation coefficient is obtained in the same way as Equation 13 by operating on the rank transformed data [74].

2.2.10. Partial Correlation Coefficient

The Partial Correlation Coefficient (PCC) technique is used when there exists a strong correlation among different input parameters which may affect the input/output correlations. PCC accounts for the correlation between input and QoI excluding the effects of other input parameters. For a system with two input parameters of x_1 and x_2 and the QoI of y, the PCC is a metric of the correlation between x_1 and y, while eliminating indirect correlations due to potential relationships that may exist between x_1 and x_2 as well as x_2 and y in the form of [73]:

$$r_{(x_1,y)|x_2} = \frac{r_{x_1,y} - r_{x_1,x_2} . r_{x_2,y}}{\left[\left(1 - r_{x_1,x_2}^2\right)\left(1 - r_{x_2,y}^2\right)\right]^{1/2}} \tag{14}$$

2.2.11. Partial Rank Correlation Coefficient

The Partial Rank Correlation Coefficient (PRCC) method is an extension of the PCC using the rank transformation technique as a test of monotonicity between input parameters and QoI while accounting for relationships between input parameters [75, 76].

2.2.12. Regression Analysis

Regression analysis can be used for probabilistic sensitivity analysis [77]. In this method (which is most suitable for independent parameters), the impact of input parameters on the QoI is investigated using the regression coefficients [78]. Usually, a relationship should be first fitted between input parameters and the QoI. In the linear form, it is:

$$y_i = \beta_0 + \sum_{j=1}^{m} \beta_j x_{j,i} + \varepsilon_i \tag{15}$$

where y_i is the QoI for ith realization, and $x_{j,i}$ is the ith data point of jth input parameter, β_j are regression coefficients, and ε is the error term. The regression coefficients can be used as a metric for sensitivity analysis.

2.3. Segmented Input Distributions Sensitivity Methods

In the segmented input distributions sensitivity method, the input parameters are divided or segmented into two or more empirical distributions based on the results of QoI distribution partitioning [76]. Typically, the median value of the QoI distribution is chosen as the dividing point. Therefore, the input parameters are divided into group 1 (those parameters that generate QoI less than the median) and group 2 (those parameters that generate QoI more than the median). Next, a series of tests are conducted to compare the characteristics (e.g., means, medians, and variances) of these segmented input distributions. These statistical quantities are compared to determine whether the samples originated from the same population [61]. If the segmented input distributions are statistically identical, the QoI is not sensitive to that parameter. If not, the QoI is sensitive to that input parameter, and the T value (discussed below) from the test statistic can be used to perform the sensitivity ranking among various input parameters.

Since there is not enough knowledge of the segmented input random samples and their distributions, non-parametric statistical tests (distribution-free models) need to be used. In the following, four non-parametric statistical tests are discussed. The first two (i.e., Smirnov and Cramer-von Mises) compare the empirical distributions with a null hypothesis of the distributions originating from the same population. The last two (i.e., Mann-Whitney and Squared-Ranks) compare means and variances, respectively, of the empirical distributions. Tied values are also assumed not to exist.

2.3.1. Smirnov Test

The Smirnov Test (ST) is based on the comparison of two empirical cumulative distribution functions, $\mathrm{eCDF}_1(x)$ and $\mathrm{eCDF}_2(x)$, resulted from input parameter segmentation. The degree of similarity between two CDFs indicates the degree of sensitivity of QoI to that parameter. The test statistic is computed as:

$$T_{\mathrm{smf}} = \max \left| e\mathrm{CDF}_2(x) - e\mathrm{CDF}_1(x) \right| \tag{16}$$

2.3.2. Cramer-von Mises Test

The Cramer-von Mises Test (CVMT) follows an approach similar to the Smirnov test; however, it uses slightly different test statistics as follows:

$$T_{\mathrm{cvm}} = \frac{n_1 n_2}{(n_1 + n_2)^2} \sum \left[e\mathrm{CDF}_2(x) - e\mathrm{CDF}_1(x)\right]^2 \tag{17}$$

where n_1 and n_2 are the numbers of samples utilized to estimate the distributions.

For both T_{smf} and T_{cvm}, a larger value corresponds to a larger difference between two segmented parts and indicates a higher correlation between the independent and dependent variables.

2.3.3. Mann-Whitney Test

The Mann-Whitney Test (MWT) is used to compare the means of two independent samples. Two CDFs (e.g., $X1$ and $X2$) are ordered as a single sample, and ranks are assigned to each element based on this ordering (assuming there is no tie). The test statistic is computed as:

$$T_{\mathrm{mwh}} = \sum_{i=1}^{n} \mathrm{Rank}(X1_i) \tag{18}$$

Theoretically, if T_{mwh} of the single sample becomes either very small or very large compared to the other, those two sample means are different. Since this test is two-tailed (i.e., the mean of $X1$ could be larger or smaller than the mean of $X2$), the sensitivity ranks are based on a normalized value of T_{mwh} [61]. The smaller values of T_{mwh} indicate the more sensitive parameters because the means of the distributions show a greater difference based on the partitioning of input data.

2.3.4. Squared-Ranks

In Squared-Ranks Test (SRT), the variances of two independent samples (let's say $X1$ and $X2$) are compared. As opposed to the Mann-Whitney test, the ranks are not based on the raw data, but based on the absolute difference between the random sample (e.g., $X1_i$) and the sample mean (e.g., μ_{X1}). The test statistic is computed as:

$$T_{\mathrm{sqr}} = \sum_{i=1}^{n} \left[\mathrm{Rank}(U1_i)\right]^2 \; ; \quad U1_i = |X1_i - \mu_{X1}| \tag{19}$$

2.4. Graphical Methods

Graphical methods refer to those methods that present the sensitivity analysis results in the form of graphs and charts. They provide a visual indication of how an QoI is impacted by variation in input parameters [79]. For example, a scatter plot can be used to visualize the impact of individual input parameters on an QoI [80].

2.5. Other Methods

Borgonovo and Plischke (2016) [81] classified the sensitivity analysis into local and global methods.

- Local sensitivity analysis techniques: If the assessment is performed around a point of interest in the model input parameters space, then the results are valid as a local sensitivity model. Examples include Tornado diagrams, one-way sensitivity functions, differentiation-based methods, and scenario decomposition through finite change sensitivity indices.
- Global sensitivity analysis techniques: Examples include: screening methods (e.g., sequential bifurcation and the Morris), variance-based, moment-independent, and value of information-based sensitivity methods.

Many other classifications and methods exist, some of which can be found in [82–86]. These methods are mainly based on the correlation of input parameters and the QoI either directly or in the form of surrogate-based global sensitivity models. These techniques are not discussed or used in this report.

3. Sensitivity to Material and Modeling Variability

This section provides an in-depth review of several recent sensitivity analyses and Tornado diagrams on seismic performance evaluations of RC frames.

3.1. Porter et al. (2002)

Porter et al. (2002) [3, 87] investigated the sources of uncertainties that have the largest impact on the repair costs of a seven-story hotel building with a perimeter moment frame lateral force-resisting system that included non-ductile detailing typical of 1960s construction. They used a deterministic sensitivity analysis with Tornado diagram to present the importance of each RV, Figure 1. The basic RVs are:

- Ground motion intensity, (S_a)
- Details of ground motion (GM)
- Building mass (m)
- Viscous damping (ξ)
- Parameters of the force-deformation relationship for the structural elements ($F-d$)
- Capacity of building assemblies to resist damage (ASS_{cap})
- Contractor unit costs ($Unit_{\$}$)
- Contractor overhead and profit ($O\&P$)

Since the Tornado diagram requires three values for each RV, they chose to use the 10th, 50th, and 90th percentiles for ground motion intensity. For a normal distribution, with COV of 0.1, the 10th and 90th percentiles correspond to 0.872 X_n, and 1.128 X_n, respectively, where X_n refers to the nominal value of X. They reported that ASS_{cap} and ground motion intensity and details are the most sensitive variables.

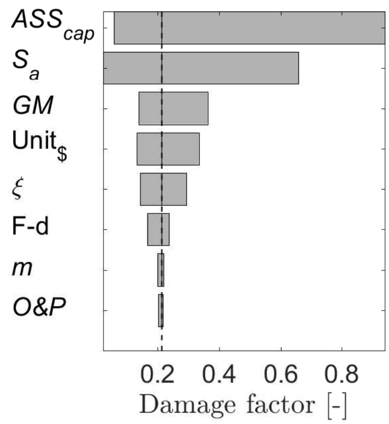

Fig. 1. Results of sensitivity analysis; modified from Porter et al. (2002) [3]

3.2. Mosalam et al. (2005-2009)

Lee and Mosalam (2005) [67] performed a seismic demand sensitivity analysis on seven-story reinforced concrete shear walls using first-order second moment (FOSM) method and classical method. A 2D model was prepared in OpenSees based on fiber flexibility formulation for beam-column elements. Shear-wall members were modeled using beam-column elements aligned with the centerline of the shear wall. A flexible SSI at the foundation level is modeled using spring-type elements in the vertical direction. They considered the following RVs:

- Ground motion intensity measure (S_a)
- Ground motion profile (GM)
- Mass (M_s)
- Viscous damping (D_p)
- Strength ($Streng$) through concrete compressive strength, and yield stress of the reinforcement
- Stiffness ($Stiff$) through initial tangent stiffness of concrete and Young's modulus of the reinforcement

They developed Tornado diagrams in two ways: 1) classical method using the 10th and 90th percentiles of the RVs, 2) FOSM-based method in which the engineering demand parameters (EDPs) are assumed to have lognormal distributions with estimated means and STDs from the FOSM results, and the 10th and 90th percentiles of these EDPs are estimated. It is noteworthy that only the GM parameter is randomly selected (using MCS) because of its nature. Figures 2(a), 2(b) and 2(c) show a reasonable match between two methods. Three

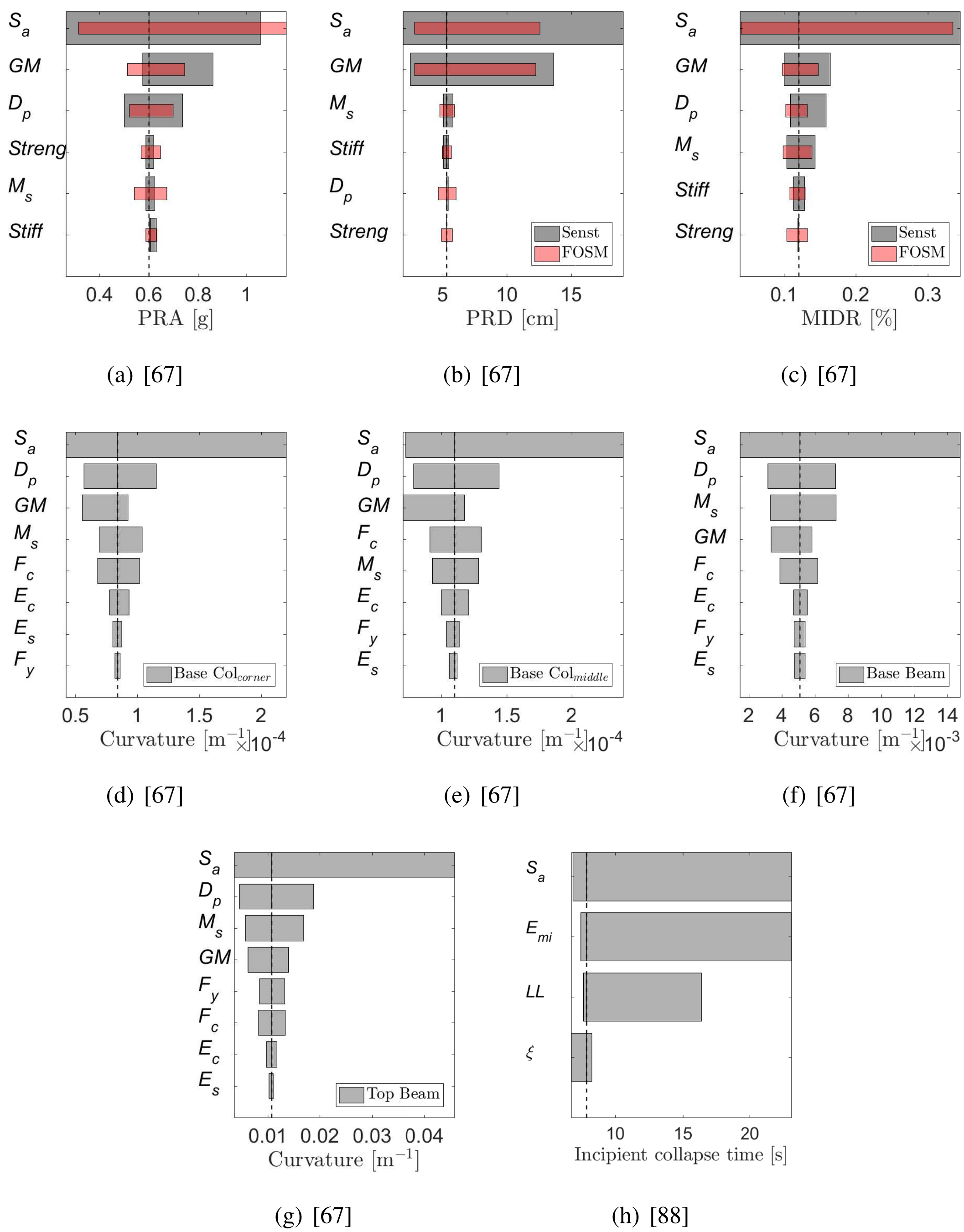

(a) [67] (b) [67] (c) [67]

(d) [67] (e) [67] (f) [67]

(g) [67] (h) [88]

Fig. 2. Results of sensitivity analysis; modified from Mosalam et al. (2005-2009) – Part 1

global EDP are used: peak absolute roof acceleration (PRA), peak absolute roof displacement (PRD), and maximum inter-story drift ratio (MIDR). Tornado diagrams showed that the intensity measure (IM) parameters and ground motion profile are the dominant sources of uncertainty for all global EDPs. It is important to note the edges of each swing from the classical method and FOSM are not necessarily matching unless the relationship between the EDP and RV is monotonic. They also investigated the sensitivity of local EDPs (i.e., the curvature at the critical point) and reported that after the IM parameter, viscous damping is the second significant source of uncertainty. However, depending on the beam or column and their location in the structure, the sensitivity of material parameters is different, See Figures 2(d) to 2(g).

Talaat and Mosalam (2009) [88] studied the element removal algorithms in dynamic analysis of an RC column member and unreinforced masonry (URM) infill wall. Modeling uncertainty was investigated as part of this research in the context of the deterministic sensitivity assessment of URM. Four parameters are used:

- Seismic hazard level (S_a) with higher and lower hazard levels of 1%/50yr and 3%/50yr
- Wall stiffness (E_{mi}) with deterministic strain, and uncertain strength f_{m0} (with lognormal distribution and the bounds with 0.997 confidence interval)
- Live load (LL) with maximum and minimum gravity loads correspond to full and no occupancy
- Damping (ξ) with min and max of 2% and 10%

They used the incipient collapse time as a sensitivity metric, and found out it is more sensitive to spectral acceleration and less to damping ratio, Figure 2(h). Therefore, their Tornado diagram is based on failure time and includes a global metric. Moreover, this Tornado diagram does not have equal/balanced wings and the right side is much bigger than the left one.

Binici and Masalam (2007) [89] provided a comparative sensitivity study showing the impact of fiber-reinforced polymer (FRP) on the ranking of various parameters in RC columns. A fiber-discretized frame element was used to simulate the compression zone of the FRP-confined region through the use of a bond model. The retrofitted plastic hinge element employs a distributed plasticity model with displacement-based frame elements. A circular RC cantilever column was modeled using five integration points (geometric nonlinearity is also included). The lap splices were modeled using an effective steel strain concept. The following RVs were considered for sensitivity analysis:

- Concrete compressive strength (f_c); COV = 0.1
- Concrete tensile strength (f_t); COV = 0.2
- Steel yield stress (f_y); COV = 0.05
- Concrete cover (c); COV = 0.2
- Concrete softening parameter (s); COV = 0.1
- Concrete tensile fracture energy, (G_{ft}); COV = 0.2
- Concrete compressive fracture energy (G_{fc}); COV = 0.2
- Concrete dilatation strain (ε_{dl}); COV = 0.1
- FRP modulus of elasticity (E_f); COV = 0.15
- FRP rupture strain (ε_{rup}); COV = 0.15

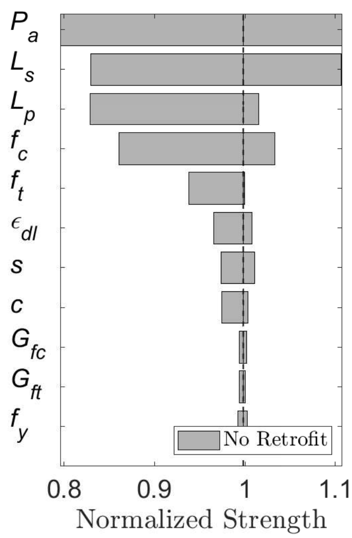

(a) [89]

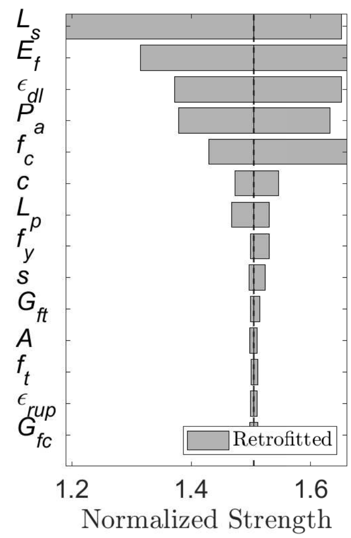

(b) [89]

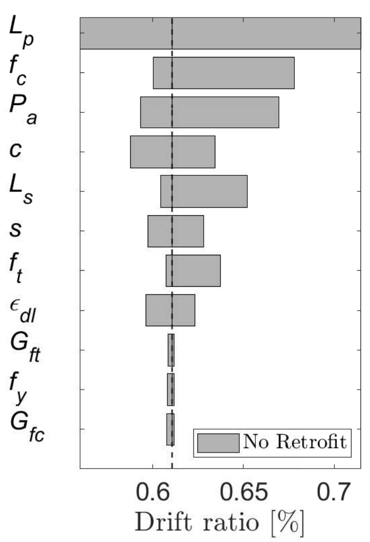

(c) [89]

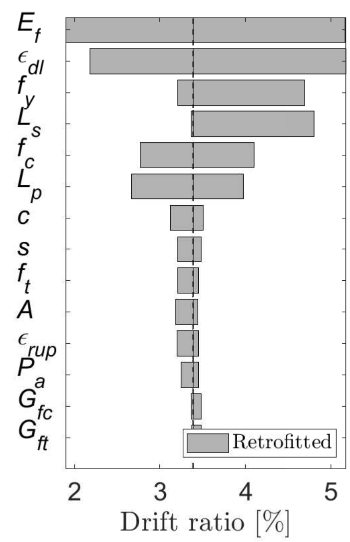

(d) [89]

Fig. 3. Results of sensitivity analysis; modified from Mosalam et al. (2005-2009) – Part 2

- Plastic hinge length (L_p); COV = 0.2; Note: Characteristic length $l_c = L_p \times$ weight of the integration point
- Splice length (L_s); COV = 0.15
- Bond stress parameter (A); COV = 0.33

- Applied axial load (P_a); COV = 0.25

Two QoIs were considered, i.e., strength and ultimate drift ratio, and computed by a simple pushover analysis (no seismic analysis). Figures 3(a) to 3(d) compare the Tornado diagrams for original and retrofitted columns. It is found that, for the existing column, parameters such as L_p, f_c and L_s are important sources of uncertainty. While for the retrofitted column, parameters such as E_f, ε_{dl} and f_y are more important RVs. For the un-retrofitted column, the axial load is also an important variable. Both fracture energy terms are at the bottom of the list.

3.3. Dolšek et al. (2009-2013)

Dolšek (2009) [90] investigated the sensitivity of a four-story RC frame with a series of modeling and RTR uncertainties. 12 RVs are considered:

- Mass of the 1st, 2nd, 3rd and 4th floors (m_1, m_2, m_3, m_4)
- Concrete strength (f_c)
- Steel strength (f_y)
- Effective slab width (b_{eff})
- Damping (ξ)
- Initial stiffness of the columns ($\Theta_{y,c}$)
- Initial stiffness of the beams ($\Theta_{y,b}$)
- Ultimate rotation of the columns ($\Theta_{u,c}$)
- Ultimate rotation of the beams ($\Theta_{u,b}$)

A total of 14 ground motion records were used to analyze the system. Combining modeling and RTR variability, they performed a series of extended incremental dynamic analysis (IDA). Figure 4(a) presents the sensitivity of peak ground acceleration, which corresponds to the collapse point, PGA_C, to the RVs. The sensitivity is measured in terms of a median Spearman rank correlation coefficient, ρ_{PGA}. The median value is calculated based on the individual response of each ground motion record. The damping, ultimate and yield rotation in the columns have the greatest influence on the PGA_C. According to this figure, some RVs are positively, and some are negatively correlated with PGA_C. The masses have a minor influence; however, their impact might be positive or negative (swing effect). In general, for a particular RV, a positive (or negative) median implies that all the individual ground motion records lead to positive (or negative) correlation too (except for masses in which for a positive median we might have individual negative correlation too).

Celarec and Dolšek (2013) [91] investigated the sensitivity of two three-story asymmetric old and contemporary RC frames, and a four-story contemporary RC frame with plan symmetry. Lumped plasticity models were used for modeling with inelastic rotational hinges at their ends and a tri-linear moment-rotation relationship. OpenSees software was used for simulation. The following 8 RVs were considered:

- Concrete strength (f_c); COV = 0.2

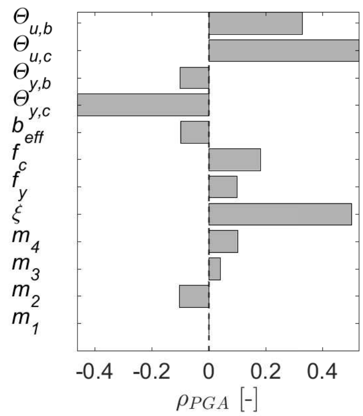

(a) [90]

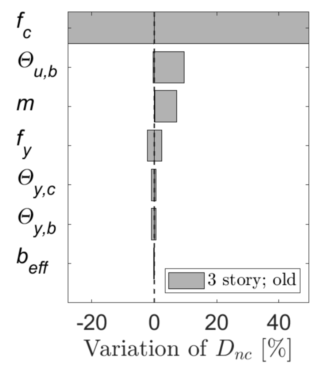

(b) 3-old; [91]

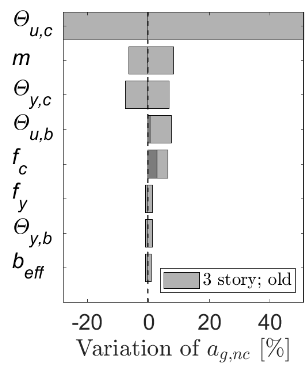

(c) 3-old; [91]

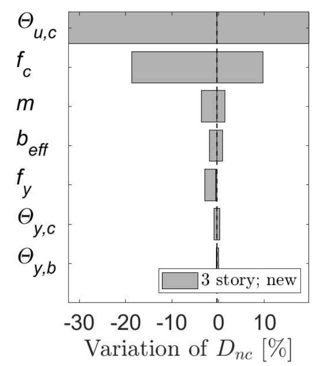

(d) 3-new; [91]

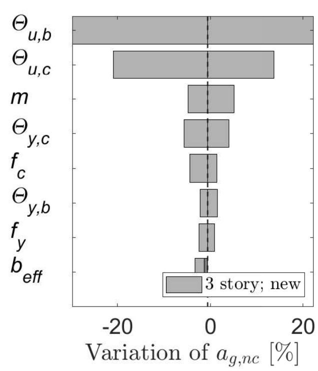

(e) 3-new; [91]

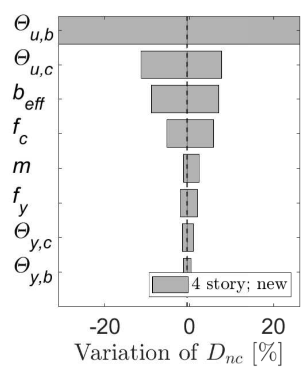

(f) 4-new; [91]

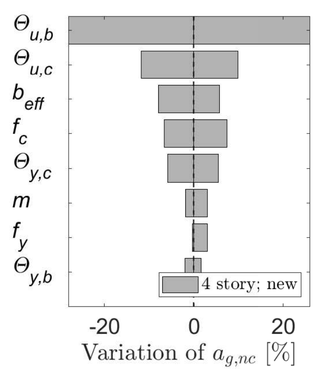

(g) 4-new; [91]

Fig. 4. Results of sensitivity analysis; modified from Dolsek et al. (2009-2013)

- Steel strength (f_y); COV = 0.05
- Effective slab width (b_{eff}); COV = 0.2

- Mass (m); COV = 0.1
- Yield rotation of the columns ($\Theta_{y,c}$); COV = 0.36
- Yield rotation of the beams ($\Theta_{y,b}$); COV = 0.36
- Ultimate rotation of the columns ($\Theta_{u,c}$); ; COV = 0.4
- Ultimate rotation of the beams ($\Theta_{u,b}$); COV = 0.6

They chose to use the 16th and 84th fractiles of each RV as the lower and upper bound in Tornado-based sensitivity analysis, and the median value as reference one. Two QoIs were used, i.e., near-collapse displacement (D_{nc}) and peak acceleration at near-collapse state ($a_{g,nc}$). The N2 method [92] was used for the seismic performance evaluation. This method is a pushover analysis that applies a monotonically increasing lateral force to the frame. Tornado diagrams are presented in Figures 4(b) to 4(g) for three frames. The results of sensitivity analysis show the greater impact of those RVs, which affect the collapse mechanism and have higher COV. It is notable that for contemporary frames, the sensitivity of QoIs to $\Theta_{u,b}$ is higher, while for order one, the $\Theta_{u,c}$ is the most sensitive RV.

3.4. Bracchi et al. (2015)

Bracchi et al. (2015) [93] performed a series of sensitivity analyses on masonry buildings by means of nonlinear static analyses. Eight different configurations of structures were used with the following six modeling variables:

- Clear height of piers (H_{pier}) with three options
- Percentage of cracked stiffness vs. initial stiffness (Crc_{stiff}) with three ratios of 50%, 75% and 100% of reduced E and G
- Spandrel length ($Spandrel$) for both beams and columns
- Percentage of load distributions from floors ($Ldist_f$)
- Vertical load distribution on piers ($Ldist_p$)
- Connections of orthogonal walls ($Wall_{ortg}$) with two options of fully coupled and uncoupled

In addition, four responses are used as a metric in the Tornado diagram (i.e., stiffness, ultimate displacement, yielding acceleration, and acceleration). Results are presented in Figures 5(a) to 5(d). The sensitivity is expressed by the quantity $\frac{1}{p-value}$ in both X and Y directions. One may note that $p-value$ ranges from 0.0 to 1.0 (where 0.0 means the hypothesis can be rejected and 1.0 it cannot). Therefore, a higher value of $\frac{1}{p-value}$ means a higher influence of the corresponding modeling uncertainty on the control parameter. Overall, cracked stiffness and orthogonal walls are the two most influencing parameters. However, depending on the control parameter and direction of the frame, the important parameter varies.

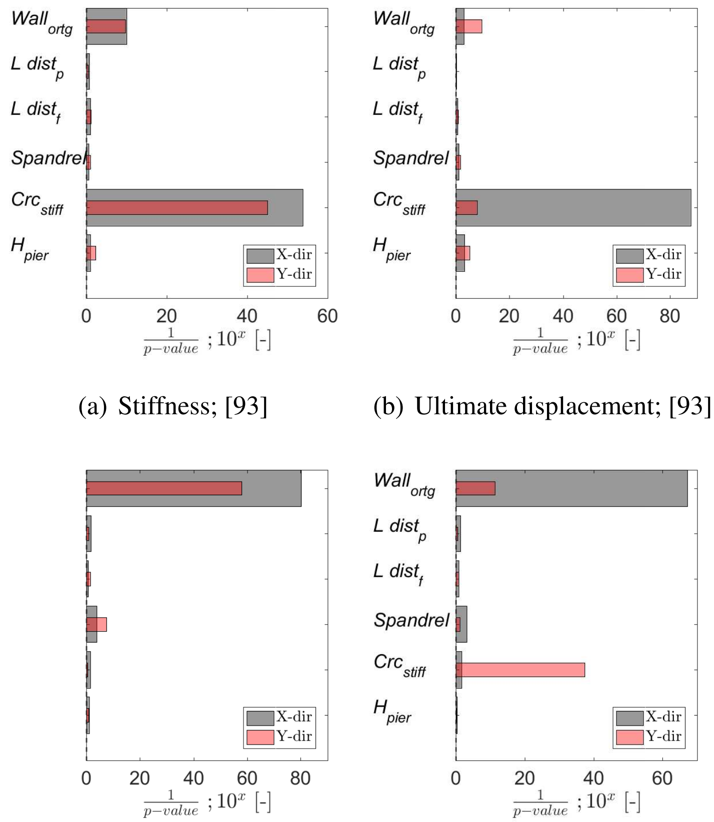

(a) Stiffness; [93] (b) Ultimate displacement; [93]

(c) Yielding acceleration; [93] (d) Acceleration; [93]

Fig. 5. Results of sensitivity analysis; modified from Bracchi et al. (2015)

3.5. Celik and Ellingwood (2010)

Celik and Ellingwood (2010) [94] studied fragility analysis of non-ductile RC frames designed for gravity loads. Various material and modeling uncertainties were considered:

- Concrete compressive strength (f_c)
- Steel yield strength (f_y)
- Structural (viscous) damping (ξ)
- Beam–column joint model parameters:
  - Bond-slip factor (α)
  - (Normalized) joint shear strength ($(\bar{\tau}_{jh})_{max}$)
  - Various joint shear strains, $(\gamma_j)_{cr}$, $(\gamma_j)_y$, $(\gamma_j)_{max}$, $(\gamma_j)_{res}$

They provided sensitivity analysis and tornado diagrams for frames with different heights and different seismic intensity levels. In all cases, damping ratio and concrete compressive strength are the most sensitive RVs. The generated Tornado diagrams are in three seismic hazard levels. Except for the first two highly sensitive RVs, the shape and the order of

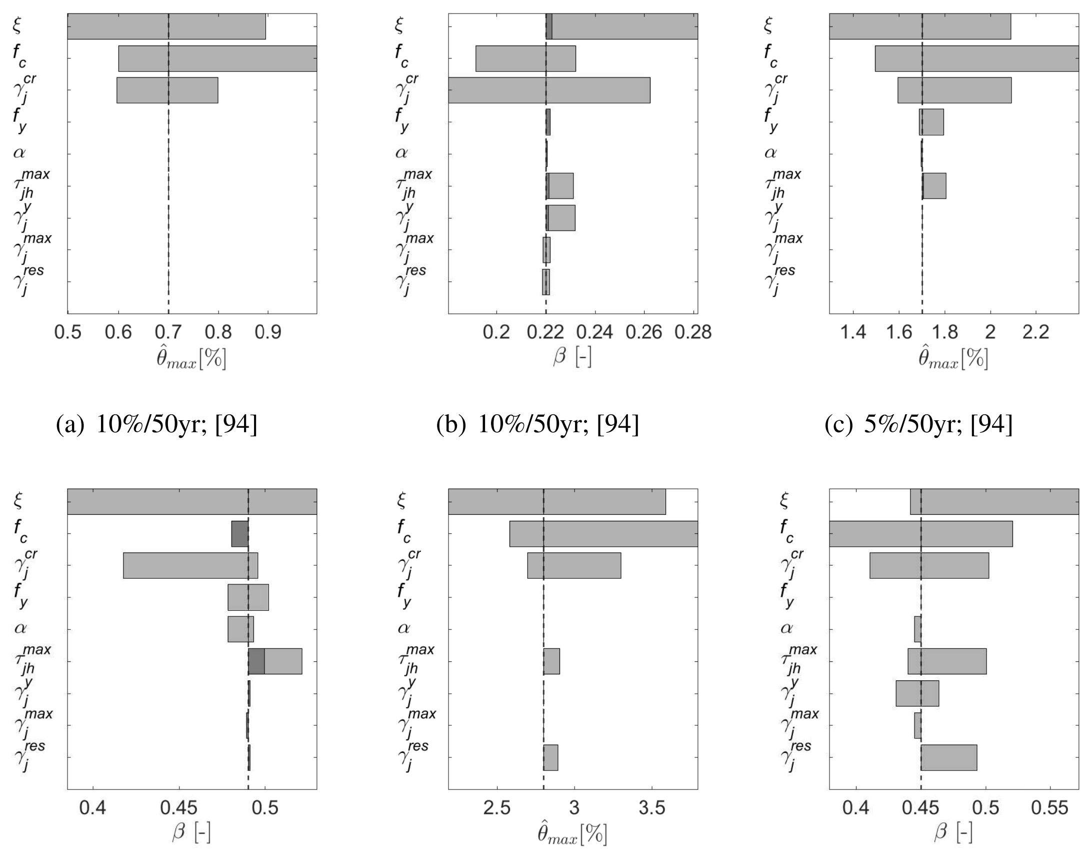

(a) 10%/50yr; [94]
(b) 10%/50yr; [94]
(c) 5%/50yr; [94]
(d) 5%/50yr; [94]
(e) 2%/50yr; [94]
(f) 2%/50yr; [94]

Fig. 6. Results of sensitivity analysis; modified from Ellingwood et al. (2010)

the Tornado diagram changes depending on hazard level. Moreover, the provided Tornado diagrams are for median, $\bar{theta}_{max}$, and logarithmic standard deviation, β, of the fitted lognormal distribution in that hazard level. Figures 6(a) to 6(f) present the results only for the three-story frame, while the original paper includes six- and nine-story frames too. To combine the ground motion records from Cloud analysis with model uncertainty, they used the simplified method with a random combination.

3.6. Li et al. (2020)

Li et al. (2020) [95] investigated the sensitivity and uncertainty in aging RC bridges with 22 modeling parameters. Using the sensitivity analysis, 10 critical parameters were identified. They reported that the uncertainty in modeling parameters may lead to the difference in the trajectory of seismic hysteretic response. The following RVs are considered:

- Concrete weight (λ_w)

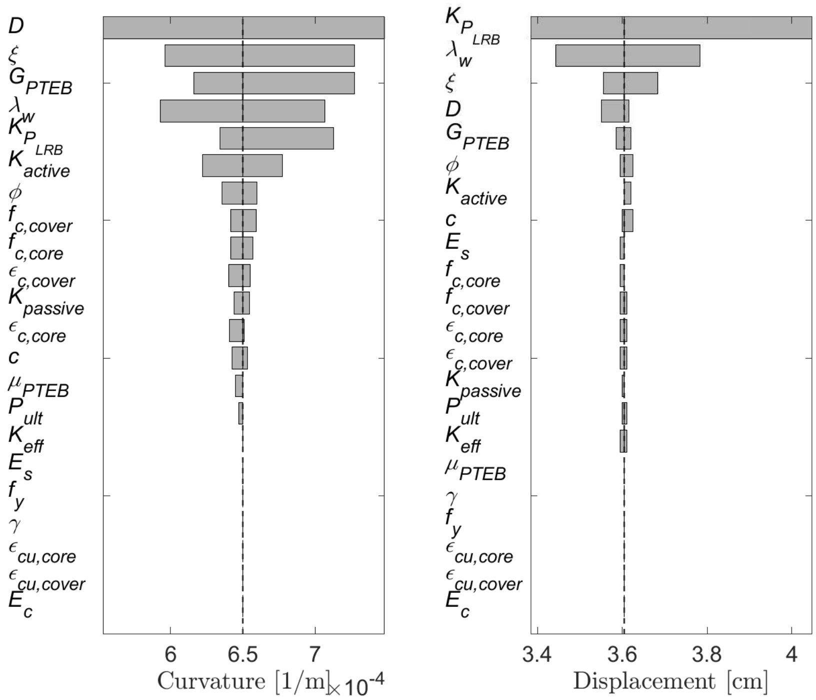

(a) E1; [95]

(b) E1; [95]

Fig. 7. Results of sensitivity analysis: part I; modified from Li et al. (2020)

- Pier diameter (D)
- Concrete cover thickness (c)
- Longitudinal reinforcement diameter (ϕ)
- Damping ratio (ξ)
- Young's modulus of concrete (E_c)
- Peak strength of cover concrete ($f_{c,cover}$)
- Peak strain of cover concrete ($\varepsilon_{c,cover}$)
- Ultimate strain of cover concrete ($\varepsilon_{cu,cover}$)
- Peak strength of core concrete ($f_{c,core}$)
- Peak strain of core concrete ($\varepsilon_{c,core}$)
- Ultimate strain of core concrete ($\varepsilon_{cu,core}$)
- Young's modulus of steel rebar (E_s)
- Yield strength of steel rebar (f_y)
- Post-yield to initial stiffness ratio (γ)
- Friction coefficient of PTEB (μ_{PTEB})
- Shear modulus of PTEB (G_{PTEB})

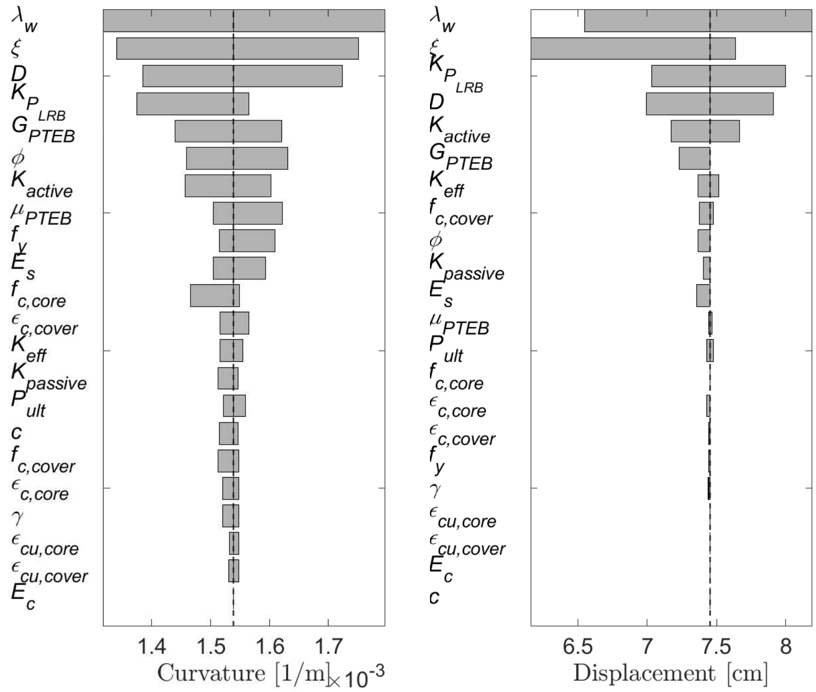

(a) E2; [95] (b) E2; [95]

Fig. 8. Results of sensitivity analysis: part II; modified from Li et al. (2020)

- Post-yield stiffness of LRB (K_{P-LRB})
- Abutment ultimate capacity (P_{ult})
- Abutment passive stiffness ($K_{passive}$)
- Abutment active stiffness (K_{active})
- Pounding effective stiffness (K_{eff})

They conducted the sensitivity analyses under two ground motion levels: E1 and E2 correspond to the earthquake with a return period of 475 and 2500 years, respectively. For each level, they used 22 pairs (44 components) of records which are scaled to first-mode spectral acceleration. They followed the concept of traditional sensitivity analysis; however, they performed the procedure for all 44 records and took the median of EDP at the end to be used in Tornado diagram. Overall, five EDPs were investigated: (1) curvature of the column, (2) relative displacement of LRB, (3) relative displacement of PTEB, (4) abutment deformation, and (5) abutment deformation.

Subsequently, they developed 10 Tornado diagrams (5 EDPs and 2 seismic levels), in which four of which are shown in Figures 7(a) to 8(b) based on curvature and LRB relative displacement under two seismic levels. The five most critical RVs are concrete weight, pier diameter, longitudinal reinforcement diameter, damping ratio, and peak stress of cover concrete.

3.7. Stocchi et al. (2019)

Stocchi et al. (2019) [4] investigated the sensitivity of EDP with respect to structural modeling and its typology. Two benchmark models were used: BANDIT (different frames modeling) and SMART2013 (different wall modeling). For each one, different realizations of structural models including low-, medium-, and high-complexity numerical models have been developed. Uncertainty in structural models originates from five RVs: concrete modulus of elasticity, fracture energy, tensile strength, steel yield stress, and damping ratio. Results were compared for six EDPs:

- MIDR [%]: maximum interstory drift ratio
- EFDO [%]: eigenfrequency drop off is linked with the stiffness of a structure, and can be interpreted as a structural damage index
- DUCT [−]: Ductility index is defined as the ratio between the maximum displacement over the last value of the displacement for which the structure remains elastic.
- DER [−]: Hysteretic energy over total input energy is defined as the ratio between the hysteretic energy over the total input energy.
- ZPA [m/s^2]: Zero-period acceleration is defined as the pseudo-acceleration estimated either when the period is null or when the frequency tends to infinity.
- AMPR [−]: Amplification ratio is defined as the ratio between the maximum pseudo-acceleration over the ZPA.

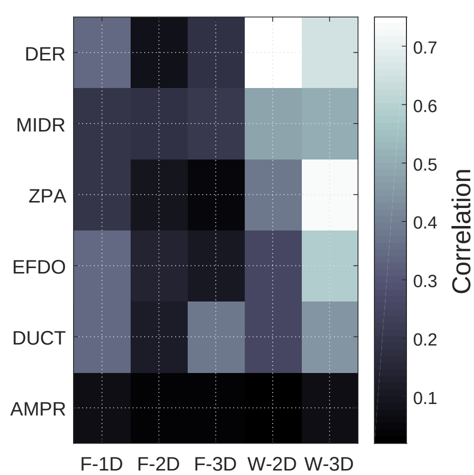

Fig. 9. Results of sensitivity analysis; modified from Stocchi et al. (2019) [4]

They reported the sensitivity of the EDPs in different modeling techniques, and presented the results in terms of correlation, Figure 9. According to the results, ZPA is one of the most sensitive EDPs, while AMPR is the least sensitive index.

3.8. Barbato et al. (2010)

Barbato et al. (2010) [96] performed sensitivity analyses using both the FOSM algorithm (with direct differentiation method – DDM) and traditional min/max methods. In the FOSM-DDM, they considered three different "relative index" (RI) rankings to develop the Tornado diagrams:

- RI-1: RI ranking based on sensitivities normalized in the deterministic sense, i.e., multiplied by the nominal/mean value of the sensitivity parameter and divided by the mean of the response quantity.
- RI-2: RI ranking based on sensitivities normalized in the probabilistic sense, i.e., multiplied by the STD of the sensitivity parameter and divided by the mean of the response quantity.
- RI-3: RI ranking based on the relative marginal contributions of the random material parameters to the total variance of the response.

Likewise, for the traditional method, the lower and upper bounds are defined as follows:

- Minimum and maximum values when the probability distribution is defined over a finite interval (uniform or beta distributions)
- 10% and 90% fractiles when the probability distribution is defined over an infinite (e.g., normal) or semi-infinite (e.g., lognormal or exponential distributions).

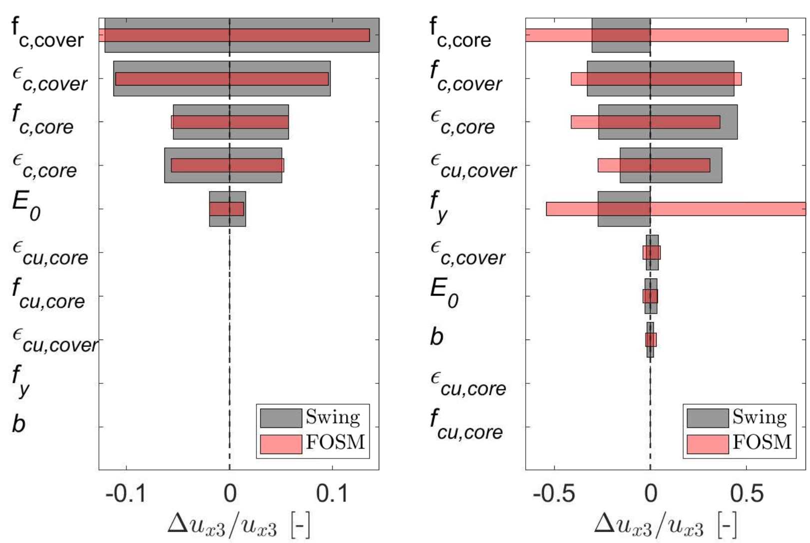

(a) P_{tot}=300 kN; [96] (b) P_{tot}=600 kN; [96]

Fig. 10. Results of sensitivity analysis; modified from Barbato et al. (2010)

All the simulations were performed on a three-story RC building including soil-structure-foundation interaction and pushover analysis. The following modeling and material parameters were considered:

- Confined concrete peak strength ($f_{c,core}$)
- Confined concrete strain at peak strength ($\varepsilon_{c,core}$)
- Confined concrete residual strength ($f_{cu,core}$)
- Confined concrete strain at which the residual strength is reached ($\varepsilon_{cu,core}$)
- Unconfined concrete peak strength ($f_{c,cover}$)
- Unconfined concrete strain at peak strength ($\varepsilon_{c,cover}$)
- Unconfined concrete strain at which the residual strength is reached ($\varepsilon_{cu,cover}$)
- Steel Initial stiffness (E_0)
- Steel Yield strength (f_y)
- Steel Post-yield to initial stiffness ratio (b)

Several Tornado diagrams have been developed under variable axial loads. Figures 10(a) and 10(b) present two samples for the P_{tot} of 300 kN and 600 kN, respectively. The RI is expressed as the relative change in the horizontal roof emplacement, u_{x3} corresponding to the parameters' lower and upper bounds using the two above-discussed methods. They found out that the FOSM-DDM estimates the classical method with good accuracy for the low-to-moderate level of inelastic behavior. However, for the highly inelastic range, there is a considerable discrepancy between them.

3.9. Ma et al. (2019)

Ma et al. (2019) [97] studied several material and modeling variables in an RC bridge pier with OpenSees. They considered the following main RVs (note that all RVs are bounded):

- Damping ratio (ξ); COV = 0.3
- Volume mass (m); COV = 0.1
- Pier diameter (D); COV = 0.05
- Longitudinal reinforcement diameter (d); COV = 0.05
- Concrete cover thickness (c); COV = 0.05
- Concrete compressive strength (f_c); COV = 0.2
- Steel yield strength (f_y); COV = 0.1

For each RV, the lower and upper bound is based on the applied COV (shown above) on the mean values. They applied the cloud analysis technique for sensitivity assessment, along with Morris one-at-a-time method. The presented Tornado diagrams are based on both mean and STD of drift predictions. Three different site conditions were considered (I: V_{S30} $>$ 510 m/s; II: 260 m/s $< V_{S30} <$ 510 m/s; III: 150 m/s $< V_{S30} <$ 260 m/s), as well as two ground motion types, i.e., near-fault and far-field. For sites I and III, 15 records have been used, while for site II a total of 35 records were chosen. They also considered two seismic design levels (by adjusting the PGA values): frequent earthquake (475 years return period) - E1 - and rare earthquake (2500 years return period) - E2. Therefore, a total of 24 Tornado

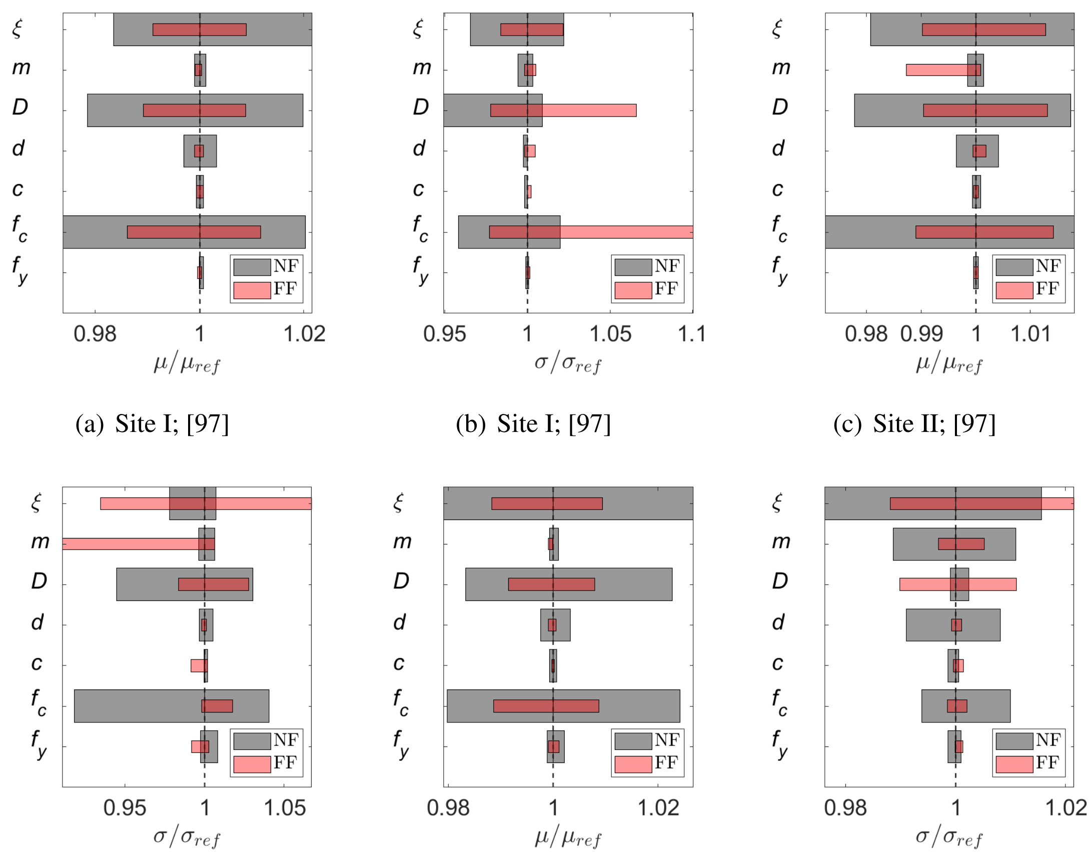

(a) Site I; [97] (b) Site I; [97] (c) Site II; [97]

(d) Site II; [97] (e) Site III; [97] (f) Site III; [97]

Fig. 11. Results of sensitivity analysis; modified from Ma et al. (2019)

diagrams were developed. Figures 11(a) to 11(f) present some of those only for E1 (note that the authors of this paper have normalized and combined those plots from their original form to be more informative). The results show that the Tornado-based sensitivity diagram is sensitive to input ground motion records and site characteristics. The damping ratio, pier diameter, and concrete strength are the most important RVs in the majority of cases.

3.10. Haselton et al. (2008)

Haselton et al. (2008) [5] conducted comprehensive research combining three sources of uncertainty in RC frames: material, modeling, and design RVs. They considered a fully inter-element correlation between the parameters of different elements. A lumped plasticity model was used for all simulations. The following 10 RVs have been used:

- Plastic rotation capacity ($\theta_{cap,pl}$); COV = 0.6
- Hysteretic energy capacity (normalized) (λ); COV = 0.5

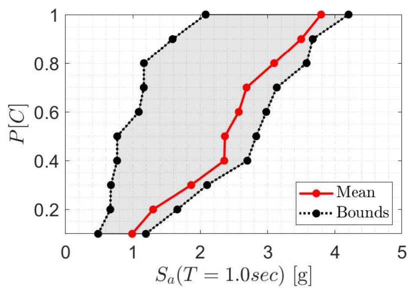

(a) Plastic rotation capacity

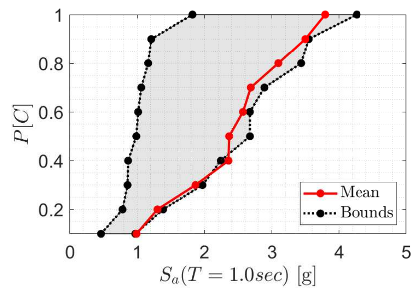

(b) Hysteretic energy capacity

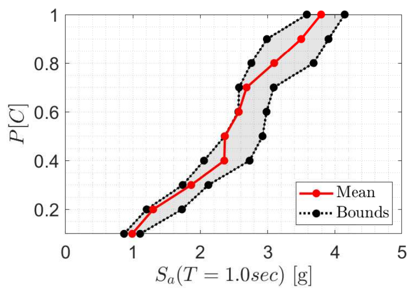

(c) Post-capping stiffness

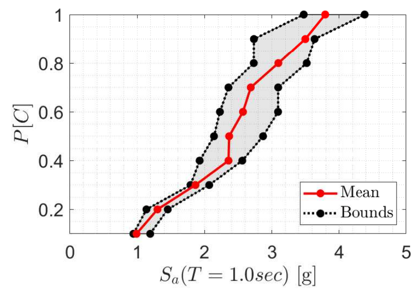

(d) Element strength

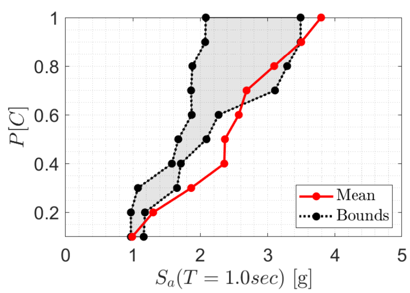

(e) Strong-Column Weak-Beam

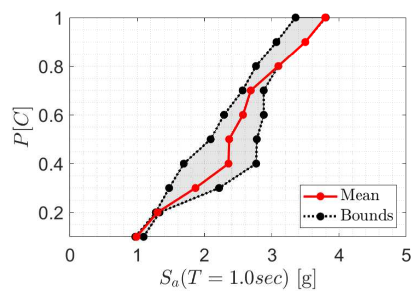

(f) Element initial stiffness

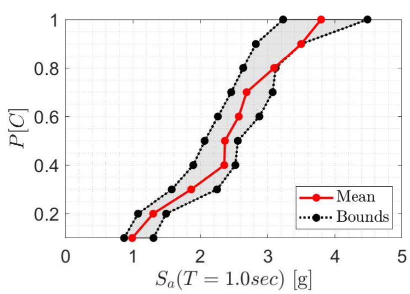

(g) Element hardening stiffness

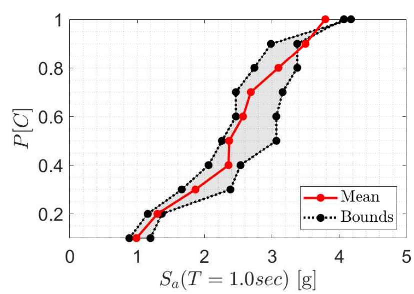

(h) Dead load and mass

Fig. 12. Sensitivity of individual RVs to variation of collapse cumulative distribution function ($P[C]$); modified from [5]

- Post-capping stiffness (K_c); COV = 0.6
- Element strength (M_y); COV = 0.12
- Strong-Column Weak-Beam design ratio (SCWB); COV = 0.15
- Element initial stiffness (K_e); COV = 0.36
- Element hardening stiffness (K_s); COV = 0.5
- Damping ratio (ξ); COV = 0.6
- Dead load and mass (DL); COV = 0.1
- Beam design strength ($\phi M_n/M_u$); COV = 0.2

They performed a special version of "dynamic" sensitivity analysis with $\mu \pm \sqrt{3}\sigma$, along with 10 ground motions. Having also a total of 10 RVs, they developed $2 \times 10 + 1$ models and performed a full IDA for each one to find their sensitivity to collapse. For any individual RV, the variation in collapse CDF is plotted in Figure 12 for mean and lower/upper bounds. The most notable observation (aside from the sensitivity of collapse to each RV), is the non-uniform pattern of the CDFs, and unproportional distance of the mean from its lower and upper bounds (in fact in some cases, the mean CDF crosses the bounds).

For each series of simulations, they fitted a Log-normal distribution to estimate the mean collapse capacities. Finally, these values were used to develop a Tornado diagram, Figure 13. Also, one may note that they chose to use a generic intensity measure parameter, $S_a(T = 1sec)$ to compare all these models because the fundamental period of the structure varies as the stiffness and mass change as RV. Overall, the element plastic rotation capacity and hysteretic energy capacity are the two most important RVs followed by strong-column weak-beam ratio. At the bottom of this diagram, we see the damping ratio indicates that the damping value does not have a large impact on the collapse capacity (note that this finding is in contrast with other Tornado diagrams summarized in this report). However, they stated that the damping formulation may be an important factor in collapse simulation.

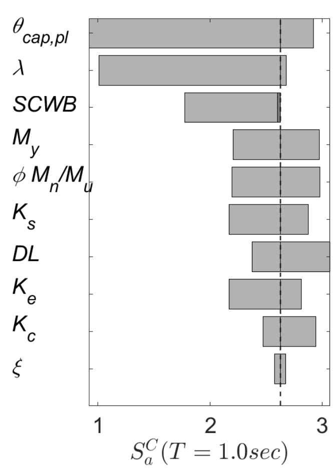

Fig. 13. Results of sensitivity analysis; modified from Haselton et al. (2008) [5]

3.11. Kim et al. (2013)

Kim et al. (2013) [98] conducted a sensitivity analysis on the design variables of staggered wall structures. Two six-story RC frame structures were used with and without a middle corridor in plan design. Perform3D was used for modeling with lumped plasticity technique. They used both the Tornado diagram and FOSM methods using seven ground motion records scaled to the maximum considered earthquake level. They chose ±2 STD as the bounds. The following RVs were used:

- Concrete compressive strength of link beam (f_c^b); COV = 0.145
- Steel yield stress of link beam (f_y^b); COV = 0.05
- Concrete compressive strength of wall (f_c^w); COV = 0.145
- Steel yield stress of wall (f_y^w); COV = 0.05
- Concrete compressive strength of column (f_c^c); COV = 0.145
- Steel yield stress of column (f_y^c); COV = 0.05
- Damping ratio (ξ); COV = 0.4

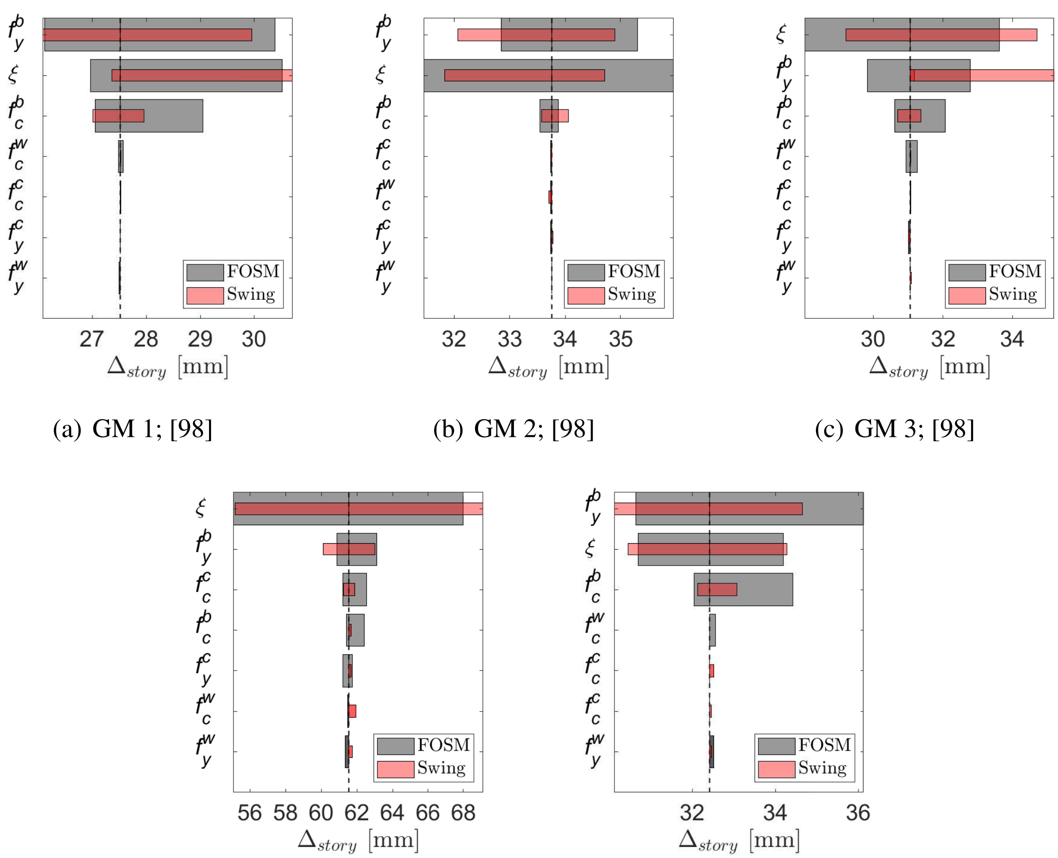

(a) GM 1; [98]

(b) GM 2; [98]

(c) GM 3; [98]

(d) GM 4; [98]

(e) GM 5; [98]

Fig. 14. Results of sensitivity analysis; modified from Kim et al. (2013)

They generated a Tornado diagram for each ground motion separately and did not integrate them, as shown in Figures 14(a) to 14(e) for five ground motions (for the case study with a corridor). Results show that the concrete ultimate strength, steel yield stress, and damping ratio are the most sensitive RVs. Moreover, comparing the results of IDA at different intensities, they reported that at lower intensity levels the steel yield stress and the concrete strength in the link beams are important RVs. At higher intensities, the column strength becomes important too.

3.12. Han et al. (2014-2015)

Han et al. (2015) [99] investigated the seismic performance and sensitivity analysis of two non-ductile RC frame buildings (three and six stories) subjected to main shock and aftershock events. The QoIs were taken to be loss-related parameters, i.e., direct loss (i.e., repair or replacement cost), downtime (summation of irrational and rational downtime), fatalities (occur when a building partially collapsed), and total loss (as opposed to traditional QoIs). They used a total of 60 mainshock-aftershocks sequences. The objective of their sensitivity analysis was to quantify the important RVs for the post-quake decisions. Both structures are modeled as a 2D frame in OpenSees using displacement-based beam-column elements with fiber sections. The following parameters were considered in the sensitivity analysis:

- Scaled ground motion (GM); [small; moderate; large]
- Assembly capacity (AC); [$e^{\ln C-1.28\beta}$; C; $e^{\ln C+1.28\beta}$] (Note: C and β are mean and STD values of different fragility groups associated with columns, beams, Drywall, Ceilings, ...)
- Damping ratio (ξ); [2.4%; 5.0%; 7.6%]
- Reparability (RP); [0.68%; 1.00%; 1.47%]
- Evacuation (EV); [Prudent; Normal; Imprudent]
- Tagging (TG); [Prudent; Normal; Imprudent]
- Threshold repair cost (TRC); [30%; 40%; 50%] of replacement value

Tornado diagrams have been generated for three scaled ground motion levels separately. The small, moderate and large earthquakes correspond to those with mean response spectra of 90%, 50%, and 10% of the probability of exceedance in 50 years. Combining three earthquake levels, two frames, and four QoIs, they generated a total of 24 Tornado diagrams. Figures 15(a) to 15(h) illustrate diagrams only for three-story frame and small/large events. Also, we normalized and combined the diagrams (with respect to the reference value in each case). The general trend of the Tornado diagram in both buildings is very similar.

They reported that ground motion uncertainty (cross-comparing the diagrams) and assembly capacity are dominant RVs. A very similar finding has been reported by [3] (See Figure 1). The damping ratio is less impact (as also reported by [5]) yet an important RV compared to the others. The uncertainty in evacuation becomes an important RV for the fatalities under small and moderate earthquakes. The threshold repair cost is important for direct loss

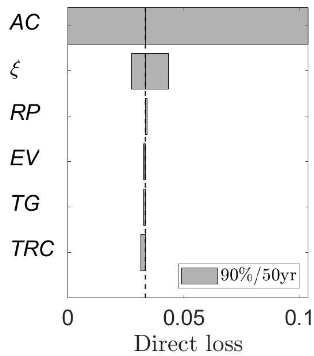

(a) Direct; [99]

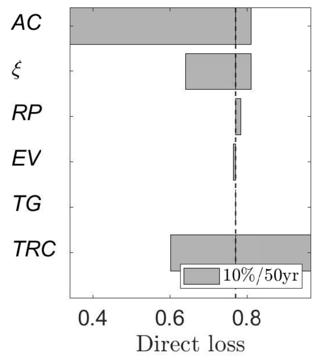

(b) Direct; [99]

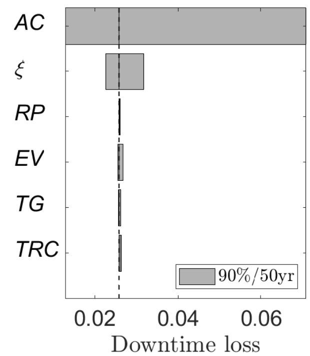

(c) Downtime; [99]

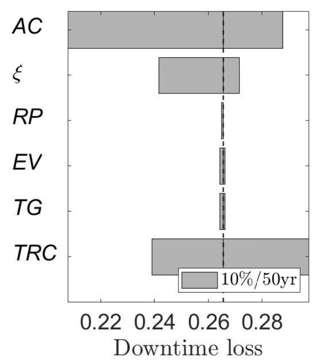

(d) Downtime; [99]

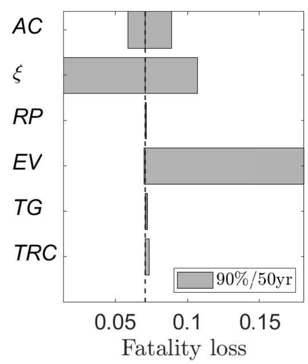

(e) Fatality; [99]

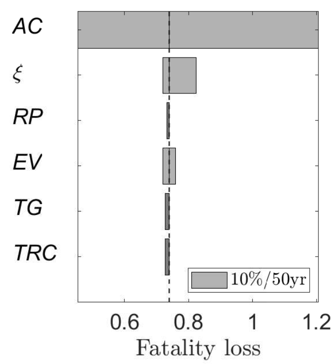

(f) Fatality; [99]

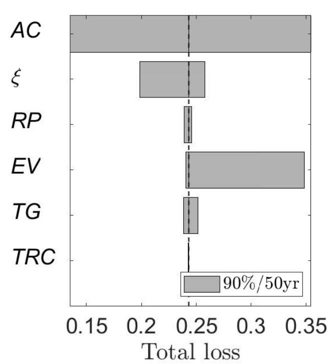

(g) Total; [99]

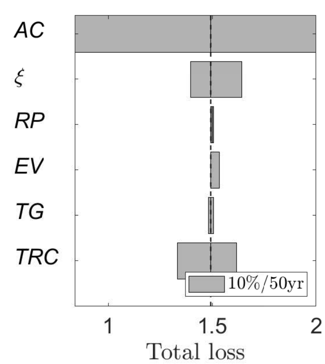

(h) Total; [99]

Fig. 15. Results of sensitivity analysis; modified from Han et al. (2014-2015) – Part 1

and downtime under larger earthquakes.

Han et al. (2014) [100] performed a very detailed sensitivity analysis on the impact of base isolation to retrofit the vulnerable old non-ductile RC frame buildings. They also considered the impact of the mainshock–aftershock (MS-AS) sequences in this process. Three types of uncertainties, i.e., structural, ground motions, and modeling were accounted for. The model is a seven-story concrete moment frame in California. The beams and columns were modeled as `Beam-With-Hinges` elements in OpenSees including two fiber-sectioned plastic hinge zones at the ends. For retrofit purposes, a base isolation system with lead-rubber bearings (LRB) is used. The LRBs were simulated using the `zerolengthSection` element with the `Isolator2spring` section. For elastomeric bearings, aging and increase in temperature are modeled by K_p and Q_d, respectively. The following RVs have been used for sensitivity analysis:

- Concrete compressive strength (f_c); COV = 0.18
- Steel yield stress (f_y); COV = 0.11
- Damping ratio (ξ); COV = 0.76
- Beam-column joint model parameters (all uniform distribution)
  - λ_1: normalized force ratio at yield point
  - λ_2: normalized force ratio at post-yield point
  - λ_{max}: normalized force ratio at maximum point
  - λ_3: normalized force ratio at ultimate point
- Isolation system-related parameters (all uniform distribution)
  - Initial post-yield stiffness (K_{pi})
  - Initial characteristic strength (Q_{di})
  - Service time (t_s)
  - Temperature (θ)

A total of 32 as-recorded MS-AS sequences were used. The aftershocks mostly occurred within a week after the mainshock (i.e., no repair in between) and all the sequences are far-field ground motions. All the sequences were amplitude-scaled to the $S_a(T_1)$ at three hazard levels, i.e., 50%, 10% and 2% in 50 years. Three QoIs were also used, i.e., the peak inter-story drift ratio (IDR), the peak shear strain (PSS), and the peak floor acceleration (PFA). Sensitivity analysis was performed using the probabilistic version of the OAT Tornado diagram method. Each time, all the scaled records were applied to the uncertain model and the results were presented in terms of median and logarithmic STD of the fitted lognormal distribution by maximum likelihood estimation. Bounds for sensitivity analyses were 10th or 90th percentile of RV.

They developed over 60 Tornado diagrams combining 3 hazard levels, 2 seismic scenarios, 2 models (i.e., un-retrofitted and isolated), 3 QoIs, and 2 statistical quantities (i.e., μ and β). Figures 16(a) to 16(h) illustrate some of those diagrams only for IDR at most high-intensity hazard level (i.e., 2%/50yr). Overall observations are as follows: ξ, f_c and f_y are generally the most sensitive RVs for the un-retrofitted frame. The first two are consistent with [94] (for IDR) and the third is indirectly similar (as both address the joint model). For the isolated system, t_s and θ are also among the sensitive RVs. For PFA, ξ, f_c, f_y and λ_1 have most significant influence on both buildings (+ θ for isolated frame). It seems that the general sensitivity ranking for MS and MS-AF is similar. Across three seismic hazard

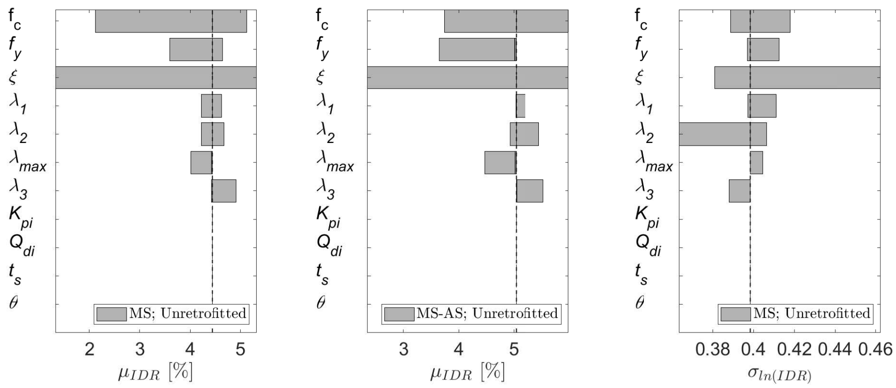

(a) 2%/50yr; [100] (b) 2%/50yr; [100] (c) 2%/50yr; [100]

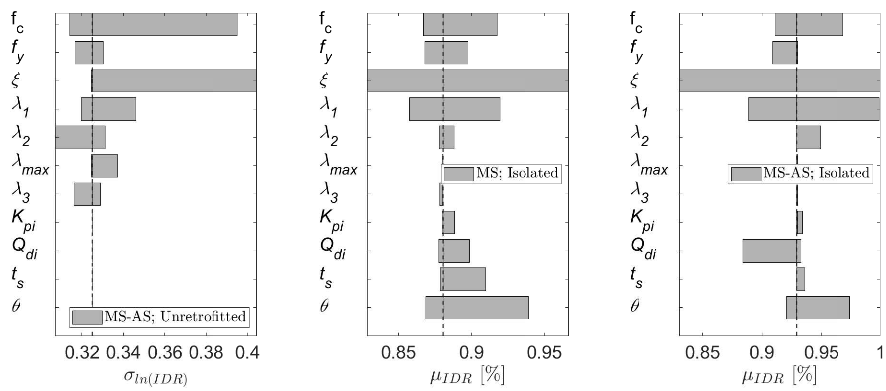

(d) 2%/50yr; [100] (e) 2%/50yr; [100] (f) 2%/50yr; [100]

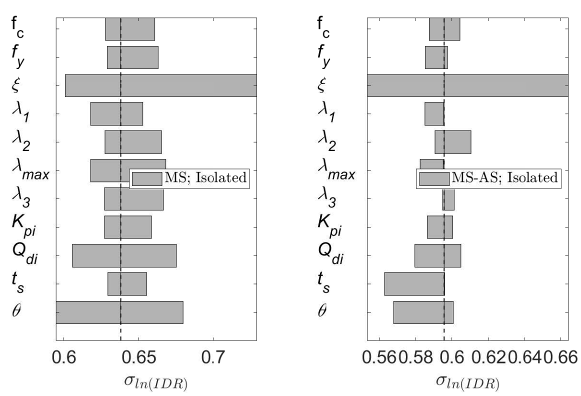

(g) 2%/50yr; [100] (h) 2%/50yr; [100]

Fig. 16. Results of sensitivity analysis; modified from Han et al. (2014-2015) – Part 2

levels (and based on IDR), the sensitivity pattern changes; however, ξ keeps its first rank (+ θ as the most important RV in an isolated frame).

3.13. Yazdani et al. (2017)

Yazdani et al. (2017) [6] provided a global sensitivity analysis of two RC frame structures (two and eight-story) using the entropy approach. This technique is consequentially similar to the mutual information index which is explained in the theory section. Their sensitivity analysis considers both the synthetic seismic excitation and structural RVs. A stochastic ground motion simulation with finite-fault method was used to generate the records. Three series of ground motions were generated with epicentral distances of 16, 52, and 90 km. Structural models were prepared in OpenSees based on lumped plasticity beam-column elements including the P-delta effect. A summary of all RVs is provided here:

- Mass (m); COV = 0.1
- Damping ratio (ξ); COV = 0.4
- Strength parameters (Strn): f_c (COV = 0.175) and f_y (COV = 0.1)
- Stiffness parameters (Stif): E_c (COV = 0.08) and E_s (COV = 0.033)
- Seismic source (Sorc)
- Propagation path (Path)
- Site effect (Site)

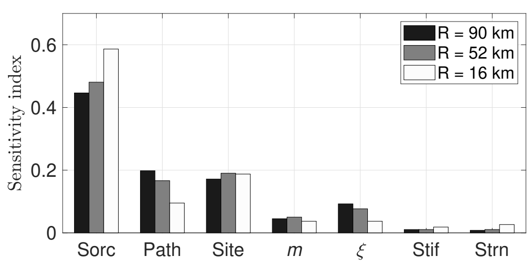

(a) MIDR

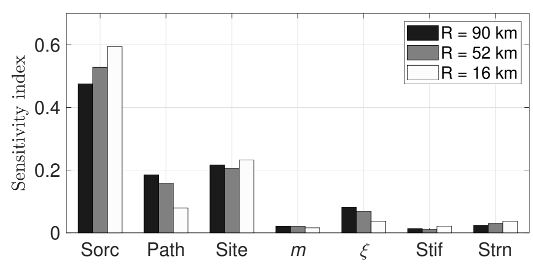

(b) PRA

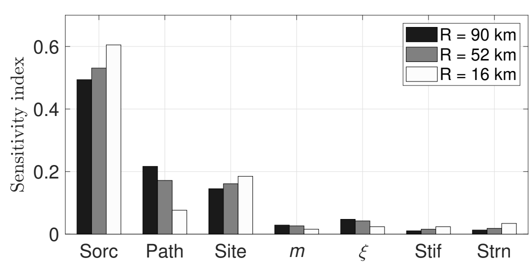

(c) PRD

Fig. 17. Sensitivity index of seven RVs based for three QoIs; modified from [6]

They investigated three QoIs in sensitivity analyses: maximum inter-story drift ratio (MIDR), peak absolute roof acceleration (PRA), and peak absolute roof displacement (PRD). Figure

17 summarizes the results in terms of the sensitivity index (results are for a two-story frame while the other one is similar). Results depend on the site location and QoI. In general, the sensitivity of ground motion RVs is higher than structural properties. More specifically, the seismic source has a dominant effect. In addition, the damping ratio is the most sensitive RV among the structural parameters.

3.14. Cantagallo et al. (2014)

While nearly all the current application of sensitivity analysis using Tornado diagram is limited to material and modeling RVs with some limited contributions from loading uncertainty, [7] developed Tornado diagram for 10 different 3D RC building portfolio using three ground motion selection and scaling techniques. They used a force-based fiber frame model using the commercial software Midas. For the first 9 structures, columns are fiber models, and beams are linear elastic. For structure #10, both the beams and columns were fiber models. Diaphragms were modeled in all cases and the same nonlinear concrete and steel material properties were used for 10 structures, Figure 18.

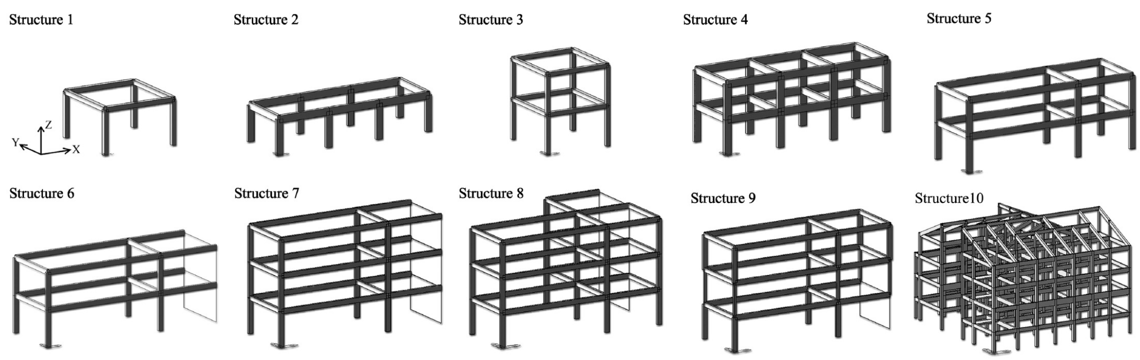

Fig. 18. Sensitivity of type and complexity of the RC buildings; adapted from [7]

They initially chose 61 ground motion records, and used 20 of them for scaling of each frame based on three approaches:

- Comb1: records selected according to the minimization of the scale factor
- Comb2: records selected according to an additional spectrum-compatibility criterion
- Comb3: Similar approach as of Comb2 but different records

Since the only variables are ground motion-related ones, two variables were considered, i.e., $S_a(T^*)$ and RTR variability. They used a method based on Poisson's recurrence law to scale the records into the median and 10% and 90% percentiles. Figure 19 presents the drift swings as RTR variability for each structure and each of the three combination methods. One intuitive observation is that drift variability increases by increasing the complexity and irregularity of the structures.

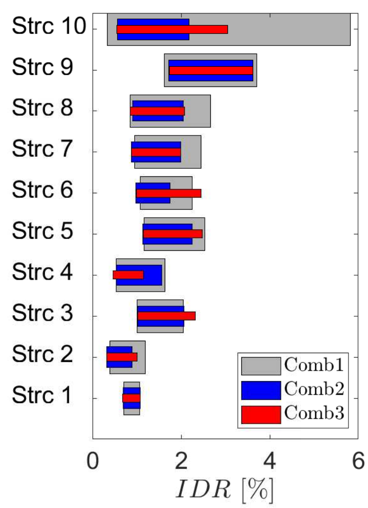

Fig. 19. Results of sensitivity analysis; modified from Cantagallo et al. (2014) [7]

3.15. Kim et al. (2020)

Kim et al. (2020) [8] studied the effects of construction quality on the sensitivity of fragility functions including the material and modeling details uncertainty. They used an old RC building from the 1980s as the case study. Models were built in OpenSees using the displacement-based beam-column element, i.e., `Concrete02` and `Steel01`. The following RVs were considered for sensitivity analysis:

- Concrete compressive strength (f_c)
- Steel yield stress (f_y)
- Longitudinal reinforcement ratio (ρ_l)
- Volumetric ratio of transverse reinforcement (ρ_w)

They performed a sensitivity analysis using two upper bounds and two lower bounds for each RV (totally $4 \times 4 + 1 = 17$ simulations). They used 50 ground motion records and performed a Cloud analysis. The relative sensitivity of each RV is evaluated by comparing the seismic fragility curves considering all RVs using the collected swing for each damage level. Figure 20 shows variation in the relative sensitivity of each RV as a function of continuous spectral acceleration and four different limit states (LS). As seen, f_c is the dominant RV in nearly all cases. For serviceability LS and low-intensity excitation, f_y shows higher sensitivity. Moreover, for collapse prevention and shear failure LSs, ρ_w plays more role.

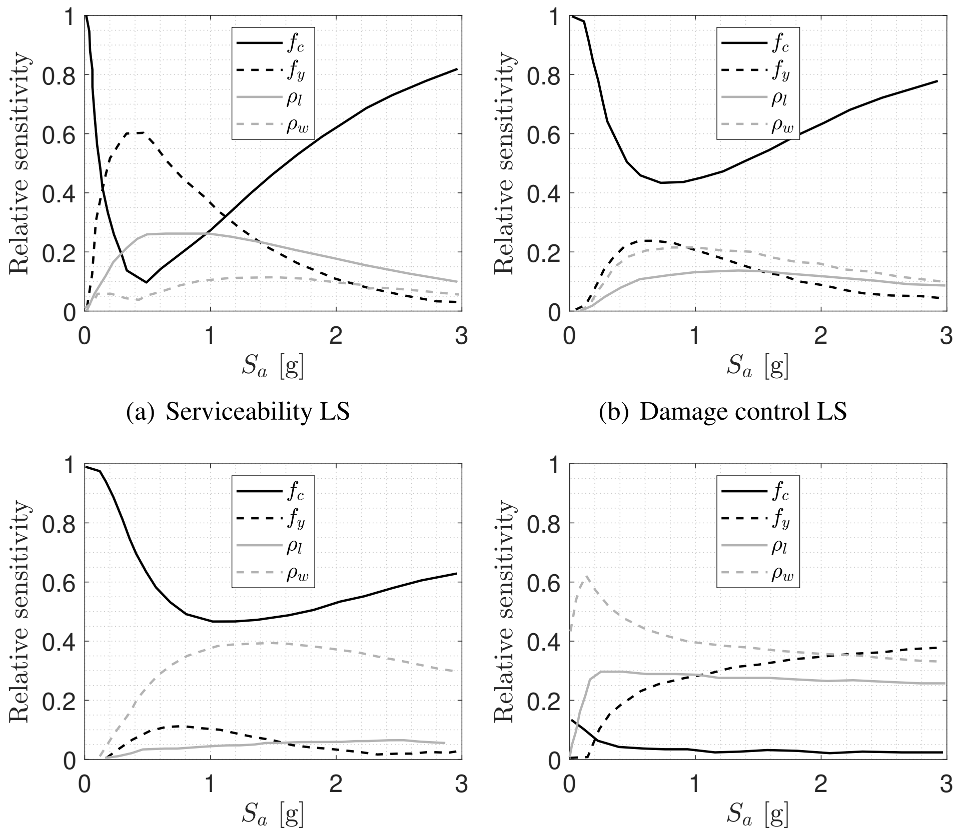

(a) Serviceability LS

(b) Damage control LS

(c) Collapse prevention LS

(d) Shear failure LS

Fig. 20. Relative sensitivity of four RVs based on fragility functions; adopted from [8]

3.16. Swensen et al. (2018)

Swensen et al. (2018) [9] studied the sensitivity of the post-yield stiffness ratio, as well as the hinge length in the seismic performance of several 2D frame structures. They used three modeling techniques, i.e., concentrated hinge elements with moment-rotation (M-R) relationships, hinge-length elements with moment-curvature (M-C) relationships, and fiber sections (FBR). They also used three software to generalize the results, i.e., OpenSees, and Perform3D. The RVs are:

- Post-yield stiffness ratio (α): 0.05%, 2% and 5% (for M-R).
- Plastic hinge length (L_p): 0.50D, 0.75D and 1.00D and D represents the member depth (for M-C and FRB).

They applied both the far-field and near-fault ground motion records to the frames (seven time-histories from each one). In the moment-rotation relationship, the hinge response was assumed to be bilinear, and the post-yield stiffness values were defined as above. The moment-curvature hinge models in OpenSees are based on `beamWithHinges` element. For the fiber models, they reported a non-convergence problem in SAP2000 models, and thus, its results were excluded from sensitivity analysis.

Figure 21 reports the results of some of the sensitivity analyses. As seen, the mean IDR can differ by up to 30% depending on the software choice and parameter used in modeling. They reported that differences using identical modeling options (moment-rotation hinges with nearly elastic-perfectly plastic behavior) can be as high as 10%. In terms of fragility, the median of being below a certain damage state can vary by 20%+ depending on the modeling parameters.

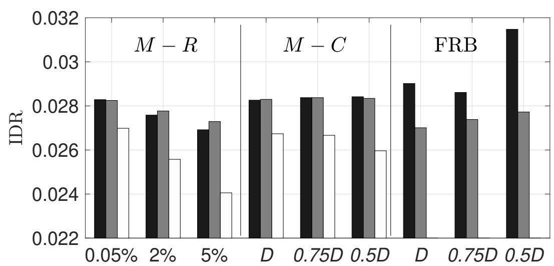

(a) 2 story

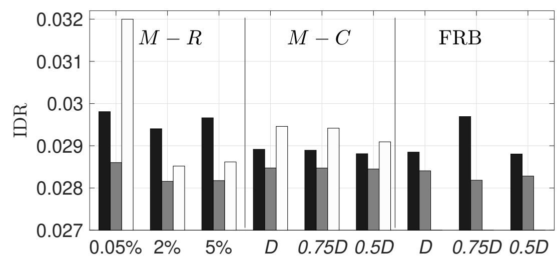

(b) 3 story

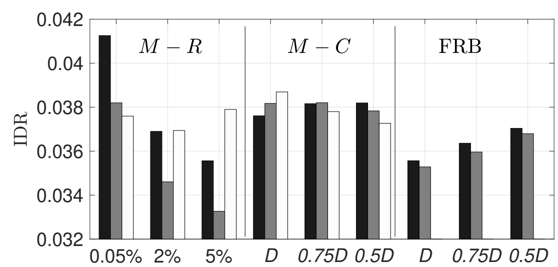

(c) 9 story

Fig. 21. Sensitivity of the mean IDR to modeling and software choice (black, gray and white); adopted from [9]

3.17. Choudhury et al. (2018)

Choudhury et al. (2018) [10] evaluated the sensitivity of the RC frames with infill walls. They compared three models of four-story frames: bare frame, open ground story frame, and fully infilled frame. This study is probably among the few that compared various statistical and graphical methods in sensitivity analysis, e.g., displacement sensitivity radar charts, response sensitivity bar diagrams, Tornado diagrams, Sobol indices, least absolute shrinkage and selection operator (LASSO) regression, and weighted pie charts. The following RVs were considered for sensitivity analysis:

- Width of column (B_c); COV = 0.0079
- Depth of beam (D_b); COV = 0.0094
- Equivalent viscous damping (ξ); COV = 0.76

- Concrete compressive strength (f_c); COV = 0.124
- Steel yield stress (f_y); COV = 0.038
- Masonry prism strength (f_m); COV = 0.24
- Unit weight of infill (γ_m), or infill load (IL); COV = 0.1
- Weight density of concrete (γ_c); COV = 0.1
- Width of equivalent diagonal strut used for modeling masonry infill walls (W_s). This value is different for ground (W_s^{gr}) and upper (W_s^{up}) stories; COV = 0.394
- Ultimate strain at failure in masonry (ε_m); COV = 0.43

Sensitivity analysis was performed with seven records and the results were presented separately for each one. In all cases, the results were normalized to the median value. Figure 22 illustrates the variation of RVs for three frames (only for one of the ground motion records). These plots present the continuous variation of the RVs and thus, are a very good method to capture any potential nonlinearity/curvature in response quantity. For both bare frame and open ground story frame, B_c, f_c, IL, and ξ incur a large variation in the estimates of roof displacement. However, for the infilled frame, there is practically no variation in response output due to a change in B_c, D_b, f_c, f_y, γ_c, IL, ξ and ε_m, while the two most influential RVs are W_s and f_m.

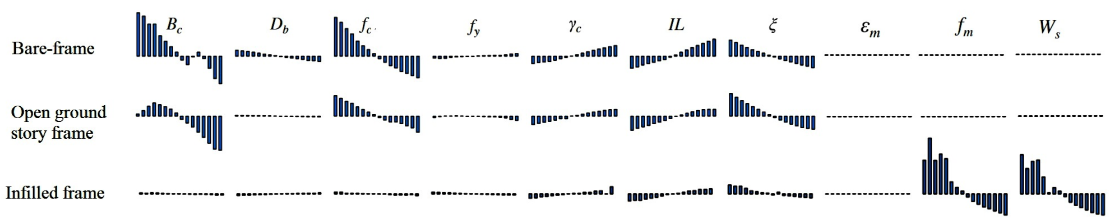

Fig. 22. Continuous variation of normalized displacement as a function of RV variation, only for one ground motion; adopted from [10]

They also performed Tornado analysis by varying the parameters to their 16% and 84% percentiles. Figures 23(a) to 23(c) present the Tornado diagrams for three frames in terms of normalized displacement. Again, for both bare frame and open ground story frame, B_c, f_c, and ξ are among three sensitive RVs. For the infilled frame, W_s and f_m are top RVs.

Furthermore, they performed an extra sensitivity analysis with Sobel's first indices. A higher index is indicative of a more sensitive RV. While it is not clear how they combined the RVs to capture the interaction effect, they provided separate Sobel index graphs for individual ground motion records and material RVs. A similar observation as of previous methods was observed. Finally, they performed LASSO regression with similar observations as of previous methods.

3.18. Yu et al. (2017)

Yu et al. (2017) [101] investigated the sensitivity of the RC frame structures to a column loss, considering the uncertainties in gravity loads, material properties, and construction

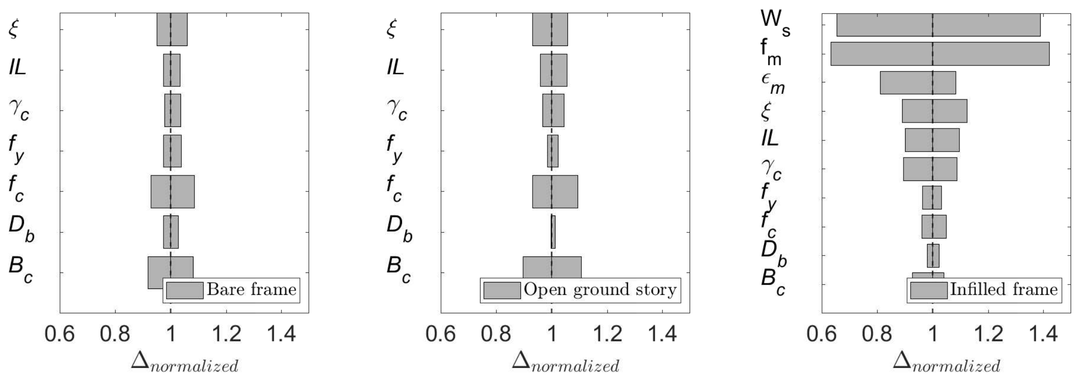

(a) [10] (b) [10] (c) [10]

Fig. 23. Results of sensitivity analysis; modified from Choudhury et al. (2018)

geometries. Two RC frames were tested using different span aspect ratios (both frames were eight-story with 4 spans; one span LF = 8.4 m and the other TF = 6.0 m). OpenSees FE code was used for simulation with displacement-based fiber elements for both beams and columns, each of which includes five integration points. The corotational transformation was also implemented. Since the column removal scenario can be conducted on either exterior (E) or interior (I) columns, a total of 4 parent models were developed: TF-E, TF-I, LF-E, and LF-I. A total of 17 RVs were used:

- Gravity loads:
  - Floor dead load (DL_f); COV = 0.1
  - Roof dead load (DL_r); COV = 0.1
  - Live load (LL); COV = 0.4
- Concrete properties
  - Compressive strength (f_c); COV = 0.18
  - Tensile strength (f_t); COV = 0.18
  - Modulus of elasticity (E_c); COV = 0.077
- Reinforcement properties
  - Steel yield strength longitudinal bars (f_y); COV = 0.093
  - Steel yield strength transverse stirrups ($f_{y,t}$); COV = 0.107
  - Steel ultimate strength (f_u); COV = 0.08
  - Modulus of elasticity (E_s); COV = 0.033
- Construction geometries
  - Beam width (B_b)
  - Beam height (H_b)
  - Span length (L)
  - Longitudinal reinforcement areas in beam ($A_{s,beam}$)
  - Longitudinal reinforcement areas in columns ($A_{s,col}$)

- Transverse stirrup area ($A_{s,t}$)
- Concrete cover (t)

The capacity curves were derived using the quasi-static pushdown analysis. They vary the RVs by one STD to develop the Tornado diagrams. Tornado diagrams were developed for two damage criteria (DC):

- DC-I: first yielding (plastic-hinge formulation) of steel rebar in RC beams
- DC-II: the ultimate load-resisting capacity

Figures 24(a) and 24(h) present the Tornado diagrams for those selected DC and four modeling scenarios in terms of the load factor, α, the ratio between the recorded gravity load corresponding to incremental vertical displacement and the nominal gravity load. For DC-I, DL_f and f_y are the important RVs, while for DC-II, DL_f and f_u are the sensitive RVs. Furthermore, the effect of $A_{s,beam}$ on both DC is also considerable. The tornado diagrams are more symmetric for DC-I than DC-II. Also, the bars in the tornado diagrams for LF are more skewed than for TF.

3.19. Grubišić et al. (2019)

Grubišić et al. (2019) [11] conducted a series of probabilistic simulations to investigate the impact of numerical modeling techniques on uncertainty quantification and sensitivity analysis of RC planar frames. A central bay RC frame from the ground floor was chosen from a typical mid-rise building. The numerical model is then calibrated, and subjected to cyclic horizontal load. OpenSees was used for modeling based on two modeling approaches:

- Lumped plasticity model with Takeda hysteresis rules [102]. M_u (ultimate bending moment) corresponds to the moment at the fracture of the first major longitudinal reinforcement; M_y (yielding moment) corresponds to the first longitudinal reinforcement yielding of each element individually; M_{cr} (cracking moment) corresponds to the initial cracking of concrete.
- Distributed plasticity using `BeamWithHinges` elements which consider force-based distributed plasticity over specified plastic hinge lengths near the element ends.

The following RVs were incorporated:

- Steel yield strength (f_y); COV = 0.08
- Steel modulus of elasticity (E_s); COV = 0.06
- Confined concrete compressive strength (f_{c1C}); COV = 0.15
- Confined concrete compressive strain (ε_{c1C}); COV = 0.15
- Unconfined concrete compressive strength (f_{c1U}); COV = 0.15
- Unconfined concrete compressive strain (ε_{c1U}); COV = 0.15
- Confined concrete crushing strength (f_{c2C}); COV = 0.2
- Confined concrete crushing strain (ε_{c2C}); COV = 0.2
- Unconfined concrete crushing strength (f_{c2U}); COV = 0.2

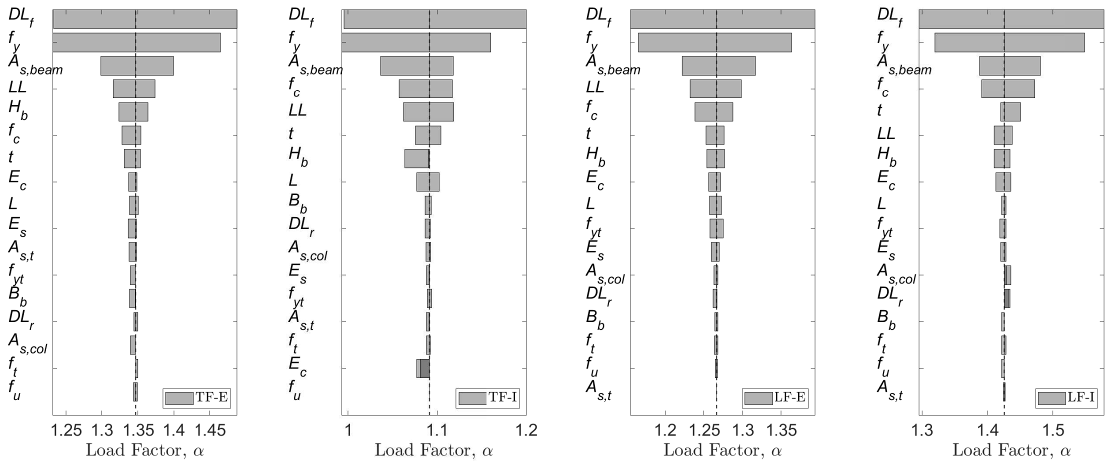

(a) DC-I; [101] (b) DC-I; [101] (c) DC-I; [101] (d) DC-I; [101]

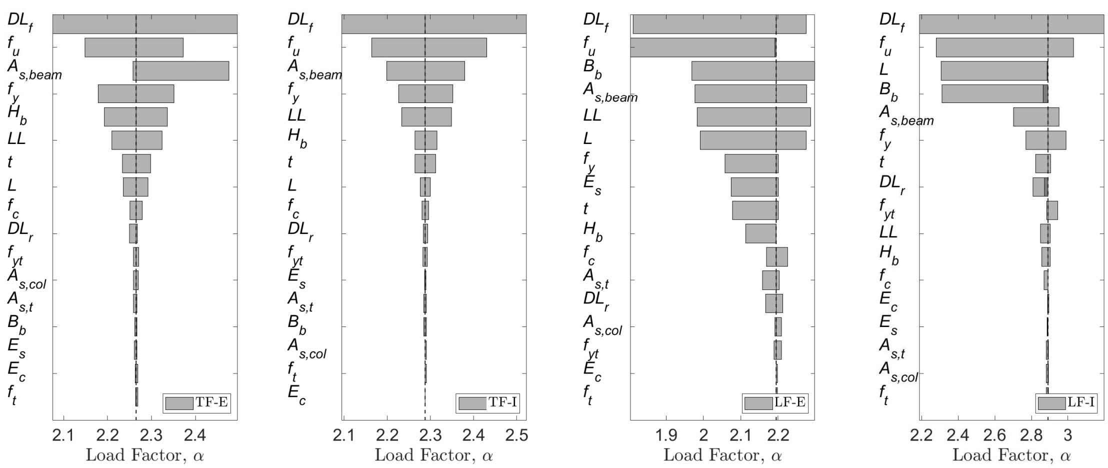

(e) DC-II; [101] (f) DC-II; [101] (g) DC-II; [101] (h) DC-II; [101]

Fig. 24. Results of sensitivity analysis; modified from Yu et al. (2017)

- Unconfined concrete crushing strain (ε_{c2U}); COV = 0.2
- Vertical load per column (F_v); COV = 0.1
- Length of the column (L_{col}); COV = 0.01
- Length of the beam (L_{beam}); COV = 0.01
- Depth of the concrete cover for both columns and beams (c_{cover}); COV 0.25
- Cross section depth of the column (H_{col}); COV = 0.05
- Cross section depth of the beam (H_{beam}); COV = 0.05

- Plastic hinge length for both columns and beam (L_p); COV = 0.1

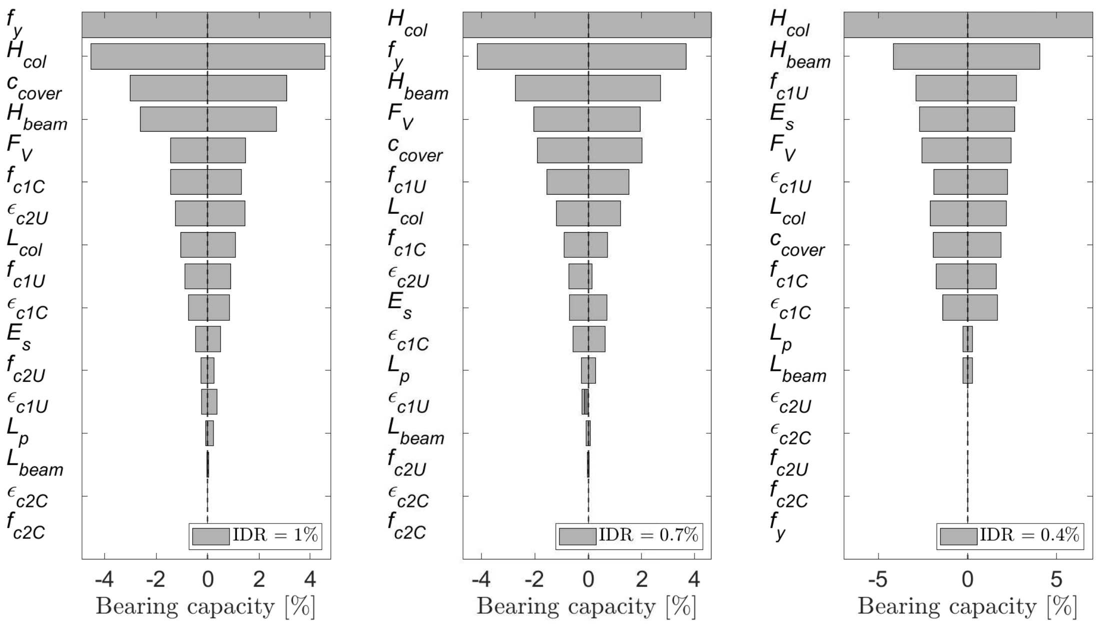

(a) [11] (b) [11] (c) [11]

Fig. 25. Results of sensitivity analysis; modified from Grubisic et al. (2019)

They performed a series of reliability analyses using different methods such as MCS (10e5 samples), FORM and SORM, and Mean-Value First-Order Second-Moment (MVFOSM). They also conducted the sensitivity analysis in two ways:

- Performing a total of 1000 MCS pushover analyses for individual RVs while keeping the remaining RVs at their mean value. With this method, a range of sensitivity is obtained ($\pm$1 STD) for each RV. Figure 26 shows some of those 17 RVs. According to this method, f_y, H_{col}, c_{cover}, H_{beam}, F_V and f_{c1C} are most important RVs. In a nonlinear region, after exceeding the yield strength of the longitudinal reinforcement, the geometry-related RVs were much more important compared to the material RVs.
- Classical Tornado diagram by varying each RV to their 16 and 84th percentiles. Results are developed for three IDRs as shown in Figures 25(a) to 25(c). In the predominant linear range of the system (0.4% IDR), the height of the beam and column are the most important RVs. Moving towards higher drift ratios, the impact of f_y is dominant.

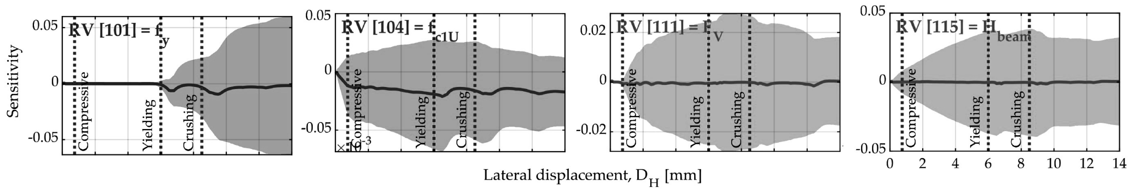

Fig. 26. Sensitivity range for individual RVs by MCS; adapted from Grubišić et al. (2019) [11]

3.20. Faggella et al. (2008)

Faggella et al. (2008) [12] investigated the seismic demand sensitivity analysis of a 3D RC building subjected to three-component earthquake excitation. A four-story frame is used as a case study and its model was developed by OpenSees using force-based fiber elements. The following RVs were incorporated:

- Mass (m); COV = 0.1
- Damping ratio (ξ); COV = 0.4
- Concrete compressive strength (f_c); COV = 0.064
- Concrete modulus of elasticity (E_c); COV = 0.08
- Steel yield strength (f_y); COV = 0.1
- Steel modulus of elasticity (E_s); COV = 0.033
- Ground motion details (GM); COV = -
- Ground motion intensity measure, $S_a(T_1)$; COV = 0.84

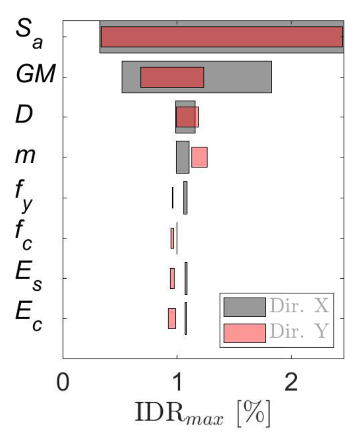

Fig. 27. Results of sensitivity analysis; modified from Faggella et al. (2008) [12]

For selecting appropriate bounds for ground motion intensity, they first drove the probability distribution for $S_a(T_1)$ from the seismic hazard analysis. The ground motions were scaled for an IM with a probability of exceedance of 50%/50 yr. Next, A MCS based on the ensemble of 20 three-component records is performed. Tornado diagrams were based on 10% and 90% fractiles from each RV. Figure 27 presents the Tornado diagram for maximum IDR in both X and Y directions. $S_a(T_1)$ and *GM* RTR variability are the predominant RVs followed by damping and the mass.

3.21. Segura et al. (2022)

Segura et al. (2022) [103] performed a sensitivity analysis using OAT Tornado diagram on an RC circular bridge column. A detailed fiber-based model was developed in OpenSees and is subjected to an intensifying artificial acceleration. There are three advantages in using such a dynamic excitation: the overall number of transient simulations remains in a manageable range (i.e., $2N+1$, where N is the number of variables), the results are independent of specific ground motion records, and the sensitivity analysis can be evaluated at different seismic intensities.

Extensive data collection and statistical post-processing is used to develop appropriate distributional models for each property. The following material parameters were considered to be random:

- Steel yield stress (f_{ym}); COV = 0.046 (Grade 60), 0.039 (Grade 80), 0.034 (Grade 100)
- Steel peak tensile stress (f_u); COV 0.043 (Grade 60), 0.034 (Grade 80), 0.037 (Grade 100)
- Steel fracture strain (ε_f); COV = 0.136 (Grade 60), 0.127 (Grade 80), 0.128 (Grade 100)
- Steel elastic modulus (E_s); COV = 0.033 (for all three grades)
- Steel strain hardening ratio (b)' COV = 0.194 (Grade 60), 0.176 (Grade 80), 0.130 (Grade 100)
- Unconfined concrete elastic modulus (E_{c0}); COV = 0.114 (for all f'_c values)
- Unconfined concrete peak compressive stress (f_{c0}); COV = 0.155 (for f'_c = 28 MPa), 0.125 (for f'_c = 35 MPa), 0.075 (for f'_c = 41 MPa)
- Unconfined concrete peak compressive strain (ε_{c0}); COV = 0.187 (for f'_c = 28 MPa), 0.193 (for f'_c = 35 MPa), 0.186 (for f'_c = 41 MPa)
- Concrete tensile rupture stress (f_t); COV = 0.211 (for f'_c = 28 MPa), 0.193 (for f'_c = 35 MPa), 0.185 (for f'_c = 41 MPa)
- Confined concrete elastic modulus (E_{cc}); COV = 0.150 (for f'_c = 28 MPa), 0.156 (for f'_c = 35 MPa), 0.154 (for f'_c = 41 MPa)
- Confined concrete peak compressive stress (f_{cc}); COV = 0.119 (for f'_c = 28 MPa), 0.102 (for f'_c = 35 MPa), 0.063 (for f'_c = 41 MPa)
- Confined concrete peak compressive strain (ε_{cc}); COV = 0.155 (for f'_c = 28 MPa), 0.166 (for f'_c = 35 MPa), 0.172 (for f'_c = 41 MPa)
- Concrete softening modulus (E_{ccdeg}); COV = 0.171 (for f'_c = 28 MPa), 0.144 (for f'_c = 35 MPa), 0.100 (for f'_c = 41 MPa)

Figure 28 presents the results of the sensitivity analysis as a Tornado diagram with respect to the percentage difference in the drift envelope value determined at four different shaking intensities as compared to the model with all material properties set at their mean value. The shaking intensities are represented by $S_a(T_1)$. For the case study column, $S_a(T_1)$ = 0.5g represents low ductility demand; $S_a(T_1)$ = 1g and 3g are representative of design-level ductility limits for bridges classified as Recovery and Ordinary according to the Caltrans Seismic Design Criteria; and $S_a(T_1)$ = 4.5g represents the intensity for which the median model is expected to reach collapse-level drift demands, assumed herein as a drift ratio of 0.1 rad.

According to these results, drifts are most sensitive to material properties that define the hardening branch of the concrete stress-strain curve and the elastic branch of the reinforcing steel stress-strain curve. Drifts are likely to be insensitive to E_{deg}, only marginally sensitive to b, f_u, and ε_f, and moderately sensitive to E_{c0}, f_{cc}, and ε_{cc}. Results also demonstrate the outcome of sensitivity analysis depends on the shaking intensity.

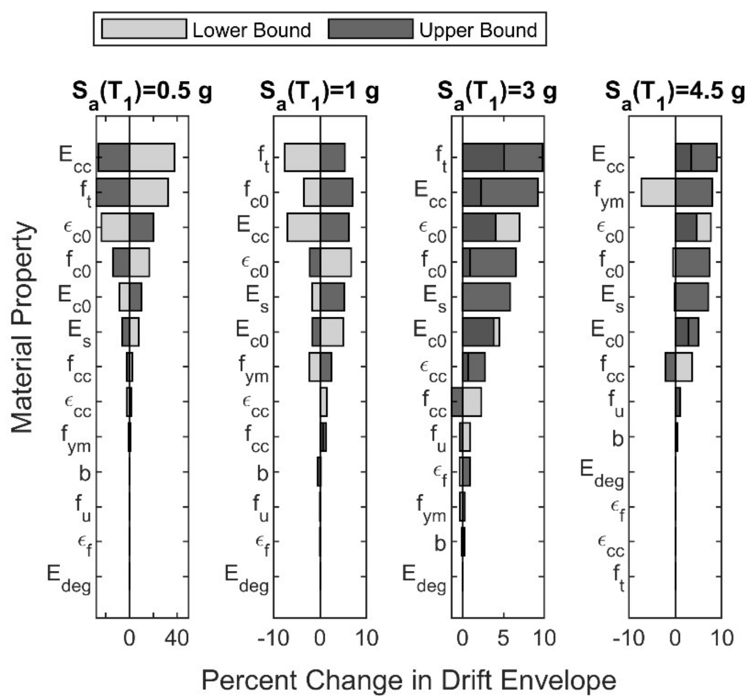

Fig. 28. Results of sensitivity analysis; modified from Segura et al. (2022)

4. Sensitivity to Beyond "Material and Modeling" Variability

Sensitivity analysis is not limited to RC structures, and there are several examples of its application on different engineering structures. While the focus of this report is to provide a detailed application, method, type of RVs, and the results of sensitivity analysis for RC structures, many other valuable findings can be uncovered by exploring other publications. Therefore, the objective of this section is to provide some comparative results that can be found in the literature on sensitivity analysis of structures. Each sub-section discusses a topic that is directly or indirectly related to the sensitivity analysis. They cover topics that are beyond the sensitivity analysis of a structure with material and/or modeling uncertainty. For example, the impact of software, the choice of demand parameter, the choice of analysis technique, etc. are all discussed in this section.

4.1. Sensitivity to Software

Some researchers investigated the sensitivity of the adopted software in the response quantification of structural systems. [9] compared three software platforms, i.e., OpenSees, Perform3D, and SAP2000 for nonlinear response sensitivity of three frame structures, and reported the choice of software is more pronounced at the local/element level than at the global/system level. Alwaeli et al. (2017) [104] compared ZEUS-NL (with two (initial and improved) 2D nonlinear models using two-node fiber-based frame elements) wiht PERFORM-3D (3D four-node fiber-based model). They reported that both software can sufficiently predict global deformation. However, the four-node model in PERFORM-3D showed better performance in accounting for the 3D effects of deformation compatibility between lateral and gravity force-resisting systems. [13] compared some medium size specialized software for masonry buildings (e.g., 3Muri and 3DMacro), as well as some more general FE packages such as DIANA and ANSYS, and some university codes like Code ASTER. The crack profiles resulted from pushover analysis among different methods present sensitivity of the response with considerable variation, see Figure 29. Moreover, Asgarian et al. (2010) [105] compared the deterministic seismic response of a high-rise concrete tower analyzed using ANSYS, ABAQUS, and OpenSees. They reported some discrepancies in the linear range between uni-axial and multi-axial element formulations. As for the nonlinear analyses, the discrepancy moves to earlier times.

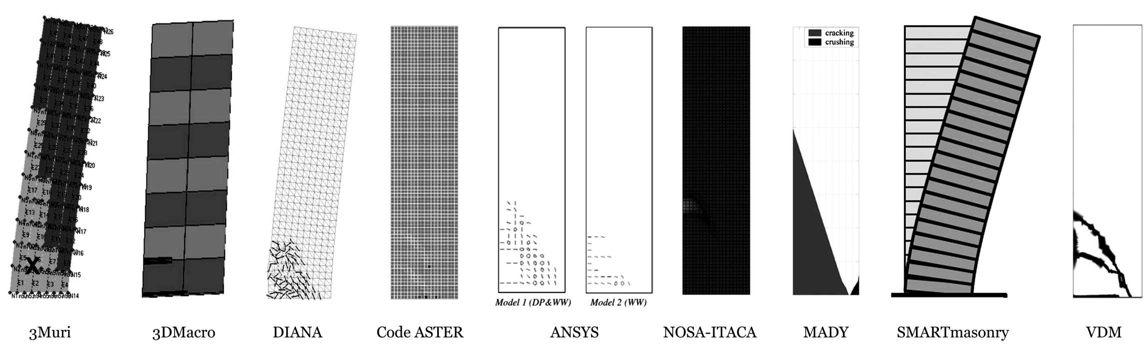

Fig. 29. Sensitivity of cracking/damage/fracture map of a column at collapse point to the software choice; adapted from [13]

4.2. Indirect Sensitivity Assessment

While the majority of sensitivity analysis techniques yield clear conclusions, ranking the RVs based on their relative sensitivity (e.g., swings in Tornado diagram, or any type of sensitivity index), some applications indirectly present the results of sensitivity analysis. The most famous form is the sensitivity in seismic fragility functions. This can be divided into three parts:

4.2.1. Type-I

Sensitivity in fragility curves due to random variations in the material properties or modeling parameters. For example, Figure 30(a) compares fragility curves at a limit state using the lower and upper bound of material/modeling RVs for each one. IM-dependent sensitivity in the probability of failure, P_f, can be tracked in this figure. Examples of this type of sensitivity is addressed in [106] for cable-stayed bridges, [107] for pile-group-supported bridges on liquefiable soil, [46] for transmission towers.

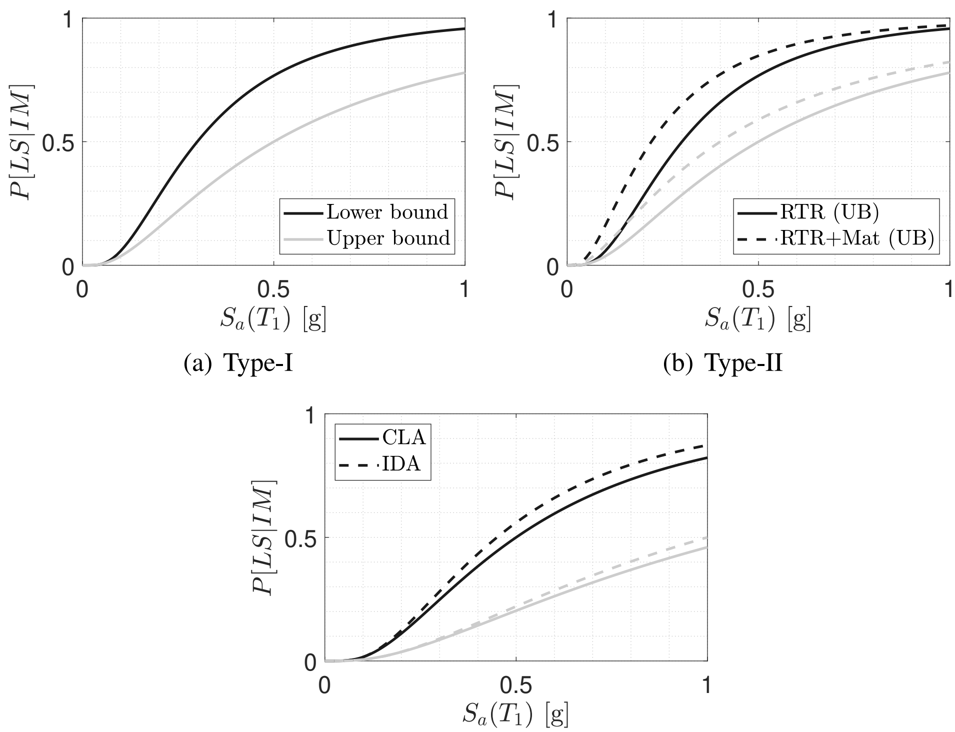

(a) Type-I (b) Type-II

(c) Type-III

Fig. 30. Indirect sensitivity assessment through seismic fragility functions

4.2.2. Type-II

Sensitivity in fragility curves due to incorporating additional sources of uncertainties. For example, Figure 30(b) compares upper and lower bound fragility curves for two uncertain scenarios: (1) only ground motion variability, and (2) ground motion and material variability. As seen, each of the upper and lower bound fragility curves is sensitive to incorporating extra (here material) sources of uncertainty. Examples of this type of sensitivity are addressed in [106] for cable-stayed bridges.

Haddad et al. (2019) [108] compared fragility functions based on the confidence factor method at three knowledge levels (KL), i.e., KL1, KL2, KL3 with increasing achieved knowledge. Any change in KL will affect the uncertainty source and thus, changes the fragility function.

4.2.3. Type-III

Sensitivity in fragility curves due to adopted probabilistic analysis technique. It is well-established that fragility curves are sensitive to the probabilistic seismic analysis technique. For example, Figure 30(c) compares the fragility curves in two limit states resulted from IDA and CLA methods. Examples of this type of sensitivity are addressed in [106] for cable-stayed bridges, [109] for highway bridges. The sensitivity of fragility curves to the ground motion meta-features is also categorized under this group [110].

Zhong et al. (2012) [111] conducted research on sensitivity analysis and importance measures for RC columns from seismic fragility estimates. They differentiated between the concept of sensitivity and importance. Sensitivity analysis is used to determine to which parameter(s) the reliability of a structural component is most susceptible [112]. Assuming $f\left(\mathbf{r},\Theta_f\right)$ to be the joint PDF of basic RVs in $\mathbf{r}$ with a set of distribution parameters Θ_f (e.g., mean, standard deviation, correlation). The sensitivity vector is computed using the proposed model by [113]:

$$\delta = \sigma.\nabla_{\Theta_f}\beta \tag{20}$$

where σ is the diagonal matrix with diagonal elements given by the standard deviation of each RV in $\mathbf{r}$, ∇_{Θ_f} is the gradient function, and β is the reliability index.

The importance measure shows the contribution of each RV to the variability of the limit state function. The importance vector is defined using [114] model:

$$\gamma^T = \frac{\alpha^T.\mathbf{J}_{\mathbf{u}^*,\mathbf{z}^*}.\mathbf{SD}'}{||\alpha^T.\mathbf{J}_{\mathbf{u}^*,\mathbf{z}^*}.\mathbf{SD}'||} \tag{21}$$

where α is a vector of the negative normalized gradient of limit state function at the design point in standard normal space, $\mathbf{J}_{\mathbf{u}^*,\mathbf{z}^*}$ presents the Jacobian matrix of the probability transformation from original to standard normal space, and $\mathbf{SD}$ is the diagonal matrix consisting of standard deviations of equivalent normal variables.

They implemented this method on two columns (one is shown here). Figure 31(a) presents the sensitivity measures for the deformation and shear fragility estimates for the means of the random variables in $\mathbf{r}$ for S_a = 0.95g and PGV/PGA = 0.19 sec (selected based on hazard map and for strong motions). These values are computed for the "expected value of the RV", $E(.)$. As seen, the yield stress of confining concrete and concrete compressive strength, and spacing of transverse reinforcement are top sensitivity RVs. In this context, the positive sign of the sensitivity measure indicates that the RV serves as a resistance (capacity) variable, while the negative sign means that the RV acts as a load (demand) variable.

Likewise, Figure 31(b) presents the importance measures. As seen, a lot of extra RVs are added to account for the random errors in demand (D) and capacity (i.e., ε_D and ε_C), the parameters in the demand and capacity models (i.e., θ_D^i and θ_C^i), and mean model errors (i.e., σ_D and σ_C). The importance measures suggest that the random errors in the probabilistic capacity and demand models represent the principal sources of uncertainty.

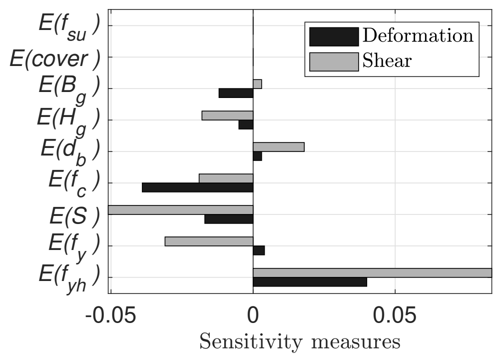

(a) Sensitivity measures for the mean, $E(.)$, of each RV

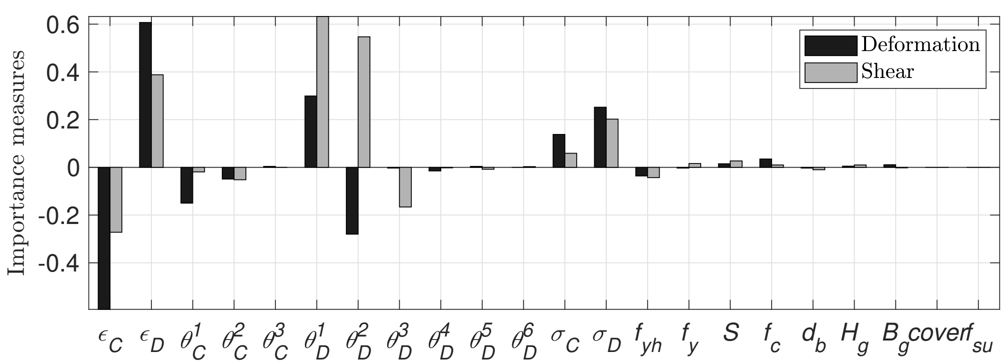

(b) Importance measures for each RV

Fig. 31. Comparison of sensitivity and importance measures for the deformation and shear fragility estimates

4.3. Sensitivity to EDP Effect

Conducting any type of sensitivity analysis requires the determination of a series of random variables and also the target QoI (or EDP). In general, the selected QoI should be (1) a good representation of the input-output relationship for the case study structure (which is typically used by the engineers), and (2) a good representation of the loss model for the subsequent decision-making steps (which is typically used by the stakeholders). Upon reviewing the literature, the following major groups can be identified:

4.3.1. Group-I: Direct QoIs

Direct QoIs are structural EDPs that are computed from the structural analyses. These quantities can be obtained directly from FE software (e.g., displacement, acceleration, or stress), or they can be computed as a separate indicator (e.g., damage index). The latter one is more complex and typically requires a combination of several single-variable QoIs. For example, a damage index might be a function of structural height, peak displacement, crack length, and the amount of dissipated energy. At any rate, the direct QoIs can be classified into two main groups:

- Local QoIs: those who might be a good representative for a particular (typically critical) location of the structure. In the case of frame structures, this can be the inter-story drift ratio at first floor. QoIs such as maximum inter-story drift ratio (MIDR), maximum floor acceleration (MFA), and normalized hysteretic energy (NHE) are typically used for frame structures [110]. Another example can be cracking stress at the dam heel/toe.
- Global QoIs: are more generic and account for the global response of the structure. For example, roof displacement in buildings or crest displacement in dams. Ductility, strength, and energy dissipation are also categorized in this group [115].

4.3.2. Group-II: Indirect QoIs

Group-II QoIs refer to the QoI which are indirectly computed from the results of structural analysis by combining them with hazard models and loss estimation. Examples of this type of QoI can be found in [116, 117], where [116] compared the results of sensitivity analysis using three methods of Tornado diagram, FOSM, and LHS using the variable in life-cycle cost (LCC) analysis of an offshore platform structure. Lamprou et al. (2013) [117] used repair cost as a metric (calculated based on drift- and acceleration-sensitive components) for life-cycle loss estimation and global sensitivity assessment.

4.3.3. Group-III: Failure-based QoIs

Sometimes the sensitivity is measured based on the duration in which the structural system can endure the applied stressor [118]. In case the stressor has a dynamic nature, the metric can be based on the "elapsed time" (from the beginning of loading to the target limit state) or the "failure time" (corresponds to collapse/un-convergence of the structure). However, if the simulations are based on a quasi-static loading protocol, the sensitivity analysis can be developed based on the number of cycles at the collapse point.

Figures 32(a) and 32(b) compare the sensitivity of time-dependent cracking DI in a concrete dam with respect to concrete strength (i.e., f_t and f_c) [119]. Using the failure time as a metric, the system is highly sensitive to f_t and practically insensitive to f_c. Also, Figure

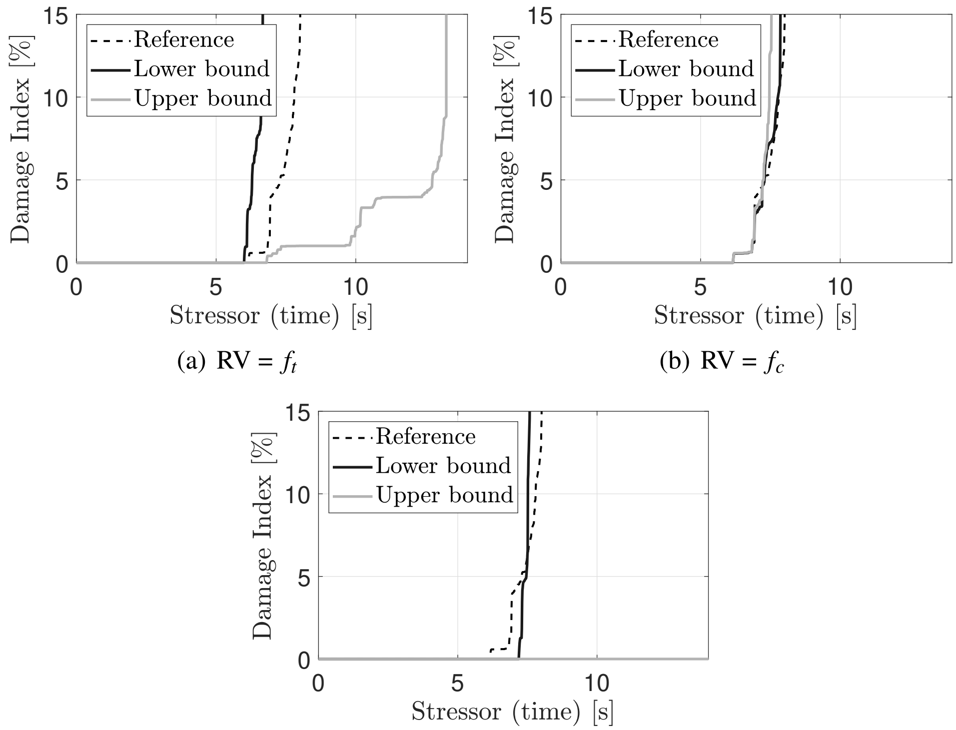

(a) RV = f_t

(b) RV = f_c

(c) Multi RVs

Fig. 32. Sensitivity analysis through the concept of failure time (i.e., Group-III)

32(c) presents the results for the combined sensitivity of all RVs, and as seen the upper bounds of all RVs make the system very resilient to shaking and do not cause any damage (the curve associated with upper bound is a flat line with zero DI). The simulations benefit from an intensifying acceleration function that dynamically pushes the structure from its linear elastic to nonlinear range, and finally causes collapse [120]. A similar approach is also reported by [121] and [122] for mass and reinforced concrete structures, respectively. A similar idea has been used by [123] for sensitivity analysis of the failure time in RC frames under post-earthquake fire.

One should not forget that apart from the QoI itself, the threshold value which is considered to extract the sensitivity results is very important. This is because not all epistemic RVs are activated in the entire range of response quantity. Parameters such as the elasticity of the system are active since the beginning (i.e., under the low-intensity loading protocols); however, these parameters, which are related to the damage (e.g., yielding, cracking, or crushing), might be active only under medium to high-intensity loading. For example, [107] developed different Tornado diagrams for pile-supported bridges based on first-yield curvature and ultimate curvature values. Liel et al. (2009) [124] developed two Tornado diagrams for a four-story frame structure using four meta-RVs (i.e., beam/column ductility/strength) and two limit states, i.e., collapse and 1% drift ratio. They showed that column strength is the most sensitive RV for the median collapse capacity, followed by column ductility. Comparing two limit states, they found that modeling RVs are more significant for the collapse limit state.

4.4. Sensitivity to Individual Ground motion Record

Several studies in Section 3 were based on probabilistic seismic analysis methods, e.g., [5, 67, 90, 94]. In all cases, the results of sensitivity analysis were presented in the form of mean or median, as well as the lower and upper bounds (such as 10-90% or 16-84%). So far, none of the research provided a detailed relationship between the ground motion record and the sensitive RVs.

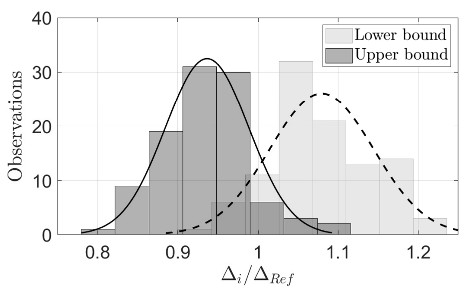

(a) E_c distribution

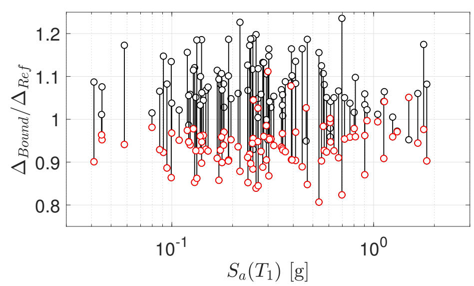

(b) $E_c - S_a(T_1)$

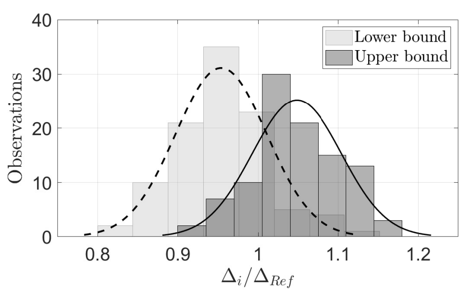

(c) ρ_c distribution

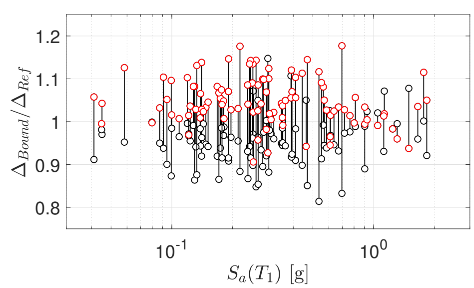

(d) $\rho_c - S_a(T_1)$

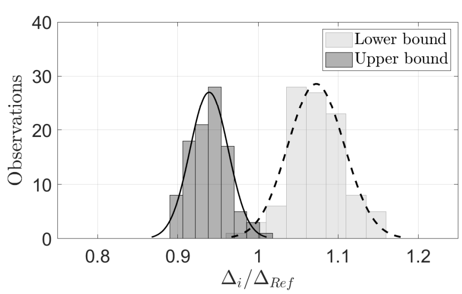

(e) η_c distribution

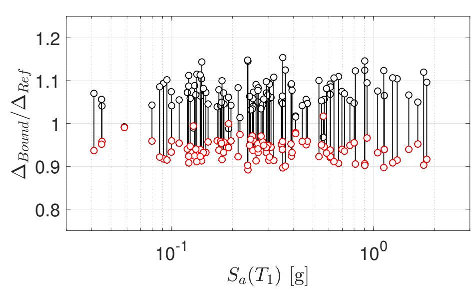

(f) $\eta_c - S_a(T_1)$

Fig. 33. Detailed sensitivity analysis with individual ground motion records; generated with data from [14]

Hariri-Ardebili and Boodagh (2018) [14] provided detailed information for sensitivity analysis of a cantilever-type concrete structure with over 100 ground motion records. Three concrete properties were assumed to be random: modulus of elasticity (E_c), mass density (ρ_c), and hysteretic damping (η_c). In each case, a separate sensitivity analysis was performed with lower and upper bound (LB/UB) values.

The first column in Figure 33 illustrates the distribution of normalized lower and upper bound drift values with respect to the reference one. As seen, increasing E_c decreases the mean and standard deviation of the fitted normal distribution. This is consistent with the physics of the problem because increasing E_c makes the system more rigid. However, this is not always the case, and for some of the ground motion records, the trend is the opposite. Indeed, the LB and UB have considerable overlap. A similar discussion is valid for ρ_c and η_c, where the overlap between two distributions is larger for ρ_c. The second column in Figure 33 shows the relation between the LB and UB with the intensity of the applied ground motion. There is absolutely no correlation between the seismic intensity ($S_a(T_1)$) and the normalized bound value. This has been tested for other intensity measure parameters such as $S_a(T_1)$, PGA, PGV, cumulative absolute velocity (CAV), Arias intensity, etc. and no significant correlation was observed too. This confirms the unreliable result of sensitivity analysis when a single ground motion record is used.

Nasrollahzadeh et al. (2022) [15] analyzed two four- and eight-story RC frame structures with the IDA method combined with modeling uncertainty in the backbone curve used to model the beams and columns. More precisely, the frames were developed with OpenSees' lumped plasticity model using a tri-linear backbone curve as constitutive relation. Four modeling parameters in beams (b) and columns (c) are assumed to be variable:

- Cyclic deterioration capacity (λ); COV = 0.5 (RV1: λ_b, RV2: λ_c)
- Ratio of capping to yield moment (M_c/M_y); COV = 0.1 (RV3: $(M_c/M_y)_b$, RV4: $(M_c/M_y)_c$)
- Plastic rotation (θ_p); COV = 0.6 (RV5: θ_{p_b}, RV6: θ_{p_c})
- Post-plastic rotation (θ_{pc}); COV = 0.6 (RV7: θ_{pc_b}, RV8: θ_{pc_c})

A total of 25 LHS-based samples were drawn for each frame and combined with IDA analysis using 44 ground motions. This results in 1,100 single-record IDA curves for each frame. The seismic intensity measure capacity, IM^c, is identified for all IDA curves which correspond to the failure point. Figures 34(a) and 34(b) present two matrices showing the IM^c for the four-story and eight-story frames. These matrices, indeed, illustrate the sensitivity of failure capacity to three main factors: modeling randomness, ground motion record-to-record variability, and the frame type (or height). In general, there is no explainable pattern in IM^c showing the importance of ground motion RTR variability when it is combined with modeling/material randomness.

For each of the forty-four ground motion records, the sensitivity of collapse capacities was computed with respect to eight input RVs. The linear correlation assumption was used.

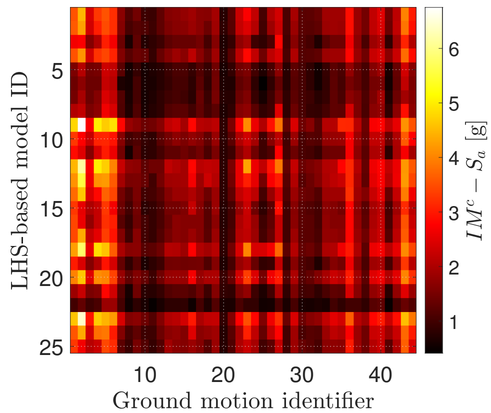

(a) Capacity points; 4-story frame

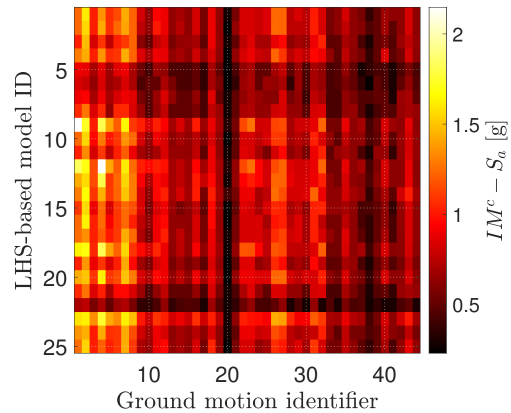

(b) Capacity points; 8-story frame

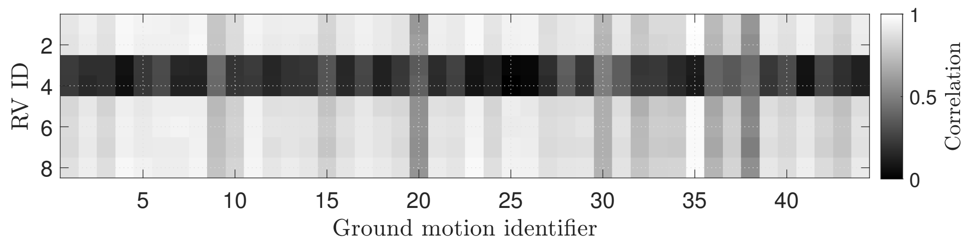

(c) Linear correlation index; 4-story frame

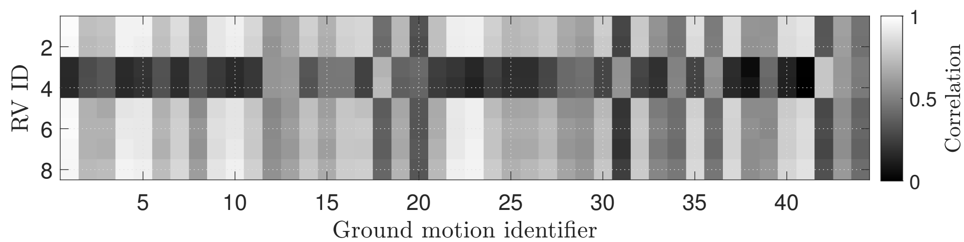

(d) Linear correlation index; 8-story frame

Fig. 34. Sensitivity of collapse capacity to ground motion and modeling uncertainty including their linear correlation with input RVs; modified from [15]

Let us assume that for a sampling of the input random vector $\mathscr{X} = \left\{\boldsymbol{x}^{(1)}, \boldsymbol{x}^{(2)}, \ldots, \boldsymbol{x}^{(N)}\right\}$, the corresponding model response is $\mathscr{Y} = \left\{y^{(1)}, y^{(2)}, \ldots, y^{(N)}\right\}$. The input-output (I-O) correlation is computed using a linear correlation coefficient between ith input and the output:

$$\rho_{I-O}^{i} \overset{\text{def}}{=} \rho\left(X_i, Y\right) = \frac{\mathbb{E}\left[\left(X_i - \mu_i\right)\left(Y - \mu_Y\right)\right]}{\sigma_i \sigma_Y} \tag{22}$$

where $\mu_i \overset{\text{def}}{=} \mathbb{E}\left[X_i\right]$, $\mu_Y \overset{\text{def}}{=} \mathbb{E}\left[Y\right]$, and σ_i and σ_Y are the standard deviations.

To evaluate the sensitivity of IM^c, each column in Figure 34(a) (or Figure 34(b)) was assumed to be $y^{(i)}$ (a vector of 25×1), while the $\mathscr{X}$ is the 25×8 matrix of LHS-based input RVs. This means that sensitivity indices are computed separately for each ground motion record. For a particular ground motion record, the sensitivity indices are recorded in an 8×1 vector, while the results of all ground motions are recorded in an 8×44 matrix, See Figures 34(c) and 34(d). According to these figures, the impact of input RVs on IM^c of four- and eight-story frames is different. For the four-story frame, RV3 and RV4 are the least sensitive variables, while all other six RVs have a much higher sensitivity index. In the case of the eight-story frame, again RV3 and RV4 have minimum sensitivity index; however, depending on the ground motion's inherent characteristics, the sensitivity matrix is very heterogeneous. It seems that a combination of different modeling uncertainties with ground motion records has a completely different local impact on the structural system (as seen in multiple plots of Figure 34).

4.5. Sensitivity for Strengthening and Rehabilitation

Sensitivity analysis can be used to evaluate the performance of the rehabilitated and strengthened RC components or frames using fiber-reinforced polymers (FRP). Sensitivity results can be used as a metric to assess the effectiveness of strengthening or to compare different rehabilitation strategies [125]. Sensitivity assessment can be limited to OAT methods and parametric studies [126], or they can be obtained from a surrogate model [127].

Coronado and Lopez (2006) [128] conducted a series of sensitivity analyses on FRP-strengthened RC beams with respect to concrete properties such as tensile strength, fracture energy, tension softening, compression model, and angle of dilatancy. In each case, the load-displacement curves were developed. They showed that depending on the failure mode, the material RVs can be significant or not. For example, for the beam failing by concrete crushing, the tensile strength and fracture energy are not important. However, for the beam failing by plate debonding, they play an important role. For continuous variables, they used three options (similar to the Tornado diagram), and for categorical ones, they used two/three options.

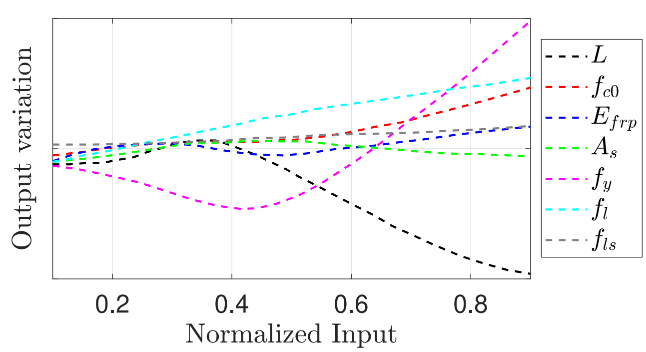

Fig. 35. Sensitivity analysis in the context of structure strengthening; adapted from [16]

Naderpour (2019) [16] performed a sensitivity analysis to estimate the capacity of FRP-strengthened circular RC columns. First, an adaptive neuro-fuzzy inference system was developed. Next, the sensitivity analysis was conducted by varying an RV OTA in its normalized range from 0.1 to 0.9 and keeping others in their median value. Figure 35 illustrates the sensitivity analysis for seven RVs: column height (L), maximum axial compressive strength of unconfined concrete (f_{c0}), modulus of elasticity of FRP (E_{frp}), the total area of longitudinal bars (A_s), yield strength of longitudinal steel (f_y), confinement pressure provided by FRP (f_l), and confinement pressure provided by transverse steel (f_{ls}).

4.6. Sensitivity of Progressive Collapse Assessment

According to ASCE/SEI 7 [129], progressive collapse is defined as "the spread of an initial local failure from element to element, which eventually results in the collapse of an entire structure or a disproportionately large part of it." The initial damage can be due to a variety of accidental events such as gas explosion, vehicular collision, blast, tornado, or other extreme loads [130]. Typically, a probabilistic analysis is required to properly capture the extent of collapse and provide a basis for risk management. As a companion to probabilistic performance assessment, sensitivity analysis provides useful information about the most affecting factors.

As discussed in Yu et al. (2017) [101] (see Section 3 and Figures 24(a) and 24(h)) progressive collapse can be modeled by column loss approach which significantly affects the results of Tornado diagram. A similar element removal study in RC frames has been reported by [88] and discussed in Figure 2(h). Farahani et al. (2018) [131] used the results of sensitivity analysis to identify the most critical elements within the RC structures whose elimination can trigger the collapse. They also modified the conventional pushdown analysis method by loading the entire structure gradually. They provided some recommendations on the location of more sensitive columns based on the size, and height of the structures.

Parisi et al. (2019) [17] discussed the results of a multilevel sensitivity analysis to characterize the progressive collapse capacity of a class of modern RC buildings. Two sensitivity scenarios are considered: (I) ultimate load capacity and corresponding maximum and residual drifts to the ultimate steel strain, and (II) location of column removal. Moreover, five performance limit states associated with increasing levels of damage are accounted for. A total of five key RVs were considered for what concerns material and geometrical properties:

- Compressive strength of concrete (f_c); COV = 0.1
- Yield strength of steel reinforcement (f_y); COV = 0.1
- Span length of primary beams (L_x); COV = 0.2
- Span length of secondary beams (L_y); COV = 0.2
- Longitudinal reinforcement ratio of primary beams (ρ); COV = 0.05

Figure 36 illustrates the Tornado diagram for different limit states. Results indicate high sensitivity to the ultimate steel strain, column location in plan, beam span, and yield steel strength. Mucedero et al. (2020) [132] also conducted a multi-level sensitivity study highlighting the role of inelastic material models in the assessment of the progressive collapse performance of RC buildings. Sensitivity to uneven application of the downward load and boundary conditions at the base of the reference structure, together with its geometry/asymmetry and material properties were also investigated. Results of sensitivity analysis were presented in the form of load-displacement curves for a middle column by gradually increasing or decreasing the values of one random variable and keeping others constant. Finally, the statistics are computed for some limit states such as yielding and crushing. A similar approach is also reported by [133] for different RC components, e.g., beams and walls.

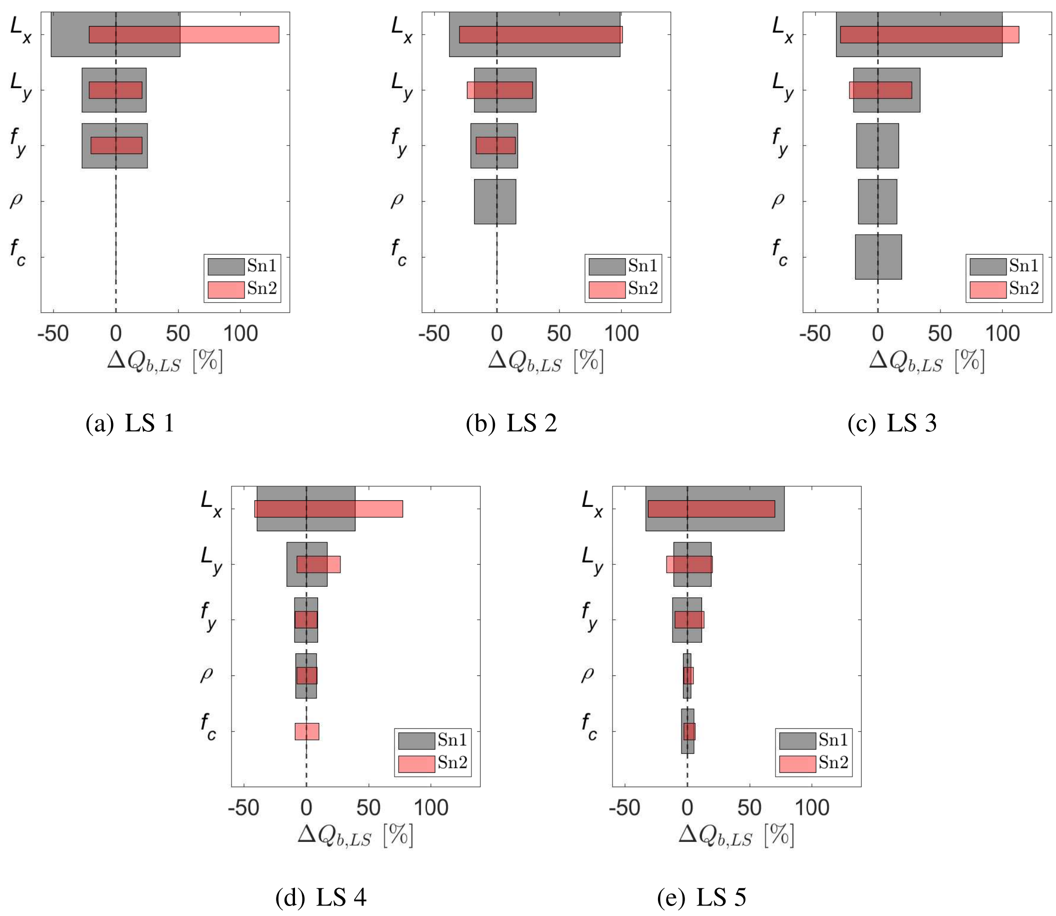

(a) LS 1

(b) LS 2

(c) LS 3

(d) LS 4

(e) LS 5

Fig. 36. Tornado diagrams of load capacity under two column removal scenarios (i.e., Sn1 and Sn2) for various limit states; adopted from [17]

4.7. Sensitivity for Life Cycle Analysis

While most of the sensitivity studies on RC structures are limited to a particular seismic scenario, this concept can be investigated in a more broad framework of life cycle analysis (LCA). An LCA is a tool to analyze the environmental impacts of a building, from construction to end-of-life; thereby identifying ways to reduce those impacts [134]. Such a comprehensive assessment requires many input parameters, which may be uncertain. A group of studies aims to determine the sensitivity of the real environmental impact according to aspects related to decisions made during the execution stage [135–140]. Sensitivity analysis can be integrated with LCA to identify the most appropriate material for construction purposes [141].

Groen et al. (2014) [142] compared seven sensitivity analysis methods (one-at-a-time, matrix perturbation, method of elementary effects, Taylor expansion, standardized regression coefficients, random balance design, and Sobol sensitivity index) applied to three types of case studies: a linear system, a nonlinear system, and a large linear system with large input uncertainties. Overall, they recommended the perturbation method for local sensitivity and the Sobol method for global sensitivity analysis.

Ferreiro-Cabello et al. (2017) [143] investigated the sensitivity of factors during the LCA and beyond the control of the planner or designer, e.g., distance traveled for component transport, working hours, and materials wasted during the production and construction process. Six different scenarios were studied and found that hourly yield had a minimal effect on the generated environmental impact. Sensitivity analysis was conducted by a simple parametric model evaluation.

Larsson et al. (2019) [18] provided an overview of different uncertainty sources in LCA of infrastructure projects and evaluated their influence on the results using the sensitivity analysis. They showed that besides the influence of uncertainty in emission factors, parameters such as material amounts and service life play a significant role in the variability of model output. They used variation mode and effect analysis (VMEA) for sensitivity analysis and uncertainty quantification. The quantitative form of VMEA entails a linearization of the limit state function around a nominal point, and in that respect, VMEA is equivalent to FOSM. Two measures were considered: Global Warming Potential (GWP), expressed in tonnes of CO2-equivalent, and Cumulative Energy Demand (CED), expressed in Gigajoules. Sensitivity analysis was implemented on an RC bridge. Figure 37 illustrates the results of the local sensitivity analysis of the outputs GWP/year and CED/year for the bridge LCA model. Moreover, they performed a global sensitivity analysis using the Monte Carlo method and concluded that it is similar to Tornado diagram when including uncertainties for emission factors and material amounts.

Van-Loc et al. (2018) [19] conducted a sensitivity analysis to establish the relationship between service life and design parameters and environmental exposure conditions for RC structures. An application is implemented on RC structures exposed to carbonation. The following eleven input RVs were considered:

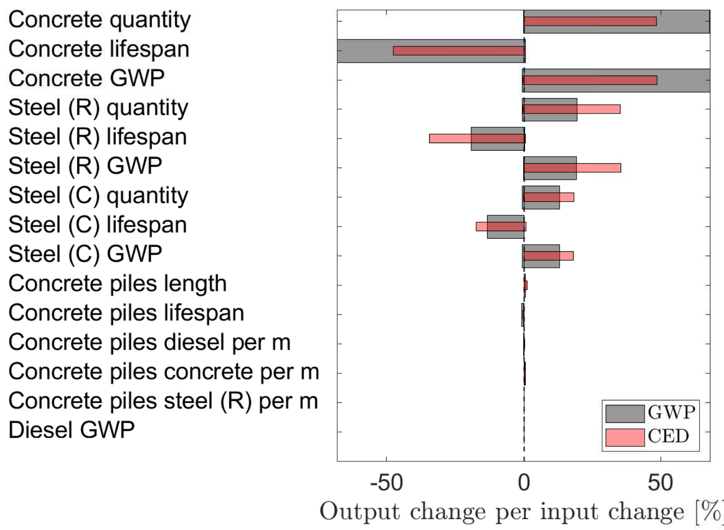

Fig. 37. Sensitivity analysis an RC bridge in the context of life cycle analysis; adapted from [18]

- Concrete mix
  - Cement content (C)
  - Water-to-cement ratio (W/C)
  - Sand-to-gravel ratio (S/G)
  - Maximum aggregate size (S_{max})
- Cement
  - Cement type (CEM)
  - Cement strength class (f_{cem})
- Concrete cover depth and initial curing period
  - Concrete cover depth (d)
  - Initial curing period (t_c)
- Environmental parameters
  - Temperature (T)
  - Relative humidity (RH)
  - CO2 concentration in the air (CO_2)

They used two sensitivity analysis methods: Sobol technique [144] and Morris method [145]. For Sobol method, sensitivity is reported based on first order, S_j, and total, S_{T_j}, indices. Moreover, Morris method presents the sensitivity based on the mean value of the elementary effects, μ_j, the absolute value of mean values, μ_j^*, and standard deviation of the elementary effects, σ_j. The relative sensitivity indices are illustrated in Figure 38. The most influential design parameters obtained are f_{cem}, W/C, and CEM. Overall, there is a good agreement between the two sensitivity analysis methods.

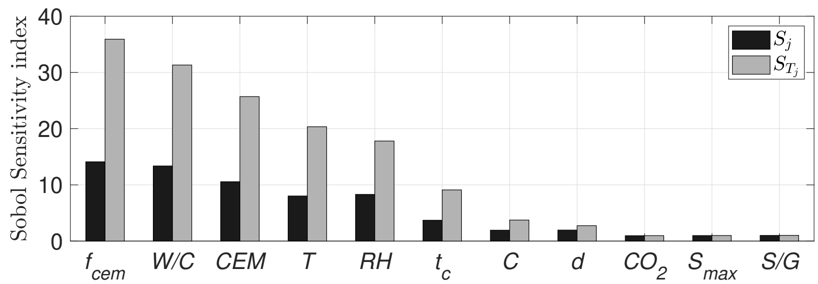

(a) Sobol method

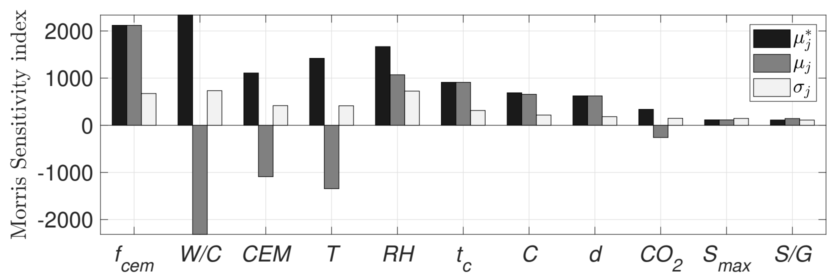

(b) Morris method

Fig. 38. Sensitivity indices of eleven RVs for LCA of RC structures exposed to carbonation; adopted from [19]

4.8. Sensitivity for Optimality in Design and Construction

As discussed before, sensitivity analysis can be used both in the framework of design and analysis. Design sensitivity analysis calculates the gradients of the objective and constraint functions with respect to design variables [146]. This includes (but is not limited to) evaluating the sensitivity of the performance measures with respect to product performance, failure probability, and construction cost. In structural engineering and mechanics, the sensitivity analysis is typically used for structural design optimization [147] with various linear and nonlinear (both material and geometric) formulations [148–150].

Sensitivity analysis has been used in various aspects of RC frames design to improve the optimal design algorithm, to control the performance objective, or to determine the sensitivity of the solution of the optimization to changes in the cost function parameters [151]. Martins et al. (2020) [152] used a sensitivity analysis with a discrete direct method to compute the sensitivities of the design objectives, the allowable values of which are dependent on the design variables. Other examples of parametric-sensitivity analysis on RC structures can be found in [153]. [154] used the results of both local and global sensitivity analysis methods to determine the contributing factors in a complex multi-parameter Bouc-Wen-Baber-Noori model. This model is used to characterize the RC columns's failure in different modes using a multi-objective optimization algorithm.

4.9. Sensitivity of RC Frames in Presence of Infill

The majority of papers discussed in Section 3 have been focused on sensitivity analysis of material and/or modeling variables in RC frame structures. However, a large percentage of RC frames includes either RC shear walls or infills (concrete or masonry). This, indeed, opens the doors for a new series of sensitivity analyses to understand the overall of this hybrid system and reevaluate the sensitive variables in the presence of another highly uncertain structural system. A detailed example of this type of sensitivity was discussed already in [10] and Figures 23(a) to 23(c). Sensitivity analysis of RC frames including masonry infill [155–158] and RC walls [159] have been investigated already. [160] discussed sensitivity analysis in the context of seismic performance of ancient mixed masonry-RC buildings.

Ricci et al. (2012) [2] conducted a very comprehensive study on the impact of infill in various sensitivity responses of RC frames. First, a series of parametric studies were designed, as shown in Figure 39. Next, Tornado diagrams were generated for each one. The parametric studies include: two design approaches (gravity load design – GLD – and seismic load design – SLD), number of stories (4 and 8), infill condition (bare frame, pilotis – the first story is bare and upper stories are infilled – and uniform – infill panels are uniformly distributed along the height), direction (X and Y), limit states (damage limitation – DL – and near collapse – NC), six RVs as discussed below:

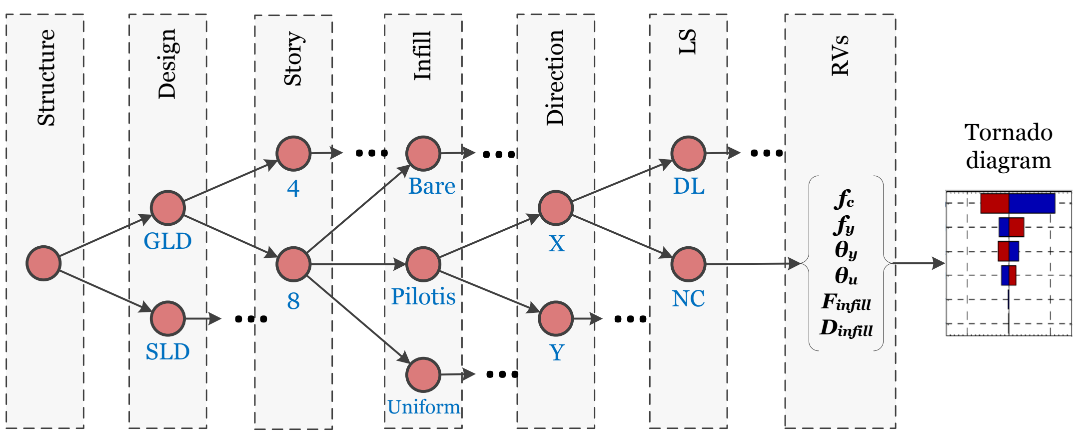

Fig. 39. Parametric sensitivity analysis RC frames in presence of infill; developed based on [2]

- Concrete compressive strength (f_c); COV^{SLD} = 0.2; COV^{GLD} = 0.31
- Steel yield strength (f_y); COV^{SLD} = 0.06; COV^{GLD} = 0.08
- Chord rotation at yielding in RC members (θ_y); COV = 0.33
- Chord rotation at ultimate in RC members (θ_u); COV = 0.41
- Loads of load-displacement relationship of the infill trusses (F_{infill}); COV = 0.3
- Displacements of load-displacement relationship of the infill trusses (D_{infill}); COV

= 0.3-0.7

Overall, 48 Tornado diagrams have been developed based on the design in Figure 39. A summary of observations about the influence of infill on sensitivity analysis of RC frames is collected in Tables 2 and 3 based on gravity and seismic design methods, respectively.

Table 2. Impact of infill on the sensitivity of RC frames based on gravity design; collected from [2]

	RV	LS	Remarks
14*RC	2*θ_u	NC	parameter with the greatest influence in each case; if it increases, collapse ductility and PGA$_{NC}$ increase
		DL	no significant influence
	2*θ_y	NC	no significant influence
		DL	achievement of DL LS is generally due to infills, if they are present in the model; for bare configurations, an increase in θ_y produces an increase both in displacement capacity and T_{eff} of the equivalent SDOF, thus resulting in no change of PGA$_{DL}$
	2*f_c	NC	when it increases, the axial load ratio in columns decreases and θ_u increases; consequently ductility at collapse and PGA$_{NC}$ increase
		DL	no significant influence
	2*f_y	NC	no significant influence
		DL	parameter with the greatest influence for bare configurations due to an increase in base shear strength C_s and displacement capacity Δ_{DL}; not important for infilled configurations when achievement of DL LS is due to infills
12*Infill	2*F_{infill}	NC	great influence on uniformly infilled configurations through the variation of collapse mechanism (i.e. 8-story structures), of maximum strength $C_{s,\max}$ and of T_{eff}; its influence is smaller than θ_u and it is different depending on the case-study structure
		DL	its influence is higher for Uniformly Infilled configurations rather than for Pilotis ones; in both cases, if it increases a beneficial decrease in T_{eff} is produced, thus resulting in an increase in PGA$_{DL}$
	2*D_{infill}	NC	except for variation of collapse mechanism (i.e., eight-story-Uniformly Infilled-longitudinal direction), when it increases the yielding displacement of the equivalent SDOF S_{dy} increases too, whereas the maximum strength $C_{s,\max}$ and the displacement capacity Δ_{col} do not change, then ductility at collapse and PGA$_{NC}$ decrease
		DL	except for the four-story-Pilotis-longitudinal direction case-study structure, if it increases T_{eff} increases and displacement capacity Δ_{DL} increases more than yielding displacement of the equivalent SDOF S_{dy}, and so collapse ductility and PGA$_{DL}$ increase

Table 3. Impact of infill on the sensitivity of RC frames based on seismic design; collected from [2]

	RV	LS	Remarks
18*RC	2*θ_u	NC	parameter with the greatest influence in each case; if it increases, collapse ductility and PGA_{NC} increase
		DL	no significant influence
	2*θ_y	NC	it becomes important just in one case study (i.e. eight-story-Uniformly Infilled-longitudinal direction) where, if it increases, a change in the collapse mechanism is produced and PGA_{NC} increases
		DL	achievement of DL LS is generally due to infills, if they are present in the model; for Bare configurations, an increase in qy produces an increase both in displacement capacity and T_{eff} of the equivalent SDOF, thus resulting in no significant change in PGA_{DL}.
	2*f_c	NC	when it increases, the axial load ratio in columns decreases and qu increases; consequently ductility at collapse and PGA_{NC} increase
		DL	only in one case (i.e. 4 stories-Uniformly-Infilled-longitudinal direction), if it increases, an increase in base shear strength C_s is observed, thus leading to a beneficial decrease in T_{eff}
	2*f_y	NC	important only for Pilotis configurations (i.e. 4- and 8- stories-Pilotis-longitudinal direction, 8 stories-Pilotis-transverse direction) where its change produces a variation of collapse mechanism
		DL	parameter with the greatest influence for bare configurations due to an increase in base shear strength C_s and displacement capacity Δ_{DL}; not important for infilled configurations when achievement of DL LS is due to infills
11*Infill	2*F_{infill}	NC	except for variation of collapse mechanism, when it increases, the yielding displacement of the equivalent SDOF S_{dy} decreases and the maximum base shear strength $C_{s,\max}$ increases
		DL	except for variation of collapse mechanism in which displacement capacity Δ_{DL} decreases (i.e., four-story-Pilotis-longitudinal direction), if it increases, an increase in base shear strength C_s and a decrease in S_{dy} are produced, thus leading to a higher ductility capacity and PGA_{DL}
	2*D_{infill}	NC	when it increases, the yielding displacement of the equivalent SDOF S_{dy} increases too, whereas the maximum strength $C_{s,\max}$ and the displacement capacity Δ_{col} do not change, and then ductility at collapse and PGA_{NC} decrease
		DL	except for variation of collapse mechanism (i.e. four-story-Pilotis-longitudinal direction), if it increases T_{eff} increases and displacement capacity Δ_{DL} increases more than yielding displacement of the equivalent SDOF S_{dy}, then ductility at collapse and PGA_{DL} increase

4.10. Sensitivity in Fundamental Period of RC Structures

Estimation of the fundamental period in reinforced concrete structures is an essential task during the initial design stage. Design guidelines provide a simple closed-form equation for a fundamental period as a function of height, i.e., $T = ah^b$. However, many researchers have shown that other variabilities contribute to the effective estimation of the fundamental period. Sensitivity analysis can be used to identify the importance of these variables, and possibly reduce the functional model [161–163].

Kose (2009) [164] proposed a neural network (NN) based sensitivity analysis on the parameters affecting the fundamental period of RC buildings with infill walls. They showed that building height, and percent of the shear wall are the most sensitive RVs, while the percentage of infill wall, number of bays, and frame type have less impact. Asteris et al. (2015) [165] performed a sensitivity analysis on parameters affecting the fundamental period of infilled RC frame structures. They developed a Tornado-like diagram comparing eleven model parameters for eight and fourteen-story frames and concluded that equivalent strut width significantly affects the estimation of the fundamental period. Somala et al. (2021) [20] used a shapely additive explanation to identify the contribution of each RV in the prediction of the fundamental period in masonry-infilled RC frames. Figure 40 presents a sample plot showing the sensitivity of output as a function of five input RVs.

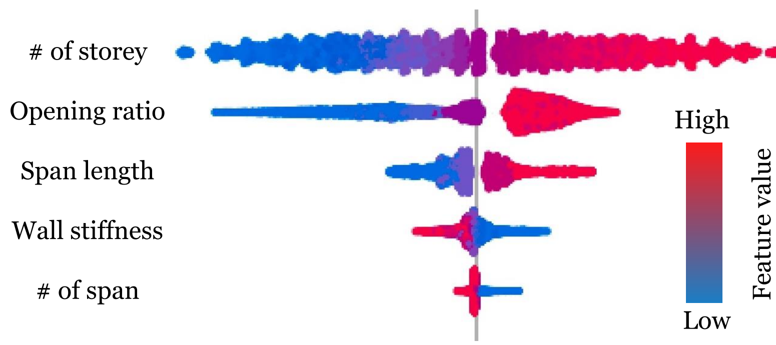

Fig. 40. Sensitivity analysis RC frames period by shapely additive explanation; adapted from [20]

4.11. Sensitivity Analysis for Failure Mode Detection

Failure mode identification is an important task in the seismic analysis of RC frame structures. The dominant failure mode of an RC beam-column element depends on multiple factors such as axial load, reinforcement detailing, aspect ratio, etc. [166]. Major failure modes for RC members are purely flexural, shear, or flexure-shear (and axial failure is a minor failure mode). Identification of dominant failure modes can be achieved by classical regression methods or more effectively using the machine learning approaches discussed in Section 4.12. Failure modes can be predicted or classified depending on the objectives of the project at hand. In either case, sensitivity analysis provides useful information about the importance of the variables in regression and classification tasks.

Failure (mode) analysis is not limited to concrete structures subjected to an external stressor (e.g., static force, or ground motion acceleration), and can be studied under various environmental conditions (e.g., material deterioration and climate change), or even other dynamic loading scenarios. For example, Guo et al. (2021) [167] conducted a global sensitivity analysis using polynomial chaos expansion on corroded RC structures. Roy and Matsagar (2021) [168] also applied the sensitivity analysis for RC structures subjected to blast loading.

Mangalathu and Jeon (2018) [169] used a series of machine-learning algorithms to classify the failure modes and predict the shear strength at RC beam-column joints. A lasso regression analysis [170] is also used to identify the relative importance of input variables on the joint shear strength. They showed that design joint shear stress is the most influential variable for the failure mode, followed by concrete compressive strength, and in-plane joint geometry. Mangalathu et al. (2020) [171] also used the machine learning idea for failure mode identification in RC shear walls. A random Forest model was used to determine the relative importance variables affecting failure mode. They reported that the aspect ratio, boundary element reinforcement indices, and wall length-to-wall thickness ratio are the critical factors, while the cross-section shape has less influence on failure modes. These two papers were followed by [172] in which the ensemble machine learning algorithms were used to classify the failure modes in RC columns. Manoj et al. (2020) [173] compared several machine learning algorithms in failure mode prediction of RC infilled frames with ten material and physical variables.

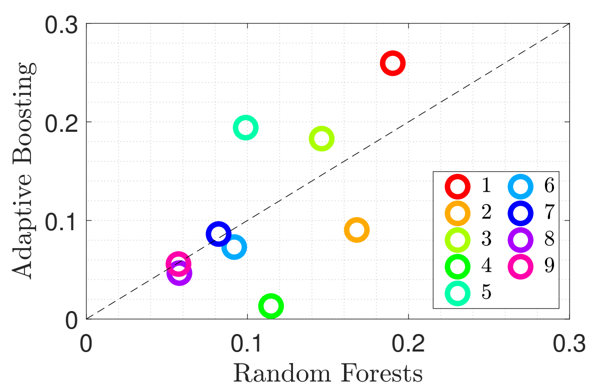

Fig. 41. Comparison of sensitivity analysis methods applied to failure mode identification; data (colored circles) collected from [21]

Huang and Burton (2019) [21] used a series of six machine learning algorithms to classify the in-plane failure modes in RC frames including infill. A database of 114 specimens was used including nine input RVs. Failure modes were considered to be: infill sliding and column flexural hinging (SF), infill sliding and column shear failure (SS), infill crushing and column flexural hinging (CF), and infill crushing and column shear failure (CS). They developed the importance variable charts using two algorithms: random forests and adaptive boosting algorithms. The importance score for each feature is evaluated according to the ability of that feature to reduce the impurity index, averaged over all base trees [170]. Figure 41 compares the consistency of two methods to identify the importance score. While the rank #1 RV is identified correctly in both methods, there is a considerable difference in other identified important RVs.

4.12. Machine Learning-Based Sensitivity Analysis

As discussed in the Introduction section, the sensitivity analysis methods can be classified into local and global ones. Most of the global sensitivity analysis techniques use the concept of surrogate meta-modeling or machine learning methods to identify the most influential random variables. Machine learning is a specific type of artificial intelligence that "learns" as it identifies new patterns in data and creates strategies to improve decision-making based on information hidden in huge data sets [23]. Both the regression and classification tasks in machine learning can be used for sensitivity analysis purposes. There are three main learning algorithms: supervised learning, unsupervised learning, and semi-supervised learning [174]. Figure 42 highlights several machine learning classes and subclasses.

It is important to note that machine learning-based sensitivity analysis is not the main theme of this report. Therefore, the detailed methods are not discussed (similar to Section 2 for other techniques). This sub-section is meant to provide a few relevant examples of such an application in the structural analysis of RC frames. Also, note that there are a large number of machine learning publications to determine the optimal concrete mix design, or to estimate the concrete strength and stiffness from different combinations. All such papers do not belong to this review as their scope is mainly at the material level and not the structural level.

Jeon et al. (2014) [175] developed some statistical models based on multiple linear regression (MLR), multivariate adaptive regression splines (MARS), and symbolic regression (SR) techniques to estimate the shear strength of RC beam-column joints. The measure of importance (a.k.a. sensitivity) for the term is the amount of increase in the residual squared error of the model fit upon the removal of the term from the regression model. They proposed such importance values based on standard deviation and generalized cross-validation for the MARS model based on ANOVA (analysis of variance) decomposition.

Gharehbaghi et al. (2020) [24] developed a predictive model for the inelastic seismic response of RC frames using a wavelet support vector machine (SVM) and a NN. A parametric sensitivity analysis was used for causal inference to evaluate the importance of each input RV. They computed a sensitivity metric very close to OAT technique, in which the sensitivity ratio for j-th RV is calculated as a ratio of swing in that RV to the summation of all swings. Figure 43 presents such sensitivity results based on SVM and NN techniques. Overall, they claimed that NN-based predicted EDPs are less sensitive to the inputs than SVM-based ones.

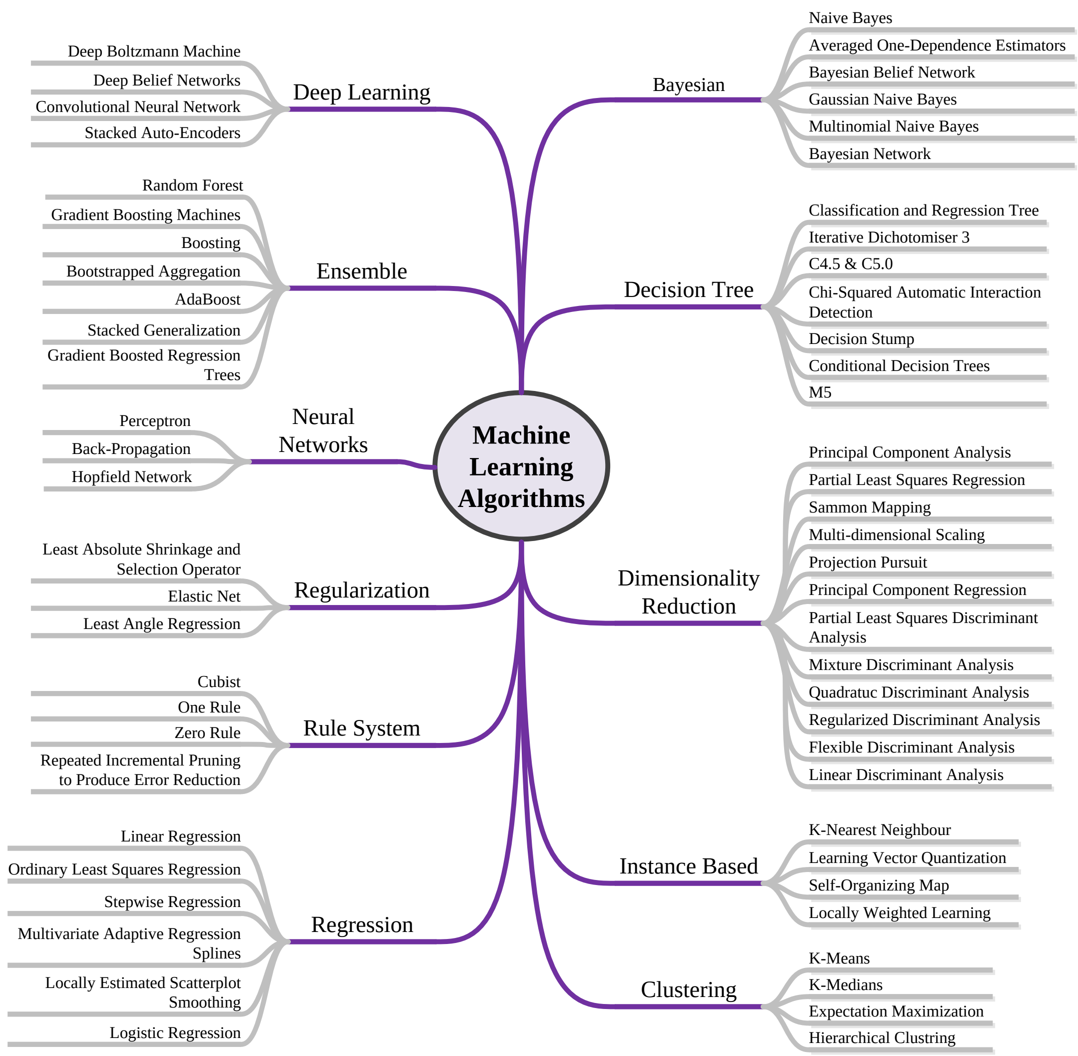

Fig. 42. A summary of machine learning algorithms; adopted from [22, 23]

Cao et al. (2017) [176] proposed an ensemble NN framework for sensitivity analysis of fracture failure in a notched concrete beam. In this approach, a series of superior NNs are developed independently and the overall sensitivity is assessed by averaging the sensitivity analysis in individual NNs. [177] developed an ANFIS model to predict the drift in RC frames and the coefficient of determination, R^2, is used as a metric for sensitivity analysis. [178] conducted a Gene expression programming (GEP) based meta-modeling and sensitivity analysis on exterior RC joints subjected to monotonic and cyclic loads. After developing the meta-model, they simply varied one of the variables at-a-time in its potential range of numbers and calculated the system response. They made some qualitative evaluations on the accuracy of these trends with respect to existing experimental results.

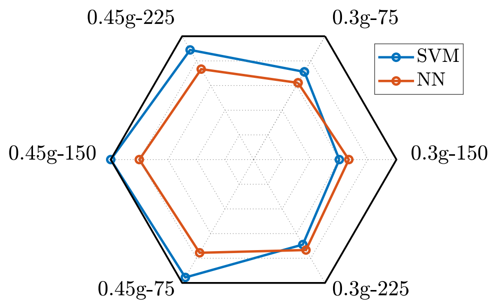

(a) EDP2; T1

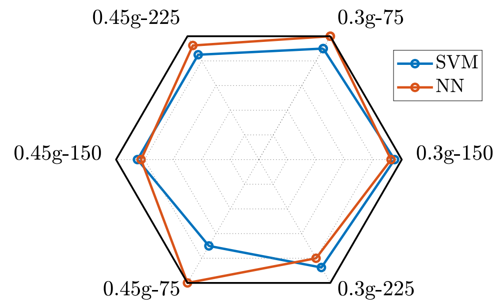

(b) EDP2; T2

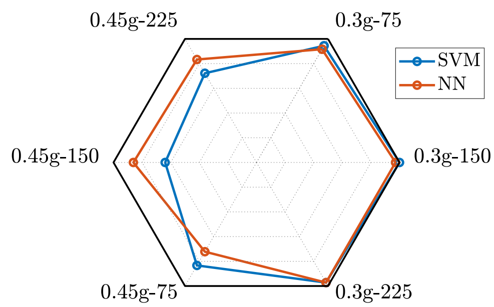

(c) EDP2; T3

Fig. 43. Mean sensitivity indices of EDPs to input variables (T_1, T_2 and T_3) based on two machine learning techniques; Two seismic level and three sample size are used; adopted from [24]

Hwang et al. (2021) [25] presented a machine learning-based methodology for predicting the seismic response and structural collapse classification of ductile RC buildings accounting for modeling uncertainties. They used both regression-based and classification-based approaches. Sensitivity analysis was conducted using extreme gradient boosting (XGBoost) algorithm [179]. The following RVs were considered for sensitivity analysis:

- Effective elastic stiffness in beams and columns (K_e^B, K_e^C)
- Pre-peak plastic rotation in beams and columns ($\theta_{p,B}$, $\theta_{p,C}$)
- Post-peak plastic rotation in beams and columns $\theta_{pc,B}$, $\theta_{pc,C}$)
- Effective yield moment strength in beams and columns ($M_{y,B}$, $M_{y,C}$)
- Post-yield (maximum) strength ratio in beams and columns ($(M_c/M_y)_B$, $(M_c/M_y)_C$)
- Column footing rotational stiffness (K_f)
- Energy dissipation capacity in beams and columns (λ_B, λ_C)
- Critical damping value (ξ)
- First-mode spectral acceleration (S_a)
- Fundamental period of the structure (T_1)
- Drift. Note: Only used for collapse response sensitivity

Figure 44 illustrates the results of sensitivity analysis on two frames and two targets using the XGBoost algorithm. As seen, depending on the frame type and the required response, the importance variables change drastically.

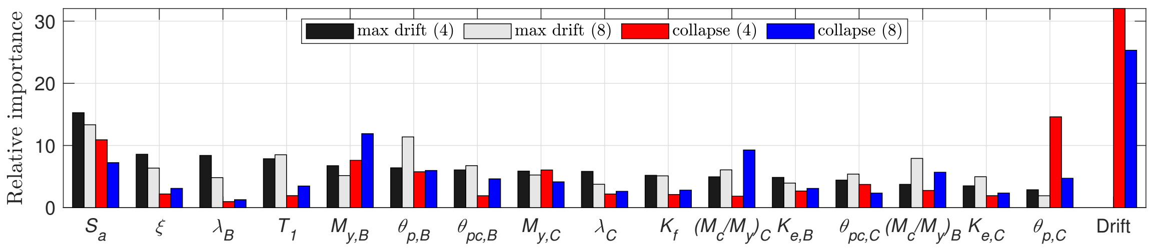

Fig. 44. Sensitivity analysis by XGBoost machine learning technique; adapted from [25]

Hariri-Ardebili et al. (2022) [26] presented a Random Forest-based machine learning methodology to identify the most sensitive variables that can be used for model reduction. They also examined the applicability of a surrogate meta-model which accelerates the performance assessment process using only a small portion of initial simulations. An RC bridge column was used as the case study, and a series of probabilistic moment-curvature analyses were conducted with OpenSees. The moment corresponding to the first steel fiber yield strain was identified as M_y^{1st}. Three additional points were identified corresponding to 10%, 20% and 30% of steel fiber yielding as $M_y^{10\%}$, $M_y^{20\%}$, and $M_y^{30\%}$. Finally, the curvature values corresponding to those four yield moments were also calculated for each realization.

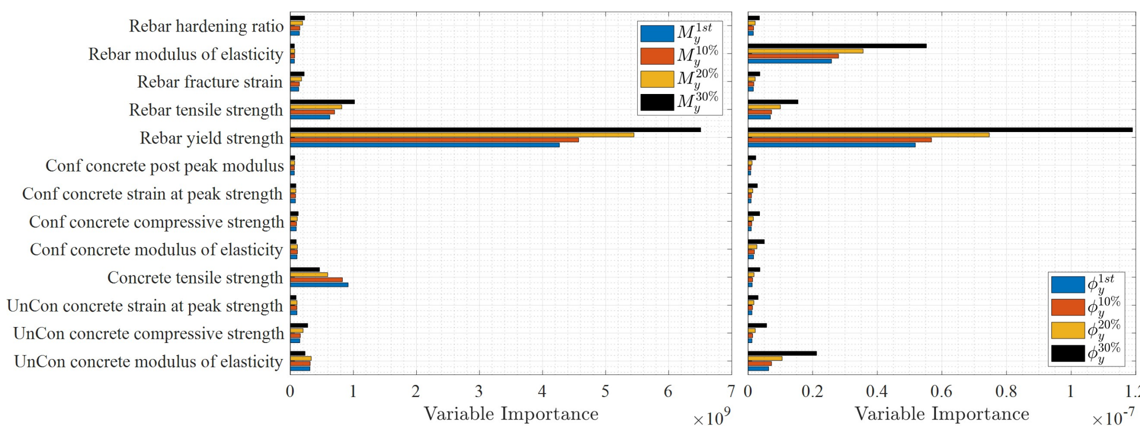

Fig. 45. Sensitivity analysis by random forest technique; adopted from [26]

A total of thirteen RVs were used for modeling all of them related to the concrete and steel mechanical properties. A full list of these RVs can be found in 3.21. Figure 45 illustrates the sensitivity of the moment and curvature values to different RVs. As expected, rebar yield strength is the most sensitive RV. For the yield moments, it is followed by rebar tensile strength, and concrete tensile strength (in reverse order for different yielding representations). For the yield curvature, the rebar yield strength is followed by rebar modulus of elasticity, steel peak tensile stress, and finally, unconfined concrete modulus of elasticity.

5. Discussion

5.1. Comparison of Sensitivity Analysis Techniques

In Section 2, comprehensive classification is provided on the conventional and widely-used sensitivity analysis techniques in structural and earthquake engineering (neglecting a deep discussion on global sensitivity analysis techniques). Also, multiple cases were shown where the results of two sensitivity analysis techniques were compared.

Several publications compare the sensitivity analysis technique to evaluate the performance of a structural system. These comparisons can be categorized into the following major groups, with the results of comparison producing different conclusions given special characteristics of the case study structure, the applied load, and the sensitivity analysis method.

5.1.1. Category-I: OAT Tornado diagram vs. FOSM

Both these techniques have similar computational demands, and they yield a close (if not the same) sensitivity ranking in most cases. However, the relative value of the swings is different in many cases. This means that although both methods may reveal that, for example, RV X_i is sensitive compared to X_j, the relative sensitivity might change a lot. Examples of such a comparison can be found in [67, 96, 98] for RC structures, [40] on port structures and soil properties as RVs (where a similar trend is reported), and [44] on gravity quay walls.

El-Din and Kim (2014) [180] compared FOSM and OAT Tornado for pile-founded fixed steel jacket platforms using both maximum top drift (MTD) and maximum inter-story drift ratio (MIDR). Results show some similarity using MIDR; however, there are some discrepancies in using MTD. [181] reported that the importance order of RVs obtained from Tornado diagram slightly differs from FOSM method for RC frames. A larger swing difference was observed for the strength-related RVs. [48] performed detailed Tornado and FOSM sensitivity analyses on a pile-supported wharf with a large number of RVs, and three QoIs. Figure 46 presents the extracted data from original drawings and replotted in a comparative mode for each QoI. According to these new plots, there is a strong linear correlation between FOSM percentage of COV contribution and Tornado swing values. Also, the ranking highly depends on the selected QoI.

5.1.2. Category-II: OAT Tornado diagram (or FOSM method) vs. MCS family

Such a comparison aims to (1) understand the shortcomings of the simple methods compared to the most comprehensive one, and (2) recommend the usage of simplified methods if they provide good enough results compared to the MCS family. [41] compared FOSM

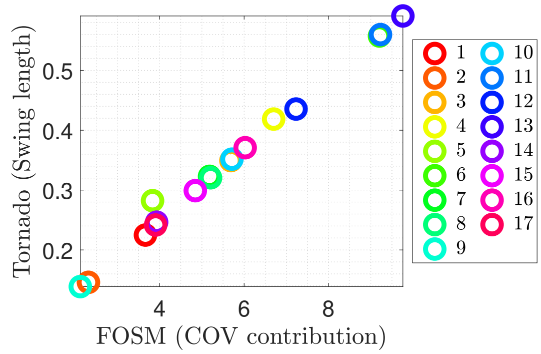

(a) Displacement ductility factor

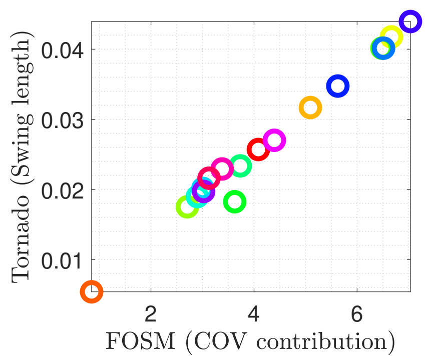

(b) Normalized residual H. displacement

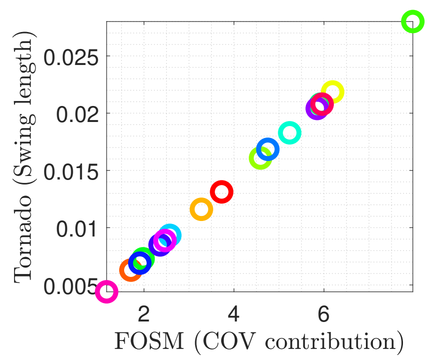

(c) Differential settlement

Fig. 46. Detailed comparison of FOSM and Tornado for a high-RV system under dynamic excitation

and MCS for sensitivity analysis in tunnel face stability in the presence of data scarcity (and reported a similar trend).

Kim et al. (2011) [182] investigated the sensitivity of steel buildings subjected to column loss using MCS, Tornado diagram, and FOSM methods. They reported the same trend with very close swing values among the three methods. [38] compared Tornado diagram and MCS for a steel moment-resisting frame with hysteretic energy dissipation devices. A similar ranking with slightly different swings is reported. [42] compared FOSM and MCS for reinforced masonry buildings based on a large database of collected data. They reported a similar level of prediction. [108] compared three methods of Tornado diagram, confidence factor, and fully probabilistic one and obtained the same ranking with slightly different values. [183] compared FOSM and MCS methods on a 3D RC frame structure. For finite element analysis the solution was also compared based on the direct differentiation method, with feed-forward/backward finite difference algorithm and their sensitivity was studied on the dispersion of results. It is found that FOSM approximation using the direct differentiation method for computing response sensitivities provides, at very low computational cost, very good estimates of the mean and standard deviation of the response quantity for low-to-average levels of material nonlinearity in the structural response.

5.1.3. Category-III: OAT Tornado diagram vs. global sensitivity method

There are few studies on this topic relevant to structural systems, for example, [184] combined the OAT perturbation method with global sensitivity analysis to evaluate the individual input factors separately. The input factors include: (1–3) level of uncertainty in the (identified) modal parameters of each of the first three longitudinal modes, (4) spatial density of measurements (number of sensors), and (5) mesh size in the FE model used in the FE model updating procedure. They showed that the level of confidence in damage identification is a function of the level of uncertainty in the identified modal parameters, the choices made in the design of experiments, and modeling errors.

5.2. A Generalized Procedure for Earthquake Engineering Practice

Sensitivity analysis determines the impact of a variation in an input parameter on output results. Mathematically, this corresponds to the partial derivative of the output function with respect to an input parameter at a given design point. While the skeleton of a classical sensitivity analysis is well-structured and has been used in numerous cases, its application in the earthquake and structural engineering requires depth discussion. More specifically, depending on the type of input and output parameters, there is another layer of "variability" in the results of sensitivity analysis. This aspect sometimes refers to as mixed (or a mixture of) epistemic and aleatory uncertainties applied to sensitivity analysis [14, 185, 186], or time-variant sensitivity analysis [187, 188].

Figure 47 provides a uniform framework for sensitivity analysis of engineering structures using the basic material and modeling random variables which are subjected to different types of stressors. A stressor refers to (1) an incrementally–increasing monotonic, cyclic, or time-dependent load; (2) an incrementally–decreasing resistance parameter or degradation in strength properties; or (3) a discrete increasing/decreasing critical parameter in a system leading to failure [118]. In earthquake engineering, the stressor is typically called an IM parameter [189]. Moreover, the generic algorithm for Tornado diagram-based sensitivity analysis is provided in Algorithm 1 in connection to Figure 47.

The stressors that can be used within the earthquake engineering framework can be classified into two main categories of deterministic/classical and probabilistic approaches. The stressors for each one can be categorized as follows:

Deterministic Monotonic Load (Sens-I): This is a classical pushover-based sensitivity analysis [43] using a monotonic (single or multi-mode) invariant load vector [190, 191]. Since this is a static method, the rate-dependent RVs (e.g., damping ratio, and dynamic magnification factor) [192] will not be activated. Examples of this method are: [92, 128, 191, 193–196].

Deterministic Cyclic Load (Sens-II): This method is similar to Type-I; however, it uses

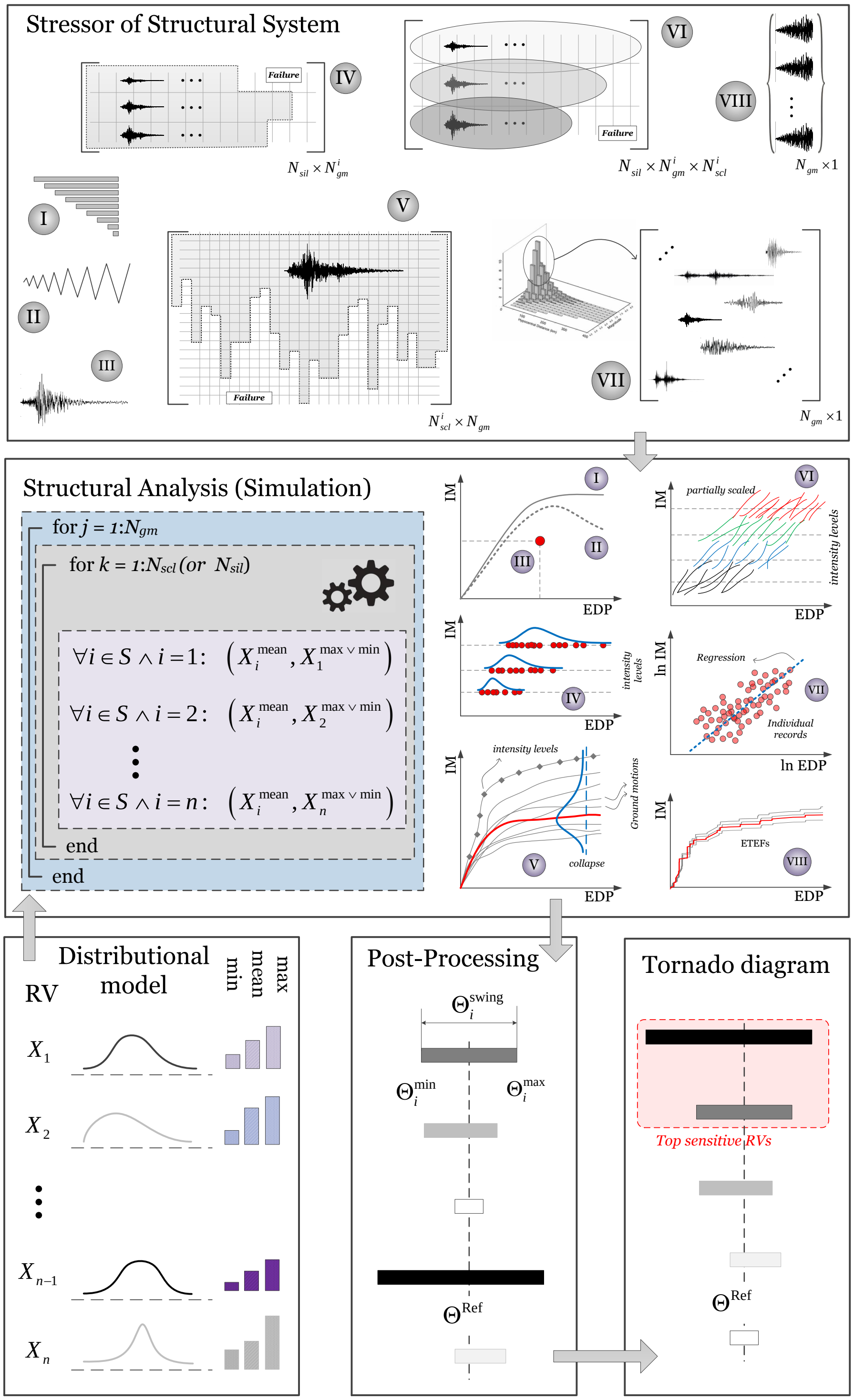

Fig. 47. Sensitivity analysis with Tornado diagram in earthquake engineering practice

Algorithm 1 Generic algorithm for Tornado diagram-based sensitivity analysis

Inputs: $\mathbf{X} = (X_1, \cdots, X_{N_{rv}})$ (basic RVs); X_i^{mean} (mean), X_i^{min} (minimum), and X_i^{max} (maximum) values of the RVs; N_{rv} number of RVs; N_{gm} number of ground motions; N_{scl} number of scale factors; N_{sil} number of seismic intensity levels.

Output: $\Theta = g(X_1, X_2, \cdots, X_i, \cdots, X_{N_{rv}})$ (response quantity); Tornado diagram.

procedure DETERMINISTIC SENSITIVITY METHODS
  $\Theta^{\text{Ref}} = g(\mathbf{X}^{\text{mean}})$
  for $i = 1, \ldots, N_{rv}$ **do**
    $\Theta_i^{\text{min}} = g\left(X_i^{\text{min}}, \mathbf{X}_{\sim i}^{\text{mean}}\right)$
    $\Theta_i^{\text{max}} = g\left(X_i^{\text{max}}, \mathbf{X}_{\sim i}^{\text{mean}}\right)$
  end for
  $\Theta_i^{\text{swing}} = \left|\frac{\Theta_i^{\text{max}}}{\Theta^{\text{Ref}}}\right| + \left|\frac{\Theta_i^{\text{min}}}{\Theta^{\text{Ref}}}\right|$ ▷ Normalized responses (centered at one)
  $\Theta_i^{\text{swing}} = \left|\frac{\Theta_i^{\text{max}} - \Theta^{\text{Ref}}}{\Theta^{\text{Ref}}}\right| + \left|\frac{\Theta_i^{\text{min}} - \Theta^{\text{Ref}}}{\Theta^{\text{Ref}}}\right|$ ▷ Error-based perspective (centered at zero)
  Sort the swings in a descending order to form the Tornado diagram.
end procedure

procedure PROBABILISTIC SENSITIVITY METHODS
  for $j = 1, \ldots, N_{gm}$ **do**
    for $k = 1, \ldots, N_{scl} (or\, N_{sil})$ **do**
      $\Theta_{j,k}^{\text{Ref}} = g(\mathbf{X}^{\text{mean}})$
      for $i = 1, \ldots, N_{rv}$ **do**
        $\Theta_{i,j,k}^{\text{min}} = g\left(X_i^{\text{min}}, \mathbf{X}_{\sim i}^{\text{mean}}\right)$
        $\Theta_{i,j,k}^{\text{max}} = g\left(X_i^{\text{max}}, \mathbf{X}_{\sim i}^{\text{mean}}\right)$
      end for
    end for
  end for
  $\Theta_{j,k}^{\text{Ref}} \sim Dist.(\eta_{j,k}^{\text{Ref}}, \beta_j^{\text{Ref}})$ ▷ $Dist.$ is a distributional model, e.g., $\mathscr{L}\mathscr{N}$
  $\Theta_{j,k}^{\text{min}} \sim Dist.(\eta_{j,k}^{\text{min}}, \beta_{j,k}^{\text{min}})$
  $\Theta_{j,k}^{\text{max}} \sim Dist.(\eta_{j,k}^{\text{max}}, \beta_{j,k}^{\text{max}})$
  Calculate the swings, $\Xi_{j,k}^{\text{swing}}$. ▷ Ξ presents any statistics
  Sort the swings in a descending order to form the Tornado diagram.
  Perform regression analysis to integrate Tornado diagrams at different SIL.
end procedure

a cyclic load vector, and it provides smaller strength in RC frame structures [197]. This method accounts for the cumulative damage, resulting in stiffness degradation and strength deterioration [198]. Therefore, it has advantage to be used for sensitivity analysis of systems with degradation- and strength-related parameters [33]. Examples of this method are presented in [199–202].

Deterministic Time-dependent Signal (Sens-III): In this method, a time (or frequency) dependent load is used to evaluate the structural system. A ground motion record is an example of a stochastic time dependent load, while a sinusoidal harmonic load is essentially characterized by its natural frequency. This type of loading is capable of activating the rate-dependent material properties. Yet, the system response highly depends on the ground motion unique meta-features [203]. Examples of this method can be found in [204].

Probabilistic Stripe Analysis (Sens-IV): This method is one of the probabilistic sensitivity analysis techniques in which the variable importance is computed using some statistical operation on the results. A stripe refers to a particular seismic intensity level (SIL) with a series of ground motion records that have been selected and scaled only for that level. Depending on the number of desired stripes, this method is called single stripe analysis (SSA), double stripe analysis (DSA), or multiple stripe analysis (MSA). Having N_{sil} stripes, and a suit of N_{gm} in each level, the process of deterministic analysis (i.e., Sens-III) should be repeated $N_{sil} \times N_{gm}$ times. Examples of this method can be found in [205–208].

Probabilistic Incremental Dynamic Analysis (Sens-V): This technique is similar to Sens-IV; however, the same group of ground motion records is successively scaled from very low-intensity seismic levels until they cause structural collapse. While the ground motion selection is easier for this method, it suffers from an unrealistically large scaling factor problem [209, 210]. It may also cause bias in some cases [211, 212]. This method can be used to evaluate the sensitivity of the EPD condition on IM (i.e., $EDP|IM$) [213] or vice versa (i.e., $IM|EDP$). However, the main application of this method is to evaluate the sensitivity at the collapse level. Examples of this method are presented in [214–218]. Assuming that a total of N_{gm} ground motions are used for IDA and each record j requires a total of N^j_{scl} scaling levels up to collapse, the process of deterministic analysis (i.e., Sens-III) should be repeated $\sum_{j=1}^{N_{gm}} N^j_{scl}$ times.

Probabilistic Adaptive Incremental Dynamic Analysis (Sens-VI): This method is created as a marriage of IDA and MSA methods. The AIDA deceptively changes the ground motions for IDA which allows the user to vary MSA-like ground motions to match the changing properties at various SILs [219]. This method partially maintains the IDA-like continuous curves. This method allows us to evaluate the sensitivity of the IM condition on any desired EDP. The sensitivity evaluation is similar to Sens-V.

Probabilistic Cloud Analysis (Sens-VII): In this method, the structure is subjected to a set of un-scaled ground motions [220]. For a pre-defined seismic hazard scenario, e.g., $< R_{rup}, M_w, V_{S30} >$, a large number of ground motion records are required (typically 100 to 200). From these results, EDP vs. IM are determined which forms a cloud of responses. Examples of this method are presented in [186, 221–224]. Assuming that a total of N_{gm} ground motions are used for CLA, the process of deterministic analysis (i.e., Sens-III) should be repeated N_{gm} times.

Probabilistic Endurance Time Analysis (Sens-VIII): This method falls in the interface of probabilistic and deterministic techniques. It uses a limited number of stressors to excite the dynamical system, thus, it benefits from deterministic techniques' advantages. However, it provides the structural responses at various SILs, therefore, it can be categorized under the probabilistic approaches. ETA method uses a special form of intensifying acceleration functions which (dynamically) pushes the structural system from linear elastic analysis to nonlinear, and finally collapse. Its computational cost is similar to Sens-III. Application of this method can be found in [120, 122, 225, 226].

6. Conclusions and Recommendations

The following points should be considered in the sensitivity analysis of structural systems:

- In both TDA and FOSM methods, the mean and standard deviation of the input parameter are predetermined, and based on that, the mean and standard deviation of the structural response is obtained. However, FOSM has been observed to lose accuracy when the relationship between input and response variables is nonlinear, which is a concern when modeling collapse [227].
- The type of the finite element formulation and the numerical model are important factors during sensitivity analysis of concrete structures [228–233]. Depending on the numerical modeling strategy, e.g., lumped plasticity, distributed plasticity, or detailed finite element model, the outcome of sensitivity analysis alters.
- Whenever it applies, the time-dependent effect of material deterioration (e.g., creep, shrinkage, and alkali-aggregate reaction), and environmental condition (e.g., climate change) should be accounted for in the sensitivity analysis of concrete structures [187, 234]. In those conditions, the developed Tornado diagram is time-dependent (i.e., different Tornado diagrams are required at different ages of structure).
- Results of a sensitivity analysis depend on the software used, and the limitations and domain of application of the adopted software should be identified properly before generalizing the results. Section 4.1 provides some insights about the choice and importance of software.
- Results of a sensitivity analysis depend not only on the input random variables but also on the target QoI (or EDP). In general, the selected QoI should be (1) a good representative of the input-output relationship for the case study structure, and (2) a good representative of the loss model for the subsequent decision-making steps. Section 4.3 identifies three major categories for QoIs that should be considered in a sensitivity analysis.
- Results of sensitivity analysis on material and modeling randomness depend on the applied stressor. There are a variety of deterministic and probabilistic methods that can be combined with sensitivity analysis. These methods have been discussed in Section 5.2 for sensitivity analysis of structural systems in the context of earthquake engineering problems. In general, a sensitivity analysis can be performed using static-type loading (neglecting the dynamic characteristics of the material), or dy-

namic loading. Dynamic loading can be applied using either real ground motion records or artificial ones. In the case of using real ground motions, the ground motion selection and scaling method plays also an important role in the outcome of sensitivity analysis.

- The methods reviewed in Section 2 are the most practical ones for sensitivity analysis of engineering structures. Nearly all of them only require some basic knowledge of statistics. However, more advanced sensitivity analysis methods can be achieved using machine learning methods and surrogate modeling. These methods typically require some knowledge about applied data science, see Section 4.12.

References

[1] Christopher Frey H, Patil SR (2002) Identification and review of sensitivity analysis methods. *Risk analysis* 22(3):553–578.

[2] Ricci P, De Risi M, Verderame G, Manfredi G (2012) Influence of infill presence and design typology on seismic performance of rc buildings: sensitivity analysis. *Proceedings of the 15th World Conference on Earthquake Engineering*, pp 24–28.

[3] Porter K, Beck J, Shaikhutdinov R (2002) Sensitivity of building loss estimates to major uncertain variables. *Earthquake Spectra* 18:719–743.

[4] Stocchi A, Richard B (2019) Sensitivity of engineering demand parameters as a function of structural typology and assessment method. *Nuclear Engineering and Design* 343:151–165.

[5] Haselton C, Goulet C, Mitrani-Reiser J, Beck J, Deierlein G, Porter K, Stewart J, Taciroglu E (2008) An assessment to benchmark the seismic performance of a code-conforming reinforced concrete moment-frame building, peer report 2007/12 (Pacific Earthquake Engineering Research Center, University of California, Berkeley, Califprnia),

[6] Yazdani A, Nicknam A, Dadras EY, Eftekhari SN (2017) Entropy-based sensitivity analysis of global seismic demand of concrete structures. *Engineering Structures* 146:118–126.

[7] Cantagallo C, Camata G, Spacone E (2014) Seismic demand sensitivity of reinforced concrete structures to ground motion selection and modification methods. *Earthquake Spectra* 30(4):1449–1465.

[8] Kim S, Moon T, Kim SJ (2020) Effect of uncertainties in material and structural detailing on the seismic vulnerability of rc frames considering construction quality defects. *Applied Sciences* 10(24):8832.

[9] Swensen DJ, Kunnath SK (2018) Consequences of modeling choices in seismic performance assessment of buildings. *Earthquake Spectra* 34(2):423–440.

[10] Choudhury T, Kaushik HB (2018) Seismic response sensitivity to uncertain variables in rc frames with infill walls. *Journal of Structural Engineering* 144(10):04018184.

[11] Grubišić M, Ivošević J, Grubišić A (2019) Reliability analysis of reinforced con-

crete frame by finite element method with implicit limit state functions. *Buildings* 9(5):119.

[12] Faggella M, Barbosa A, Conte J, Spacone E, Restrepo J (2008) Probabilistic seismic response sensitivity analysis of 3d nonlinear model of r/cbuilding structure. *Valutazione e riduzione della vulnerabilità sismica di edifici in cemento armato* .

[13] Bartoli G, Betti M, Biagini P, Borghini A, Ciavattone A, Girardi M, Lancioni G, Marra AM, Ortolani B, Pintucchi B, et al. (2017) Epistemic uncertainties in structural modeling: a blind benchmark for seismic assessment of slender masonry towers. *Journal of Performance of Constructed Facilities* 31(5):04017067.

[14] Hariri-Ardebili M, Boodagh P (2018) Taguchi design-based seismic reliability analysis of geostructures. *Georisk: Assessment and Management of Risk for Engineered Systems and Geohazards* :1–19.

[15] Nasrollahzadeh K, Hariri-Ardebili MA, Kiani H, Mahdavi G (2022) An integrated sensitivity and uncertainty quantification of fragility functions in rc frames. *Sustainability* 14(20):13082.

[16] Naderpour H, Nagai K, Haji M, Mirrashid M (2019) Adaptive neuro-fuzzy inference modelling and sensitivity analysis for capacity estimation of fiber reinforced polymer-strengthened circular reinforced concrete columns. *Expert Systems* 36(4):e12410.

[17] Parisi F, Scalvenzi M, Brunesi E (2019) Performance limit states for progressive collapse analysis of reinforced concrete framed buildings. *Structural Concrete* 20(1):68–84.

[18] Larsson Ivanov O, Honfi D, Santandrea F, Stripple H (2019) Consideration of uncertainties in lca for infrastructure using probabilistic methods. *Structure and Infrastructure Engineering* 15(6):711–724.

[19] Van-Loc T, Kiesse TS, Bonnet S, Ventura A (2018) Application of sensitivity analysis in the life cycle design for the durability of reinforced concrete structures in the case of xc4 exposure class. *Cement and Concrete Composites* 87:53–62.

[20] Somala SN, Karthikeyan K, Mangalathu S (2021) Time period estimation of masonry infilled rc frames using machine learning techniques. *Structures* (Elsevier), Vol. 34, pp 1560–1566.

[21] Huang H, Burton HV (2019) Classification of in-plane failure modes for reinforced concrete frames with infills using machine learning. *Journal of Building Engineering* 25:100767.

[22] Brownlee J (2013) A tour of machine learning algorithms. Available at https://machinelearningmastery.com/a-tour-of-machine-learning-algorithms/.

[23] Hariri-Ardebili M (2018) Risk, reliability, resilience (R3) and beyond in dam engineering: A state-of-the-art review. *International journal of disaster risk reduction* 31:806–831.

[24] Gharehbaghi S, Yazdani H, Khatibinia M (2020) Estimating inelastic seismic response of reinforced concrete frame structures using a wavelet support vector machine and an artificial neural network. *Neural Computing and Applications*

32(8):2975–2988.

[25] Hwang SH, Mangalathu S, Shin J, Jeon JS (2021) Machine learning-based approaches for seismic demand and collapse of ductile reinforced concrete building frames. *Journal of Building Engineering* 34:101905.

[26] Hariri-Ardebili M, Sattar S, Segura C, Mahdavi G (2022) Probabilistic moment curvature analysis using random forest-based ensemble regression. *Proceedings of the 12th National Conference on Earthquake Engineering* (Earthquake Engineering Research Institute).

[27] Gorris L, Yoe C (2014) Risk analysis: risk assessment: principles, methods, and applications. *Encyclopedia of Food Safety* :65–72.

[28] Konietzky H, Schlegel R (2007) Using sensitivity analysis and optimization for civil engineering and geotechnical applications. *Proceedings Optimization and Stochastic Days* 4.

[29] Oberguggenberger M, King J, Schmelzer B (2009) Classical and imprecise probability methods for sensitivity analysis in engineering: A case study. *International Journal of Approximate Reasoning* 50(4):680–693.

[30] Bucher C (2009) Robustness analysis in structural optimization. *Structure and Infrastructure Engineering* 5(4):287–293.

[31] Hezarjaribi M, Bahaari M, Bagheri V, Ebrahimian H (2013) Sensitivity analysis of jacket-type offshore platforms under extreme waves. *Journal of Constructional Steel Research* 83:147–155.

[32] Hariri-Ardebili M, Saouma V (2016) Sensitivity and uncertainty quantification of the cohesive crack model. *Engineering Fracture Mechanics* 155:18–35.

[33] Hariri-Ardebili M, Saouma V (2018) Sensitivity and uncertainty analysis of aar affected reinforced concrete shear walls. *Engineering Structures* 172:334–345.

[34] Keitel H, Dimmig-Osburg A (2010) Uncertainty and sensitivity analysis of creep models for uncorrelated and correlated input parameters. *Engineering Structures* 32(11):3758–3767.

[35] Li Z (2021) Global sensitivity analysis of the static performance of concrete gravity dam from the viewpoint of structural health monitoring. *Archives of Computational Methods in Engineering* 28(3):1611–1646.

[36] Gao Y, Gu Q, Qiu Z, Wang J (2016) Seismic response sensitivity analysis of coupled dam-reservoir-foundation systems. *Journal of Engineering Mechanics* 142(10):04016070.

[37] Rodríguez D, Brunesi E, Nascimbene R (2020) Fragility and sensitivity analysis of steel frames with bolted-angle connections under progressive collapse. *Engineering Structures* :111508.

[38] Shin DH, Kim HJ (2014) Probabilistic assessment of structural seismic performance influenced by the characteristics of hysteretic energy dissipating devices. *International Journal of Steel Structures* 14(4):697–710.

[39] Xie Y, DesRoches R (2019) Sensitivity of seismic demands and fragility estimates of a typical california highway bridge to uncertainties in its soil-structure interaction

modeling. *Engineering Structures* 189:605–617.
[40] Na UJ, Chaudhuri SR, Shinozuka M (2008) Probabilistic assessment for seismic performance of port structures. *Soil Dynamics and Earthquake Engineering* 28(2):147–158.
[41] Fellin W, King J, Kirsch A, Oberguggenberger M (2010) Uncertainty modelling and sensitivity analysis of tunnel face stability. *Structural Safety* 32(6):402–410.
[42] Lu X, Tian Y, Guan H, Xiong C (2017) Parametric sensitivity study on regional seismic damage prediction of reinforced masonry buildings based on time-history analysis. *Bulletin of Earthquake Engineering* 15(11):4791–4820.
[43] Mendes N, Lourenço PB (2014) Sensitivity analysis of the seismic performance of existing masonry buildings. *Engineering Structures* 80:137–146.
[44] Calabrese A, Lai CG (2016) Sensitivity analysis of the seismic response of gravity quay walls to perturbations of input parameters. *Soil Dynamics and Earthquake Engineering* 82:55–62.
[45] Taflanidis AA, Jia G (2011) A simulation-based framework for risk assessment and probabilistic sensitivity analysis of base-isolated structures. *Earthquake Engineering & Structural Dynamics* 40(14):1629–1651.
[46] Pan H, Tian L, Fu X, Li H (2020) Sensitivities of the seismic response and fragility estimate of a transmission tower to structural and ground motion uncertainties. *Journal of Constructional Steel Research* 167:105941.
[47] Tran QH, Huh J, Nguyen VB, Kang C, Ahn JH, Park IJ (2018) Sensitivity analysis for ship-to-shore container crane design. *Applied Sciences* 8(9):1667.
[48] Heidary-Torkamani H, Bargi K, Amirabadi R (2014) Seismic vulnerability assessment of pile-supported wharves using fragility curves. *Structure and Infrastructure Engineering* 10(11):1417–1431.
[49] Salehi F, Prasher S, Amin S, Madani A, Jebelli S, Ramaswamy H, Tan C, Drury C (2000) Prediction of annual nitrate-n losses in drain outflows with artificial neural networks. *Transactions of the ASAE* 43(5):1137.
[50] Morgan MG, Henrion M, Small M (1990) *Uncertainty: a guide to dealing with uncertainty in quantitative risk and policy analysis* (Cambridge university press).
[51] Brun R, Reichert P, Künsch HR (2001) Practical identifiability analysis of large environmental simulation models. *Water Resources Research* 37(4):1015–1030.
[52] Critchfield GC, Willard KE (1986) Probabilistic analysis of decision trees using monte carlo simulation. *Medical Decision Making* 6(2):85–92.
[53] Cullen AC, Frey HC, Frey CH (1999) *Probabilistic techniques in exposure assessment: a handbook for dealing with variability and uncertainty in models and inputs* (Springer Science & Business Media).
[54] Box GE, Draper NR (1987) *Empirical model-building and response surfaces*. Vol. 424 (Wiley New York).
[55] Hoffman F, Gardner R (1983) Evaluation of uncertainties in environmental radiological assessment models. *Radiological assessments: a textbook on environmental dose assessment* 11:1.

[56] Downing DJ, Gardner R, Hoffman F (1985) An examination of response-surface methodologies for uncertainty analysis in assessment models. *Technometrics* 27(2):151–163.
[57] Menard S (2002) *Applied logistic regression analysis*. Vol. 106 (Sage).
[58] Von Winterfeldt D, Edwards W (1993) Decision analysis and behavioral research, .
[59] Andersson FO, Åberg M, Jacobsson SP (2000) Algorithmic approaches for studies of variable influence, contribution and selection in neural networks. *Chemometrics and intelligent laboratory systems* 51(1):61–72.
[60] Scheffe H (1999) *The analysis of variance*. Vol. 72 (John Wiley & Sons).
[61] Hamby D (1995) A comparison of sensitivity analysis techniques. *Health physics* 68(2):195–204.
[62] Melchers R (1994) Structural system reliability assessment using directional simulation. *Structural Safety* 16(1-2):23–37.
[63] Nowak AS, Collins KR (2012) *Reliability of structures* (CRC Press).
[64] Nikolaidis E, Ghiocel DM, Singhal S (2004) *Engineering design reliability handbook* (CRC Press).
[65] Hohenbichler M, Rackwitz R (1982) First-order concepts in system reliability. *Structural safety* 1(3):177–188.
[66] Ibarra LF, Krawinkler H (2005) *Global collapse of frame structures under seismic excitations* (Pacific Earthquake Engineering Research Center Berkeley, CA).
[67] Lee TH, Mosalam KM (2005) Seismic demand sensitivity of reinforced concrete shear-wall building using fosm method. *Earthquake engineering & structural dynamics* 34(14):1719–1736.
[68] Melchers RE (1999) *Structural reliability analysis and prediction* (John Wiley & Son Ltd).
[69] Cornell C (1968) Engineering seismic risk analysis. *Bulletin of the Seismological Society of America* 58:1583–1606.
[70] Cornell CA (1972) First-order analysis of model and parameter uncertainty. *Proceedings of International Symposium on Uncertainties in Hydrology and Water Resources Systems, University of Arizona, Tucson, Arizona*, pp 1245–1272.
[71] Cukier R, Levine H, Shuler K (1978) Nonlinear sensitivity analysis of multiparameter model systems. *Journal of computational physics* 26(1):1–42.
[72] IM S (1993) Sensitivity estimates for nonlinear mathematical models. *Math Model Comput Exp* 1(4):407–414.
[73] Conover WJ (1998) *Practical nonparametric statistics*. Vol. 350 (John Wiley & Sons).
[74] Iman RL, Conover WJ (1979) The use of the rank transform in regression. *Technometrics* 21(4):499–509.
[75] Iman RL, Helton JC, Campbell JE (1981) An approach to sensitivity analysis of computer models: Part i—introduction, input variable selection and preliminary variable assessment. *Journal of quality technology* 13(3):174–183.
[76] Crick M, Hill M (1987) The role of sensitivity analysis in assessing uncertainty. *Un-*

certainty analysis for performance assessments of radioactive waste disposal systems.

[77] Iman RL, Shortencarier MJ, Johnson JD (1985) Fortran 77 program and user's guide for the calculation of partial correlation and standardized regression coefficients (Sandia National Labs., Albuquerque, NM (USA)),

[78] Sen A, Srivastava M (2012) *Regression analysis: theory, methods, and applications* (Springer Science & Business Media).

[79] Geldermann J, Rentz O (2001) Integrated technique assessment with imprecise information as a support for the identification of best available techniques (bat). *OR-Spektrum* 23(1):137–157.

[80] Cook RD, Weisberg S (2009) *An introduction to regression graphics*. Vol. 405 (John Wiley & Sons).

[81] Borgonovo E, Plischke E (2016) Sensitivity analysis: a review of recent advances. *European Journal of Operational Research* 248(3):869–887.

[82] Novak D, Teply B, Shiraishi N (1993) Sensitivity analysis of structures: A review. *THE FIFTH INTERNATIONAL CONFERENCE ON CIVIL AND STRUCTURAL ENGINEERTNG COMPUTING* (Edinburgh, Scotland), pp 201–207.

[83] Saltelli A (2002) Sensitivity analysis for importance assessment. *Risk analysis* 22(3):579–590.

[84] Saltelli A, Ratto M, Tarantola S, Campolongo F, Commission E, et al. (2006) Sensitivity analysis practices: Strategies for model-based inference. *Reliability Engineering & System Safety* 91(10-11):1109–1125.

[85] Marelli S, Lamas C, Sudret B, Konakli K, Mylonas C (2019) Uqlab user manual–sensitivity analysis. *Report# UQLab-V1* :3–106.

[86] Cheng K, Lu Z, Ling C, Zhou S (2020) Surrogate-assisted global sensitivity analysis: an overview. *Structural and Multidisciplinary Optimization* 61(3):1187–1213.

[87] Porter KA, Beck JL, Shaikhutdinov RV (2002) Investigation of sensitivity of building loss estimates to major uncertain variables for the van nuys testbed (PEER Report 2002/03, Pacific Earthquake Engineering Research Center, University of California, Berkeley),

[88] Talaat M, Mosalam KM (2009) Modeling progressive collapse in reinforced concrete buildings using direct element removal. *Earthquake Engineering & Structural Dynamics* 38(5):609–634.

[89] Binici B, Mosalam KM (2007) Analysis of reinforced concrete columns retrofitted with fiber reinforced polymer lamina. *Composites Part B: Engineering* 38(2):265–276.

[90] Dolšek M (2009) Incremental dynamic analysis with consideration of modeling uncertainties. *Earthquake Engineering and Structural Dynamics* 38:805–825.

[91] Celarec D, Dolšek M (2013) The impact of modelling uncertainties on the seismic performance assessment of reinforced concrete frame buildings. *Engineering Structures* 52:340–354.

[92] Fajfar P (2000) A nonlinear analysis method for performance based seismic design.

Earthquake Spectra 16:573–592.
[93] Bracchi S, Rota M, Penna A, Magenes G (2015) Consideration of modelling uncertainties in the seismic assessment of masonry buildings by equivalent-frame approach. *Bulletin of Earthquake Engineering* 13(11):3423–3448.
[94] Celik O, Ellingwood B (2010) Seismic fragilities for non-ductile reinforced concrete frames–role of aleatoric and epistemic uncertainties. *Structural Safety* 32:1–12.
[95] Li H, Li L, Zhou G, Xu L (2020) Effects of various modeling uncertainty parameters on the seismic response and seismic fragility estimates of the aging highway bridges. *Bulletin of Earthquake Engineering* :1–37.
[96] Barbato M, Gu Q, Conte J (2010) Probabilistic push-over analysis of structural and soil-structure systems. *Journal of structural engineering* 136(11):1330–1341.
[97] Ma HB, Zhuo WD, Lavorato D, Nuti C, Fiorentino G, Marano GC, Greco R, Briseghella B (2019) Probabilistic seismic response and uncertainty analysis of continuous bridges under near-fault ground motions. *Frontiers of Structural and Civil Engineering* 13(6):1510–1519.
[98] Kim J, Han S (2013) Sensitivity analysis for seismic response of reinforced concrete staggered wall structures. *Magazine of concrete research* 65(22):1348–1359.
[99] Han R, Li Y, van de Lindt J (2015) Impact of aftershocks and uncertainties on the seismic evaluation of non-ductile reinforced concrete frame buildings. *Engineering Structures* 100:149–163.
[100] Han R, Li Y, van de Lindt J (2014) Seismic risk of base isolated non-ductile reinforced concrete buildings considering uncertainties and mainshock–aftershock sequences. *Structural Safety* 50:39–56.
[101] Yu XH, Lu DG, Qian K, Li B (2017) Uncertainty and sensitivity analysis of reinforced concrete frame structures subjected to column loss. *Journal of Performance of Constructed Facilities* 31(1):04016069.
[102] Takeda T, Sozen MA, Nielsen NN (1970) Reinforced concrete response to simulated earthquakes. *Journal of the Structural Division* 96(12):2557–2573.
[103] Segura Jr CL, Sattar S, Hariri-Ardebili MA (2022) Quantifying material uncertainty in seismic evaluations of reinforced concrete bridge column structures. *ACI Structural Journal* 119(3):141–152.
[104] Alwaeli W, Mwafy A, Pilakoutas K, Guadagnini M (2017) Multi-level nonlinear modeling verification scheme of rc high-rise wall buildings. *Bulletin of Earthquake Engineering* 15(5):2035–2053.
[105] Asgarian B, Yahyai M, Mirtaheri M, Samani HR, Alanjari P (2010) Incremental dynamic analysis of high-rise towers. *The Structural Design of Tall and Special Buildings* 19(8):922–934.
[106] Pang Y, Wu X, Shen G, Yuan W (2014) Seismic fragility analysis of cable-stayed bridges considering different sources of uncertainties. *Journal of Bridge Engineering* 19(4):04013015.
[107] Wang X, Ye A, Ji B (2019) Fragility-based sensitivity analysis on the seismic performance of pile-group-supported bridges in liquefiable ground undergoing scour

potentials. *Engineering Structures* 198:109427.

[108] Haddad J, Cattari S, Lagomarsino S (2019) Use of the model parameter sensitivity analysis for the probabilistic-based seismic assessment of existing buildings. *Bulletin of earthquake engineering* 17(4):1983–2009.

[109] Zhang J, Huo Y (2009) Evaluating effectiveness and optimum design of isolation devices for highway bridges using the fragility function method. *Engineering Structures* 31:1648–1660.

[110] Kiani J, Pezeshk S (2017) Sensitivity analysis of the seismic demands of rc moment resisting frames to different aspects of ground motions. *Earthquake engineering & structural dynamics* 46(15):2739–2755.

[111] Zhong J, Gardoni P, Rosowsky D (2012) Closed-form seismic fragility estimates, sensitivity analysis and importance measures for reinforced concrete columns in two-column bents. *Structure and Infrastructure Engineering* 8(7):669–685.

[112] Hohenbichler M, Rackwitz R (1986) Sensitivity and importance measures in structural reliability. *Civil engineering systems* 3(4):203–209.

[113] Haukaas T, Der Kiureghian A (2005) Parameter sensitivity and importance measures in nonlinear finite element reliability analysis. *Journal of engineering mechanics* 131(10):1013–1026.

[114] Der Kiureghian A, Ke JB (1985) Finite-element based reliability analysis of frame structures. *Proc., 4th Int. Conf. on Structural Safety and Reliability* (International Association for Structural Safety and Reliability New York), Vol. 1, pp 395–404.

[115] Xu J, Chen Z, Zhao X, Demartino C, Ozbakkaloglu T, Xue J (2019) Seismic performance of circular recycled aggregate concrete-filled steel tubular columns: Fem modelling and sensitivity analysis. *Thin-Walled Structures* 141:509–525.

[116] Eldin MN, Kim J (2016) Sensitivity analysis on seismic life-cycle cost of a fixed-steel offshore platform structure. *Ocean Engineering* 121:323–340.

[117] Lamprou A, Jia G, Taflanidis AA (2013) Life-cycle seismic loss estimation and global sensitivity analysis based on stochastic ground motion modeling. *Engineering structures* 54:192–206.

[118] Hariri-Ardebili M, Saouma V (2017) Single and multi-hazard capacity functions for concrete dams. *Soil Dynamics and Earthquake Engineering* 101:234–249.

[119] Furgani L, Hariri-Ardebili M, Meghella M, Seyed-Kolbadi S (2019) On the dynamic capacity of concrete dams. *Infrastructures* 4(3):57.

[120] Hariri-Ardebili M, Sattar S (2021) Myths and realities about ETA. *Ocean Engineering* 221:108499.

[121] Hariri-Ardebili MA (2020) Uncertainty quantification of heterogeneous mass concrete in macro-scale. *Soil Dynamics and Earthquake Engineering* 137:106137.

[122] Segura CL, Sattar S (2020) Uncertainty in the seismic response of structural components due to material variability. *Proceedings of the 17th World Conference on Earthquake Engineering* (Sendai, Japan).

[123] Moradi M, Tavakoli H, AbdollahZade G (2020) Sensitivity analysis of the failure time of reinforcement concrete frame under postearthquake fire loading. *Structural*

Concrete 21(2):625–641.
[124] Liel A, Haselton C, Deierlein G, Baker J (2009) Incorporating modeling uncertainties in the assessment of seismic collapse risk of buildings. *Structural Safety* 31:197–211.
[125] Furtado A, Rodrigues H, Varum H, Costa A (2014) Assessment and strengthening strategies of existing rc buildings with potential soft-storey response. *9th international masonry conference (IMC), Portugal*.
[126] Chansawat K, Yim SC, Miller TH (2006) Nonlinear finite element analysis of a frp-strengthened reinforced concrete bridge. *Journal of Bridge Engineering* 11(1):21–32.
[127] Jiao P, Roy M, Barri K, Zhu R, Ray I, Alavi AH (2019) High-performance fiber reinforced concrete as a repairing material to normal concrete structures: Experiments, numerical simulations and a machine learning-based prediction model. *Construction and Building Materials* 223:1167–1181.
[128] Coronado CA, Lopez MM (2006) Sensitivity analysis of reinforced concrete beams strengthened with frp laminates. *Cement and Concrete Composites* 28(1):102–114.
[129] ASCE/SEI 7 (2010) Minimum design loads for buildings and other structures (American Society of Civil Engineers),
[130] Ellingwood BR, Smilowitz R, Dusenberry DO, Duthinh D, Lew HS, Carino NJ, et al. (2007) Best practices for reducing the potential for progressive collapse in buildings (National Institute of Standards and Technology (NIST), Gaithersburg, MD, USA),
[131] Farahani A, Kheyroddin A, Sharbatdar MK (2018) Finding critical element in the progressive collapse of rc structures using sensitivity analysis. *Civil Engineering Journal* 4(12):3038–3057.
[132] Mucedero G, Brunesi E, Parisi F (2020) Nonlinear material modelling for fibre-based progressive collapse analysis of rc framed buildings. *Engineering Failure Analysis* 118:104901.
[133] Hariri-Ardebili MA (2020) Safety and reliability assessment of heterogeneous concrete components in nuclear structures. *Reliability Engineering & System Safety* 203:107104.
[134] Buonopane SG (2008) The basics of life cycle assessment (lca) for structural engineers. *Structures Congress 2008: Crossing Borders*, pp 1–7.
[135] Cellura M, Longo S, Mistretta M (2011) Sensitivity analysis to quantify uncertainty in life cycle assessment: the case study of an italian tile. *Renewable and Sustainable Energy Reviews* 15(9):4697–4705.
[136] Crawford RH, Bartak EL, Stephan A, Jensen CA (2016) Evaluating the life cycle energy benefits of energy efficiency regulations for buildings. *Renewable and sustainable energy reviews* 63:435–451.
[137] Bueno C, Hauschild MZ, Rossignolo JA, Ometto AR, Mendes NC (2016) Sensitivity analysis of the use of life cycle impact assessment methods: a case study on building materials. *Journal of Cleaner Production* 112:2208–2220.
[138] Häfliger IF, John V, Passer A, Lasvaux S, Hoxha E, Saade MRM, Habert G (2017)

Buildings environmental impacts' sensitivity related to lca modelling choices of construction materials. *Journal of cleaner production* 156:805–816.

[139] Bahramian M, Yetilmezsoy K (2020) Life cycle assessment of the building industry: An overview of two decades of research (1995–2018). *Energy and Buildings* 219:109917.

[140] Harter H, Singh MM, Schneider-Marin P, Lang W, Geyer P (2020) Uncertainty analysis of life cycle energy assessment in early stages of design. *Energy and Buildings* 208:109635.

[141] Trejo D, Reinschmidt K (2007) Justifying materials selection for reinforced concrete structures. i: Sensitivity analysis. *Journal of Bridge Engineering* 12(1):31–37.

[142] Groen EA, Heijungs R, Bokkers EA, de Boer IJ, et al. (2014) Sensitivity analysis in life cycle assessment. *Environmental Impacts of Cultured Meat: Alternative Production Scenarios, Proceedings of the 9th International Conference on Life Cycle Assessment in the Agri-Food Sector* (ACLCA San Francisco), pp 1360–1366.

[143] Ferreiro-Cabello J, Fraile-Garcia E, Martinez-Camara E, Perez-de La-Parte M (2017) Sensitivity analysis of life cycle assessment to select reinforced concrete structures with one-way slabs. *Engineering Structures* 132:586–596.

[144] Sobol IM (2001) Global sensitivity indices for nonlinear mathematical models and their monte carlo estimates. *Mathematics and computers in simulation* 55(1-3):271–280.

[145] Morris MD (1991) Factorial sampling plans for preliminary computational experiments. *Technometrics* 33(2):161–174.

[146] Chang KH (2014) *Design theory and methods using CAD/CAE: The computer aided engineering design series* (Academic Press).

[147] Ryu Y, Haririan M, Wu C, Arora J (1985) Structural design sensitivity analysis of nonlinear response. *Computers & structures* 21(1-2):245–255.

[148] Val D, Bljuger F, Yankelevsky D (1997) Reliability evaluation in nonlinear analysis of reinforced concrete structures. *Structural Safety* 19(2):203–217.

[149] Haukaas T, Scott MH (2006) Shape sensitivities in the reliability analysis of nonlinear frame structures. *Computers & structures* 84(15-16):964–977.

[150] Habibi A, Moharrami H (2010) Nonlinear sensitivity analysis of reinforced concrete frames. *Finite Elements in Analysis and Design* 46(7):571–584.

[151] Madsen H, Hansen PF (1992) A comparison of some algorithms for reliability based structural optimization and sensitivity analysis. *Reliability and Optimization of Structural Systems' 91* (Springer), pp 443–451.

[152] Martins AM, Simões LM, Negrão JH, Lopes AV (2020) Sensitivity analysis and optimum design of reinforced concrete frames according to eurocode 2. *Engineering Optimization* 52(12):2011–2032.

[153] Nabid N, Hajirasouliha I, Petkovski M (2018) Performance-based optimisation of rc frames with friction wall dampers using a low-cost optimisation method. *Bulletin of Earthquake Engineering* 16(10):5017–5040.

[154] Li Z, Noori M, Zhao Y, Wan C, Feng D, Altabey WA (2021) A multi-objective

optimization algorithm for bouc–wen–baber–noori model to identify reinforced concrete columns failing in different modes. *Proceedings of the Institution of Mechanical Engineers, Part L: Journal of Materials: Design and Applications* :14644207211020028.

[155] Celarec D, Ricci P, Dolšek M (2012) The sensitivity of seismic response parameters to the uncertain modelling variables of masonry-infilled reinforced concrete frames. *Engineering Structures* 35:165–177.

[156] Choudhury T, Kaushik HB (2019) Treatment of uncertainties in seismic fragility assessment of rc frames with masonry infill walls. *Soil Dynamics and Earthquake Engineering* 126:105771.

[157] Stavridis A, Shing P (2010) Finite-element modeling of nonlinear behavior of masonry-infilled rc frames. *Journal of structural engineering* 136(3):285–296.

[158] Mohammad A, Faggella M, Gigliotti R, Spacone E (2014) Probabilistic seismic response sensitivity of nonlinear frame bending-shear and infill model parameters for an existing infilled reinforced concrete structure. *Proceedings of the Twelfth International Conference on Computational Structures Technology, Naples, Italy*, pp 2–5.

[159] Gallardo JA, Juan C, Santa María H, Chacón MF (2021) Damage and sensitivity analysis of a reinforced concrete wall building during the 2010, chile earthquake. *Engineering Structures* 240:112093.

[160] Milosevic J, Cattari S, Bento R (2018) Sensitivity analysis of the seismic performance of ancient mixed masonry-rc buildings in lisbon. *International Journal of Masonry Research and Innovation* 3(2):108–154.

[161] Amanat KM, Hoque E (2006) A rationale for determining the natural period of rc building frames having infill. *Engineering structures* 28(4):495–502.

[162] Masi A, Vona M (2010) Experimental and numerical evaluation of the fundamental period of undamaged and damaged rc framed buildings. *Bulletin of Earthquake Engineering* 8(3):643–656.

[163] Asteris PG, Repapis CC, Repapi EV, Cavaleri L (2017) Fundamental period of infilled reinforced concrete frame structures. *Structure and Infrastructure Engineering* 13(7):929–941.

[164] Kose MM (2009) Parameters affecting the fundamental period of rc buildings with infill walls. *Engineering Structures* 31(1):93–102.

[165] Asteris PG, Repapis CC, Tsaris AK, Di Trapani F, Cavaleri L (2015) Parameters affecting the fundamental period of infilled rc frame structures. *Earthquakes and Structures* 9(5):999–1028.

[166] Sattar S, Liel A (2017) Collapse indicators for existing nonductile concrete frame buildings with varying column and frame characteristics. *Engineering Structures* 152:188–201.

[167] Guo H, Dong Y, Bastidas-Arteaga E, Gu XL (2021) Probabilistic failure analysis, performance assessment, and sensitivity analysis of corroded reinforced concrete structures. *Engineering Failure Analysis* 124:105328.

[168] Roy T, Matsagar V (2021) Probabilistic framework for failure investigation of rein-

forced concrete wall panel under dynamic blast loads. *Engineering Failure Analysis* 125:105368.
[169] Mangalathu S, Jeon JS (2018) Classification of failure mode and prediction of shear strength for reinforced concrete beam-column joints using machine learning techniques. *Engineering Structures* 160:85–94.
[170] Friedman J, Hastie T, Tibshirani R (2001) *The elements of statistical learning*. Vol. 1 (Springer series in statistics New York).
[171] Mangalathu S, Jang H, Hwang SH, Jeon JS (2020) Data-driven machine-learning-based seismic failure mode identification of reinforced concrete shear walls. *Engineering Structures* 208:110331.
[172] Feng DC, Liu ZT, Wang XD, Jiang ZM, Liang SX (2020) Failure mode classification and bearing capacity prediction for reinforced concrete columns based on ensemble machine learning algorithm. *Advanced Engineering Informatics* 45:101126.
[173] Manoj JA, Asiya A, Navya D, Kumar GG, Davis PR (2020) Machine learning approach to failure mode prediction of reinforced concrete infilled frames. *National Conference on Structural Engineering and Construction Management* (Springer), pp 899–907.
[174] Xie Y, Ebad Sichani M, Padgett JE, DesRoches R (2020) The promise of implementing machine learning in earthquake engineering: A state-of-the-art review. *Earthquake Spectra* 36(4):1769–1801.
[175] Jeon JS, Shafieezadeh A, DesRoches R (2014) Statistical models for shear strength of rc beam-column joints using machine-learning techniques. *Earthquake engineering & structural dynamics* 43(14):2075–2095.
[176] Cao M, Pan L, Gao Y, Novák D, Ding Z, Lehkỳ D, Li X (2017) Neural network ensemble-based parameter sensitivity analysis in civil engineering systems. *Neural Computing and Applications* 28(7):1583–1590.
[177] Torkian H, Keshavarz Z (2018) Determining the drift in reinforced concrete building using anfis soft computing modeling. *Computational Engineering and Physical Modeling* 1(1):1–11.
[178] Murad Y, Abdel-Jabar H, Diab A, Hajar HA (2020) Exterior rc joints subjected to monotonic and cyclic loading. *Engineering Computations* .
[179] Chen T, Guestrin C (2016) Xgboost: A scalable tree boosting system. *Proceedings of the 22nd acm sigkdd international conference on knowledge discovery and data mining* (ACM), pp 785–794.
[180] El-Din MN, Kim J (2014) Sensitivity analysis of pile-founded fixed steel jacket platforms subjected to seismic loads. *Ocean Engineering* 85:1–11.
[181] Arshian AH, Morgenthal G (2015) Alternate path sensitivity analysis of reinforced concrete frames using first-order second-moment method. *IABSE symposium report* (International Association for Bridge and Structural Engineering), Vol. 103, pp 170–177.
[182] Kim J, Park JH, Lee TH (2011) Sensitivity analysis of steel buildings subjected to column loss. *Engineering Structures* 33(2):421–432.

[183] Barbato M, Gu Q, Conte J (2006) Response sensitivity and probabilistic response analyses of reinforced concrete frame structures. *Proceedings of the 8th NCEE* :18–22.
[184] Moaveni B, Conte JP, Hemez FM (2009) Uncertainty and sensitivity analysis of damage identification results obtained using finite element model updating. *Computer-Aided Civil and Infrastructure Engineering* 24(5):320–334.
[185] Guo J, Du X (2007) Sensitivity analysis with mixture of epistemic and aleatory uncertainties. *AIAA journal* 45(9):2337–2349.
[186] Hariri-Ardebili M, Pourkamali-Anaraki F (2019) Matrix completion for cost reduction in finite element simulations under hybrid uncertainties. *Applied Mathematical Modelling* 69:164–180.
[187] Yang IH (2007) Uncertainty and sensitivity analysis of time-dependent effects in concrete structures. *Engineering structures* 29(7):1366–1374.
[188] Wei P, Wang Y, Tang C (2017) Time-variant global reliability sensitivity analysis of structures with both input random variables and stochastic processes. *Structural and Multidisciplinary Optimization* 55(5):1883–1898.
[189] Porter K (2003) An overview of PEER's performance-based earthquake engineering methodology. *Proceedings of the 9th International Conference on Applications of Statistics and Probability in Civil Engineering (ICASP9)* (San Francisco, CA).
[190] 365 F (2000) Prestandard and commentary for the seismic rehabilitation of buildings (Federal Emergency Management Agency, Washington, DC),
[191] Chopra A, Goel R (2002) A modal pushover analysis procedure for estimating seismic demands for buildings. *Earthquake Engineering and Structural Dynamics* 31:561—582.
[192] Ghannoum W, Saouma V, Haussmann G, Polkinghorne K, Eck M, Kang DH (2012) Experimental investigations of loading rate effects in reinforced concrete columns. *Journal of Structural Engineering* 138(8):1032–1041.
[193] Freeman S (1978) Prediction of response of concrete buildings to severe earthquake motion. *Proceedings of Douglas McHenry international symposium on concrete and concrete structures*, ed Institute AC (Detroit, MI, USA).
[194] Chopra A, Goel R (1999) Capacity-demand-diagram methods based on inelastic design spectrum. *Earthquake Spectra* 15:637–656.
[195] Antoniou S, Pinho R (2004) Development and verification of a displacement-based adaptive pushover procedure. *Journal of Earthquake Engineering* 8:643–661.
[196] Giorgi P, Scotta R (2013) Validation and improvement of {N1} method for pushover analysis. *Soil Dynamics and Earthquake Engineering* 55:140–147.
[197] Koutromanos I, Stavridis A, Shing PB, Willam K (2011) Numerical modeling of masonry-infilled rc frames subjected to seismic loads. *Computers & Structures* 89(11-12):1026–1037.
[198] Panyakapo P (2014) Cyclic pushover analysis procedure to estimate seismic demands for buildings. *Engineering Structures* 66:10–23.
[199] Cheung P, Pauley T, Park R (1991) New zealand tests on full-scale reinforced con-

crete beam-column-slab sub-assemblages designed for earthquake resistance. *ACI Special Publication SP-123, Design of Beam-Column Joints for Seismic Resistance* (Detroit, MI, USA), pp 1–37.

[200] Clark P, Frank K, Krawinkler H, Shaw R (1997) Protocol for fabrication, inspection, testing and documentation of beam-column connection and other experimental specimens (SAC Joint Venture, Sacramento, CA, USA), SAC/BD-97/02.

[201] Zona A, Barbato M, Conte JP (2005) Finite element response sensitivity analysis of steel-concrete composite beams with deformable shear connection. *Journal of engineering mechanics* 131(11):1126–1139.

[202] Filiatrault A, Wanitkorkul A, Constantinou M (2008) Development and appraisal of a numerical cyclic loading protocol for quantifying building system performance (University at Buffalo, State University of New York), MCEER-08-0013.

[203] Hariri-Ardebili M, Barak S (2020) A series of forecasting models for seismic evaluation of dams based on ground motion meta-features. *Engineering Structures* :109657.

[204] Fan FG, Ahmadi G, Tadjbakhsh IG (1990) Multi-story base-isolated buildings under a harmonic ground motion—part ii: sensitivity analysis. *Nuclear Engineering and Design* 123(1):17–26.

[205] Mackie K, Stojadinovic B (2005) Comparison of incremental dynamic, cloud, and stripe methods for computing probabilistic seismic demand models. *Proceedings of the 2005 Structures Congress and the 2005 Forensic Engineering Symposium* (New York, NY), pp 1–11.

[206] Jalayer F, Cornell C (2009) Alternative non-linear demand estimation methods for probability-based seismic assessments. *Earthquake Engineering and Structural Dynamics* 38:951–972.

[207] Scozzese F, Tubaldi E, Dall'Asta A (2020) Assessment of the effectiveness of multiple-stripe analysis by using a stochastic earthquake input model. *Bull Earthq Eng* 18:3167–3203.

[208] Conde Bandini PA, Padgett JE, Paultre P, Siqueira GH (2021) Seismic fragility of bridges: An approach coupling multiple-stripe analysis and gaussian mixture for multicomponent structures. *Earthquake Spectra* :87552930211036164.

[209] Bommer JJ, Acevedo AB (2004) The use of real earthquake accelerograms as input to dynamic analysis. *Journal of Earthquake Engineering* 8(spec01):43–91.

[210] Watson-Lamprey J, Abrahamson N (2006) Selection of ground motion time series and limits on scaling. *Soil Dynamics and Earthquake Engineering* 26(5):477–482.

[211] Luco N, Bazzurro P (2007) Does amplitude scaling of ground motion records result in biased nonlinear structural drift responses? *Earthquake Engineering & Structural Dynamics* 36(13):1813–1835.

[212] Baker JW (2007) Measuring bias in structural response caused by ground motion scaling. *8th Pacific Conference on Earthquake Engineering, Singapore*, pp 1–8.

[213] Dolšek M (2015) Analytic fragility and limit states [P(EDP—IM)]: nonlinear static procedures. *Encyclopedia of Earthquake Engineering*, eds Beer M, Kougioumt-

zoglou I, Patelli E, Au I (Springer Berlin Heidelberg), pp 1–19.
[214] Vamvatsikos D, Cornell C (2002) Incremental dynamic analysis. *Earthquake Engineering and Structural Dynamics* 31:491–514.
[215] Vamvatsikos D, Cornell C (2004) Applied incremental dynamic analysis. *Earthquake Spectra* 20:523–553.
[216] Vamvatsikos D, Cornell C (2005) Developing efficient scalar and vector intensity measures for ida capacity estimation by incorporating elastic spectral shape information. *Earthquake Engineering and Structural Dynamics* 34(13):1573–1600.
[217] Mander J, Dhakal R, Mashiko N, Solberg K (2007) Incremental dynamic analysis applied to seismic financial risk assessment of bridges. *Engineering Structures* 29:2662–2672.
[218] Azarbakht A, Dolšek M (2011) Progressive incremental dynamic analysis for first-mode dominated structures. *Journal of Structural Engineering* 137:445–455.
[219] Lin T, Baker JW (2013) Introducing adaptive incremental dynamic analysis: a new tool for linking ground motion selection and structural response assessment. *11th International Conference on Structural Safety and Reliability, New York*, pp 805–811.
[220] Jalayer F (2003) *Direct probabilistic seismic analysis: implementing non-linear dynamic assessments*. Ph.D. thesis. Stanford University, Stanford, Palo-Alto, CA.
[221] Shome N (1999) *Probabilistic Seismic Demand Analysis of Nonlinear structures*. Ph.D. thesis. Stanford University, Stanford, .
[222] Padgett J, Nielson B, DesRoches R (2008) Selection of optimal intensity measures in probabilistic seismic demand models of highway bridge portfolios. *Earthquake Engineering and Structural Dynamics* 37:711–725.
[223] Jankovic S, Stojadinovic B (2004) Probabilistic performance-based seismic demand model for {R/C} frame buildings. *Proceeding of the 13th World Conferance on Earthquake Engineering* (Vancouver, B.C., Canada), pp 1–12.
[224] Ramamoorthy SK, Gardoni P, Bracci JM (2006) Probabilistic demand models and fragility curves for reinforced concrete frames. *Journal of structural Engineering* 132(10):1563–1572.
[225] Hariri-Ardebili M, Sattar S, Estekanchi H (2014) Performance-based seismic assessment of steel frames using endurance time analysis. *Engineering Structures* 69:216–234.
[226] Hariri-Ardebili M, Furgani L, Meghella M, Saouma V (2016) A new class of seismic damage and performance indices for arch dams via eta method. *Engineering Structures* 110:145–160.
[227] Gokkaya BU, Baker JW, Deierlein GG (2016) Quantifying the impacts of modeling uncertainties on the seismic drift demands and collapse risk of buildings with implications on seismic design checks. *Earthquake Engineering & Structural Dynamics* 45(10):1661–1683.
[228] Barbato M, Conte J (2005) Finite element response sensitivity analysis: a comparison between force-based and displacement-based frame element models. *Computer*

Methods in Applied Mechanics and Engineering 194(12-16):1479–1512.

[229] Barbato M, Zona A, Conte JP (2007) Finite element response sensitivity analysis using three-field mixed formulation: general theory and application to frame structures. *International journal for numerical methods in engineering* 69(1):114–161.

[230] Gu Q, Barbato M, Conte JP (2009) Handling of constraints in finite-element response sensitivity analysis. *Journal of Engineering Mechanics* 135(12):1427–1438.

[231] Scott M, Hamutçuoğlu O (2010) Analytical sensitivity of interpolatory quadrature in force-based frame elements. *International Journal for Numerical Methods in Biomedical Engineering* 26(12):1586–1595.

[232] Li Y, Huang S, Lin C, Gu Q, Qiu Z (2017) Response sensitivity analysis for plastic plane problems based on direct differentiation method. *Computers & Structures* 182:392–403.

[233] Al-Aukaily A, Scott MH (2019) Response sensitivity for geometrically nonlinear displacement-based beam-column elements. *Computers & Structures* 220:43–54.

[234] Bastidas-Arteaga E, El Soueidy CP, Amiri O, Nguyen PT (2020) Polynomial chaos expansion for lifetime assessment and sensitivity analysis of reinforced concrete structures subjected to chloride ingress and climate change. *Structural Concrete* 21(4):1396–1407.